Acute Perturbation and Activity Measurement of Rho GTPases in Living Cells

Technische Universität Dortmund
Fakultät für Chemie

Dissertation

Zur Erlangung des akademischen Grades eines
Doktors der Naturwissenschaften
(Dr. rer. Nat.)

vorgelegt von
Master of Science

Abram Calderon

aus Lansing, Michigan (U.S.A.)

Dekan: Prof. Dr. Roland Winter
1. Gutachter: Prof. Dr. Philippe Bastiaens
2. Gutachter: Prof. Dr. Martin Engelhard

Ich versichere hiermit, dass ich die vorliegende Dissertation selbstständig und ohne unzulässige fremde Hilfe erbracht habe. Ich habe keine anderen als die angegebenen Quellen und Hilfsmittel benutzt, sowie wörtliche und sinngemäße Zitate kenntlich gemacht.

_____ _____

Ort, Datum Unterschrift

ZUSAMMENFASSUNG

Zellen enthalten ein komplexes System aus Filamenten, das Zytoskelett, welches eine Vielzahl von zellulären Prozessen reguliert. In Säugerzellen unterscheidet man drei Arten dieser Filamente: Aktinfilamente, Mikrotubuli und Intermediärfilamente. Diese Arbeit beschäftigt sich hauptsächlich mit Aktinfilamenten und Regulatorproteinen, welche hauptsächlich an der Plasmamembran lokalisiert sind und die Morphologie der Zelle maßgeblich beeinflussen.

Zunächst wurde der Einfluss von niedermolekularen Wirkstoffen, welche aus Naturstoffen abgeleitet wurden, auf das dynamische Aktin-Netzwerk untersucht. Für einen dieser Wirkstoffe (LGM235) konnte selbst bei sehr geringen Konzentrationen (~85 pM) gezeigt werden, dass er einen Einfluss auf die Organisation von Aktin in Zellen hat. Aus dieser Substanz wurde ein fluoreszenzmarkiertes Analogon entwickelt, welches zellpermeabel und nicht-toxisch ist, um statische Aktinstrukturen in lebenden Zellen zu untersuchen.

Darüber hinaus wurden in dieser Arbeit eine Reihe von Biosensoren entwickelt, um die Aktivität von Signalmolekülen aus der Familie der Rho-GTPasen (Rac1, Cdc42 und RhoA) zu messen. Diese Signalmoleküle regulieren hauptsächlich das Aktin Zytoskelett. Aktivitätsmessungen mit diesen Biosensoren wurden mit Aktivitätsstörungen durch ein photoaktivierbares Rac1-Konstrukt kombiniert, um die gegenseitige Regulation der Proteine Rac1, Cdc42 und RhoA zu charakterisieren. Überraschenderweise konnte gezeigt werden, dass als Antwort auf eine akute Photoaktivierung von Rac1 die Aktivität von Rac1, Cdc42 und RhoA erhöht wurde. Es wurde jedoch eine unerwartete subzelluläre Lokalisation von photoaktivierbarem Rac1 beobachtet, welche die Messung der gegenseitige Regulation der Rho GTPasen erschweren könnte. Daher wurde ebenfalls ein optimiertes photoaktivierbares Rac1-Konstrukt entwickelt, in welchem diese Mislokalisation unterdrückt wurde.

Alternativ zur Photoaktivierung wurde eine neue, generelle Methode zur Kontrolle der Aktivität von Rho GTPasen basierend auf chemisch induzierter Dimerisierung (CID) entwickelt. Bei diesem Ansatz bindet ein niedermolekularer Wirkstoff („Dimerizer“) gleichzeitig zwei Proteindomänen und bildet so einen heterodimeren Proteinkomplex. Da keine der beiden Proteindomänen natürlicherweise in Säugerzellen vorkommt, handelt es sich hierbei um einen neuartigen, bioorthogonalen CID-Ansatz, der zur Kontrolle der Proteinfunktion genutzt werden kann. Die C-terminale Aminosäuresequenz von K-Ras wurde an eine dieser Domänen fusioniert, um eine Lokalisation an der Plasmamembran zu gewährleisten. Eine dauerhaft aktive Mutante von Rac1 wurde an die andere der beiden Domänen fusioniert. Zusätzlich wurde die Plasmamembran Lokalisationssequenz von Rac1 entfernt, sodass sich dieses Konstrukt im Zytoplasma befindet. Kurz nach Zugabe des Dimerizers auf Zellen, welche beide Fusionsproteine synthetisieren, konnte eine sehr schnelle Rekrutierung des Fusionsproteins mit der Rac1-Mutante zur Plasmamembran beobachtet werden. Diese Rekrutierung löste die Entstehung von Rac1-typischen Aktin-Fortsätzen an den Rändern der Zelle aus. Analoge Experimente mit dauerhaft aktiven Cdc42- und RhoA-Mutanten induzierten ebenfalls Änderungen im Aktin-Zytoskelett und der Zellmorphologie, welche charakteristisch für diese Signalproteine sind.

Die in dieser Arbeit entwickelten Werkzeuge können genutzt werden, um die Dynamik von Aktinstrukturen und deren Regulation durch Signalnetzwerke der Rho GTPasen zu untersuchen.

ABSTRACT

Cells contain a complex system of filaments called the cytoskeleton that regulates a variety of cellular processes. In mammalian cells, these filaments can be categorized into three groups: actin filaments, microtubules and intermediate filaments. The work presented here focuses on actin filaments, which are predominantly found beneath the plasma membrane, where they play a central role in determining cell shape.

First, small molecules based on natural products were screened for their ability to perturb actin dynamics. One of these molecules (LGM235) was shown to influence the organization of actin in cells, even at extremely low concentrations (~85 pM). A fluorescently labeled analogue of LGM235 was found to be cell permeable and non-toxic, making it useful in studying static actin within living cells.

Next, a series of biosensors was developed in order to study the activities of three members (Rac1, Cdc42, and RhoA) of the Rho GTPase family of signaling molecules that are known to regulate the actin cytoskeleton. These biosensors were tested in combination with a photoactivatable Rac1 (PA-Rac1) construct to study the crosstalk between Rac1, Cdc42, and RhoA. Surprisingly, these experiments showed that the activities of Rac1, Cdc42, and RhoA all increase in response to acute photoactivation of Rac1. However, PA-Rac1 displayed an unexpected subcellular localization that is inconsistent with that of wild-type or constitutively active Rac1, making these crosstalk measurements difficult to interpret. Therefore, an optimized photoactivatable Rac1 construct was developed that localizes primarily to the plasma membrane.

As an alternative to photoactivation, a new and more generally applicable method of controlling Rho GTPase activity, based on chemically induced dimerization (CID), was developed. In this approach, a small molecule (referred to as a "dimerizer") binds simultaneously to two distinct protein modules to form a heterodimeric protein complex. Because neither of the protein modules described here are endogenous to mammalian cells, this approach represents a novel bioorthogonal CID system that can be used to control protein function in cells. The C-terminal sequence from K-Ras was fused to one of these modules to ensure that it would localize to the plasma membrane. A constitutively active mutant of Rac1 lacking a prenylation site was fused to the other protein module and was observed largely in the cytosol. When dimerizer was added to cells expressing these two proteins, rapid recruitment of the constitutively active Rac1 mutant to the plasma membrane was observed. This recruitment, was accompanied by the formation of actin-based protrusions at the cell periphery that are typically observed upon activation of Rac1. And, similar experiments with constitutively active Cdc42 and RhoA mutants produced changes in the actin cytoskeleton and in cell morphology that are consistent with activation of these signaling molecules.

The tools described here can be used to study actin dynamics and its regulation by Rho GTPase signaling networks.

TABLE OF CONTENTS

LIST OF PUBLICATIONS

Results and methodologies presented in this thesis have contributed to the following peer-reviewed publications:

- Milroy L, Rizzo S, **Calderon A**, Ellinger B, Erdmann S, Mondry J, Verveer P, Bastiaens P, Waldmann H, Dehmelt, Arndt H (2012) Selective Chemical Imaging of Static Actin in Live Cells, *Journal of the American Chemical Society*, 134 (20): 8480–8486
- Liu P*, **Calderon A***, Konstantinidis G*, Hou J*, Chen X, Li F, Banerjee S, Hoffmann J, Theiss C, Dehmelt L, Wu Y (2014) A Bioorthogonal Small-molecule Switch System for Controlling Protein Function in Cells, *Angewandte Chemie International Edition* (submitted)
- Rizzo S, Milroy L, **Calderon A**, Bieker V, Schulz I, Tran T, Ellinger B, Sievers S, Waldmann H, Arndt H, Dehmelt L (2014) Identification of a Gain-of-function phenotype induced by a Natural Product-Inspired Compound (manuscript in preparation)
- Grässl M, Koch J, **Calderon A**, Schulze N, Mazel T, Banerjee S, Dehmelt L, Nalbant P (2014) RhoA dependent FHOD1 activity fluctuations control cellular morphodynamics (manuscript in preparation)
  *equal contribution

Part of the work described here was presented at the following conference:

- The 5th Conference on Systems Biology of Mammalian Cells, Berlin, Germany (2014)

LIST OF FIGURES

ABBREVIATIONS

% (v/v)	percent by volume
°C	degrees Celsius
A_{450}	absorbance at 450 nm
A_{650}	absorbance at 650 nm
aa	amino acid(s)
ADP	adenosine diphosphate
Arp	actin-related protein
ATP	adenosine triphosphate
AU	arbitrary units
BFP	blue fluorescent protein
bp	base pairs(s)
BSA	bovine serum albumin
C-term.	carboxy terminus (C-terminus)
Cdc42	cell division cycle 42
CFP	cyan fluorescent protein
CID	chemically induced dimerization
CMV	Cytomegalovirus
DAPI	4',6-Diamidino-2-Phenylindole
ddH_2O	dideoionized water
delCMV	a truncated CMV promoter
DMEM	Dulbecco's modified Eagle's medium
DMSO	dimethylsulfoxide
DNA	deoxyribonucleic acid
DNIC2	dynein intermediate chain 2
dNTPs	deoxyribonucleoside triphosphates
E. coli	Escherichia coli
e.g.	exempli gratia
eDHFR	*E. coli* dihydrofolate reductase
EDTA	ethylenediaminetetraacetic acid
EGFP	enhanced green fluorescent protein
ER	endoplasmatic reticulum
et al.	and others
FBS	foetal bovine serum
Fig.	figure
FKBP	FK506-binding protein
FKBP'	F36V mutant of FKBP
fM	femtomolar
For	forward
FRET	Förster resonance energy transfer
FTase	farnesyltransferase
g	gram(s)
GAP	GTPase activating protein
GBD	GTPase binding domain
GDP	guanosine diphosphate
GEF	guanine nucleotide exchange factor
GFP	green fluorescent protein
GGTase	geranylgeranyltranserase
GTP	guanosine triphosphate
hrs	hours
i.e.	id est
ICMT	isoprenylcysteine-*O*-carboxyl methyltransferase
jasp.	jasplakinolide
KRC	K-Ras C-terminus
L	Liter(s)
LB	Luria-Bertani
LOV2	Light Oxygen Voltage 2
MEM	minimum essential medium
min	minute(s)
mL	milliliter(s)
mm	millimeter(s)
mM	millimolar
n	number of cells
N-term.	amino terminus (N-terminus)
N2a	Neuro-2a
NA	numerical aperture
NES	nuclear export sequence
ng	nanogram(s)
nM	nanomolar
nm	nanometer(s)

NMR	nuclear magnetic resonance
PA	photoactivatable/photoactivation
PA-Cdc42	photoactivatable Cdc42
PA-Rac1	photoactivatable Rac1
PAK, PAK1	p21/Cdc42/Rac1-activated kinase
PBS	phosphate buffered saline
PCR	polymerase chain reaction
PDB	protein data bank
pg	picogram(s)
pH	potentium hydrogenii
pM	picomolar
Rac1	ras-related C3 botulinum toxin substrate 1
RBD	rhotekin GTPase binding domain (aa 8-89)
RCE1	Ras-converting enzyme 1
Rev	reverse
RFP	red fluorescent protein
rGBD	rhotekin GTPase binding domain (aa 7-89)
RhoA	ras homolog family member A
RhoGDI	Rho Guanine nucleotide Dissociation Inhibitor
RNA	ribonucleic acid
rpm	revolutions per minute
RT	room temperature
sec	second(s)
SV40	simian virus 40
T	temperature
TAE	tris-acetatic acid-EDTA
TIR	total internal reflection
TIRF	total internal reflection fluorescence
Tris	tris[hydroxymethyl]aminomethane
U	unit(s) of enzyme
UV	ultraviolet
V	volt(s)
WASP	Wiskott-Aldrich Syndrome Protein
wt. %	% by weight
YFP	yellow fluorescent protein
SLF'	synthetic ligand of FKBP'
TMP	trimethoprim
ΔSV40	a truncated SV40 promoter
μg	microgram(s)
μL	microliter(s)
μM	micromolar
θ	incident angle

Amino acids

Ala	alanine
Arg	arginine
Gln	glutamine
Glu	glutamic acid
Lys	lysine
Thr	threonine
E	glutamic acid
F	phenylalanine
H	histidine
L	leucine
Q	glutamine
N	asparagine
V	valine
W	tryptophan

1. INTRODUCTION

The human body is composed of a variety of cell types that perform a multitude of tasks. Frequently, the shape of a particular cell plays an important role in its function. For example, in the small intestine, epithelial cells form protrusions called microvilli near the apical surface that help them to absorb nutrients from digested food (Fig. 1.1A)[1]. Similarly, hair cells within the inner ear also form protrusions called stereocilia that allow these cells to sense forces (Fig. 1.1B)[1]. Improper stereocilia formation can lead to deafness[1]. In the brain, neurons can also form protrusions called growth cones that help to guide these cells as they grow and develop (Fig. 1.1C)[2]. In all of these examples, actin filaments play a central role in determining the shapes of the protrusions.

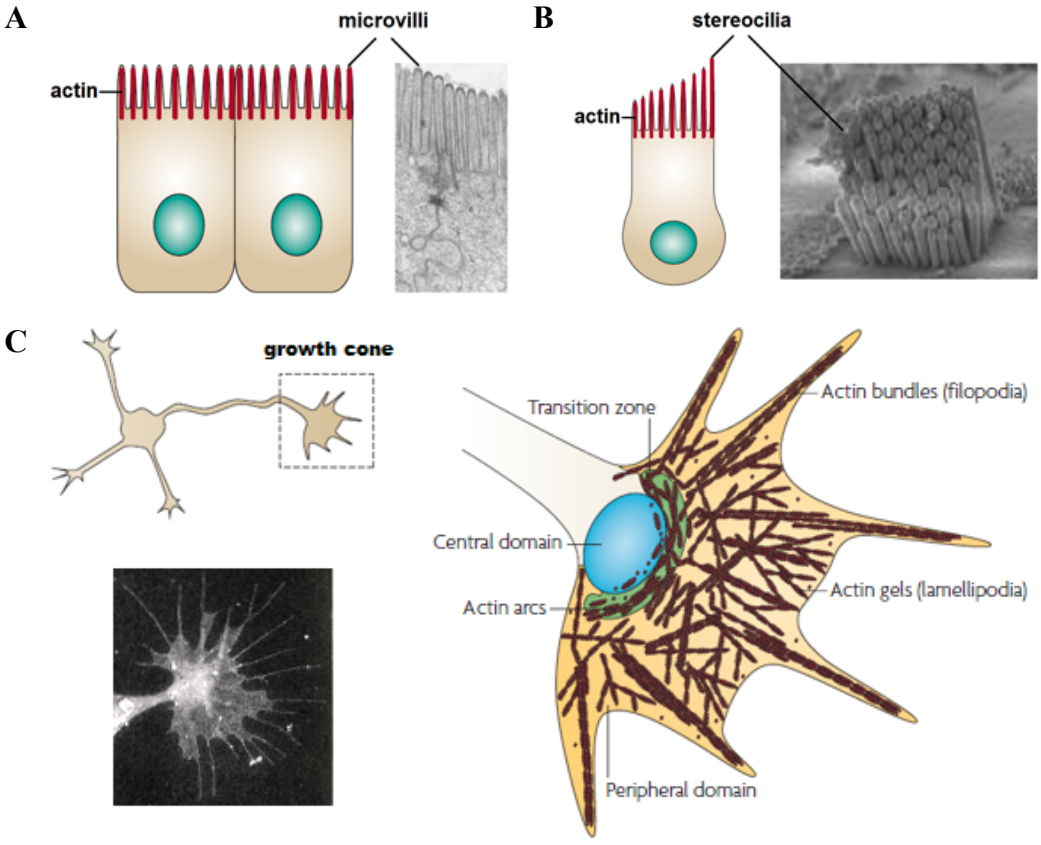

Figure 1.1: Examples of Cells that Form Actin-based Protrusions. (**A**) Epithelial cells in the small intestine form actin-based protrusions called microvilli. These protrusions increase the surface areas of the cells, making it easier for them to absorb nutrients from digested food as it passes by. (**B**) Hair cells within the inner ear also form protrusions called stereocilia that allow these cells to sense forces. If these stereocilia are improperly formed, this can lead to deafness. (**C**) Neurons can also form protrusions called growth cones that help to guide these cells as they migrate. (These figures were taken from references 1-3).

In mammalian cells, the complex system of actin filaments, intermediate filaments, and microtubules is referred to as the cytoskeleton.

1.1 Actin Can Rapidly Convert Between Monomeric and Filamentous Forms

Actin filaments are often referred to as polymers. However, this term can be misleading. Unlike other biological polymers (such as DNA, RNA, proteins, and polysaccharides) the subunits of actin filaments are not covalently bonded to each other. Rather, these subunits are held together by weak noncovalent forces. This makes it possible for actin subunits to rapidly convert between monomeric and filamentous forms (Fig. 1.2). The assembly and disassembly of actin filaments is also regulated by many accessory proteins.

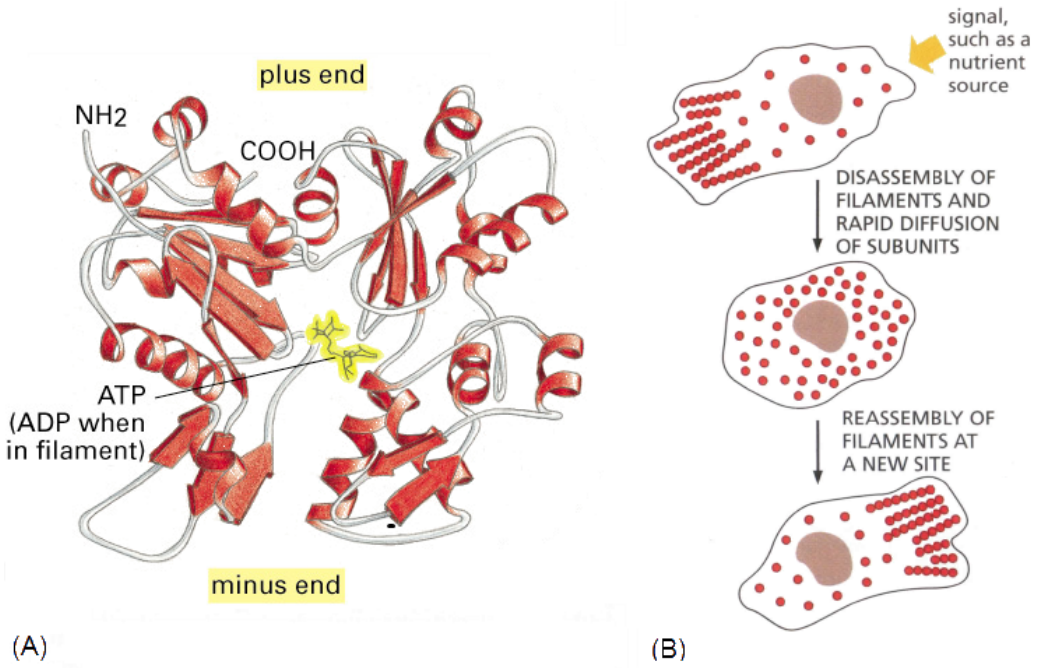

Figure 1.2: Actin Can Rapidly Convert Between Monomeric and Filamentous Forms. (A) Structure of an actin subunit. **(B)**. Cartoon demonstrating how a cell can respond to an external stimulus by rapidly rearranging its actin cytoskeleton. (These figures were taken from reference 3).

Nucleators are a group of accessory proteins that promote filament assembly. As their name suggests, nucleators function by assembling actin subunits into a "nucleus". Formation of an actin nucleus is the rate limiting step in filament assembly and proceeds slowly in the absence of a nucleator[3]. Once a nucleus of actin filaments has formed, additional actin subunits can quickly bind to and elongate this structure.

Formins are a group of actin nucleators that promote the formation of linear filaments. These enzymes form dimers that can accommodate two actin subunits. When both of these binding sites are filled, the formin dimer undergoes a conformational change that allows it to release one of the actin subunits and expose a new binding site while it remains anchored to the other subunit. A repetitive cycle of actin subunit binding followed by structural rearrangement of the formin dimer leads to nucleation and elongation of an actin filament (Fig. 1.3a). These actin filaments can be crosslinked by other accessory proteins to produce actin bundles such as those observed in microvilli, stereocilia, and filopodia (Fig. 1.1).

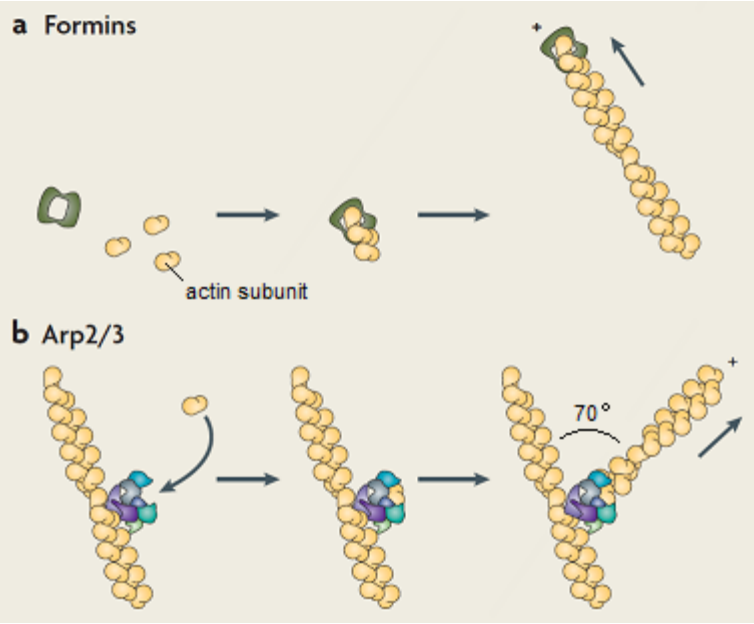

Figure 1.3: Actin Nucleation by Formins and the Arp2/3 Complex. (**a**) Formins promote the formation of linear filaments. These enzymes form dimers that can accommodate two actin subunits. When both of these binding sites are filled, the formin dimer undergoes a conformational change that allows it to release one of the actin subunits and expose a new binding site while it remains anchored to the other subunit. A repetitive cycle of actin subunit binding followed by structural rearrangement of the formin dimer leads to nucleation and elongation of an actin filament. (**b**) The Arp2/3 complex promotes the formation of a branched network of actin filaments. The Arp2/3 complex consists of seven proteins, including two Actin-Related Proteins (Arp2 and Arp3) that share significant sequence and structural similarities with actin. The Arp2/3 complex can bind to the side of an existing actin filament and promote the formation of a new filament that forms a 70° angle to the original filament. (These figures were taken from reference 2).

Actin filaments can also be nucleated by a group of proteins known as the Arp2/3 complex. This complex consists of seven proteins, including two Actin-Related Proteins (Arp2 and Arp3) that share significant sequence and structural similarities with actin. The Arp2/3 complex can bind to the side of an existing actin filament and promote the formation of a new filament that forms a 70° angle to the original filament (Fig. 1.3b). This branched network of actin filaments can lead to large-scale structures such as lamellipodia (Fig. 1.1C).

The Arp2/3 complex is highly concentrated at the leading edge of keratocyte cells (Fig. 1.4A, top)[4], where it can promote the assembly of actin filaments (Fig. 1.4A, middle) that push against the plasma membrane at the leading edge of these motile cells. This protrusive force appears to operate in conjunction with other forces to move cells in a particular direction (Fig. 1.4B). For example, while actin assembly stretches the cell at the leading edge, motor proteins (e.g., myosin II) provide a constrictive force at the trailing edge to prevent tension from building up within the cell. Similarly, loss of contacts between the cell and the substratum at the trailing edge is balanced by the formation of new contacts at the leading edge.

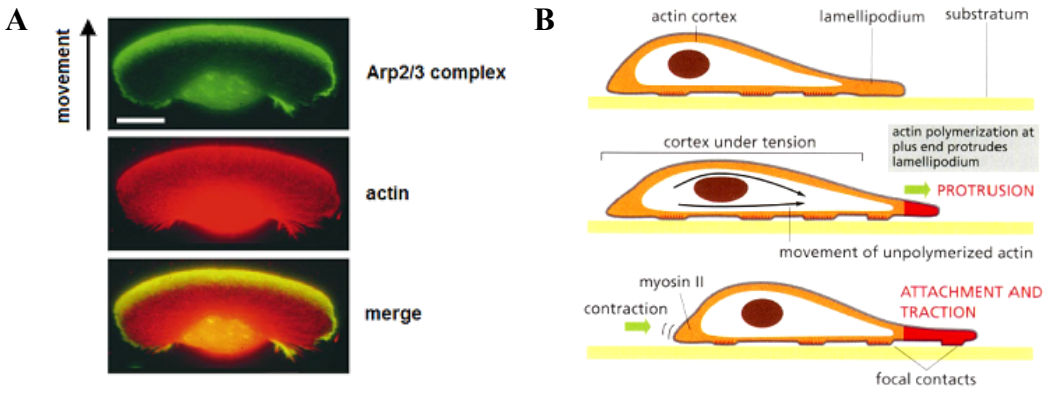

Figure 1.4: The Role of Actin Polymerization in Cell Motility. (**A**) A keratocyte was fixed, permeablized, and stained to show the localization of the Arp2/3 complex and actin within this motile cell. The Arp2/3 complex was stained using antibodies while actin was stained with a fluorescently-labeled phalloidin. (**B**) This image shows a model of the forces involved in cell motility. As newly formed actin filaments push against the plasma membrane at one end of the cell, motor proteins (e.g., myosin II) provide a constrictive force at the opposite end of the cell to prevent tension from building up within the cell. Similarly, loss of contacts between the cell and the substratum at the trailing edge is balanced by the formation of new contacts at the leading edge. (These figures were taken from references 3-4).

Interestingly, small molecules that disrupt actin dynamics have been isolated from various natural sources (Table 1.1)[3,5-8]. These natural products can be used as tools to study the actin cytoskeleton. For example, fluorescently labeled phalloidins are frequently used to stain actin filaments in fixed and permeabilized cells (Fig. 1.4A, middle). Alternatively, these natural products can be used as templates to develop new tools to study actin dynamics[5,8].

Table 1.1: Small Molecules That Interfere With Actin Dynamics

Small Molecule	Interferes With Actin Dynamics by ...	Isolated From
phalloidin	binding to and stabilizing filaments	*Amanita phalloides* (death cap mushroom)
jasplakinolide	binding to and stabilizing filaments	*Jaspis splendans* (sea sponge)
chondramide C	binding to and stabilizing filaments	*Chondromyces crocatus* (myxobacterium)
cytochalasin	capping filament plus ends	*Helminthosporium dematioideum* (mold)
swinholide	severing filaments	*Theonella swinhoei* (sea sponge)
latrunculin	binding to subunits and preventing their assembly into filaments	*Latrunculia magnifica* (sea sponge)

1.2 Rho GTPases are Signaling Molecules that Influence Actin Dynamics

Extensive studies have shown that Rho GTPases play a central role in coordinating actin dynamics in cells. For example, Hall et al. showed that selective activation of RhoA, Rac1, or Cdc42 led to distinct rearrangements in the actin cytoskeletons of serum-starved Swiss 3T3 cells (Fig. 1.5)[9]. Activation of RhoA led to the formation of stress fibers (Fig. 1.5B) while activation of Rac1 or Cdc42 led to the formation of actin-based protrusions at the cell periphery; lamellopodia were formed in response to activation of Rac1 (Fig. 1.5C) and filopodia were formed in response to activation of Cdc42 (Fig. 1.5D).

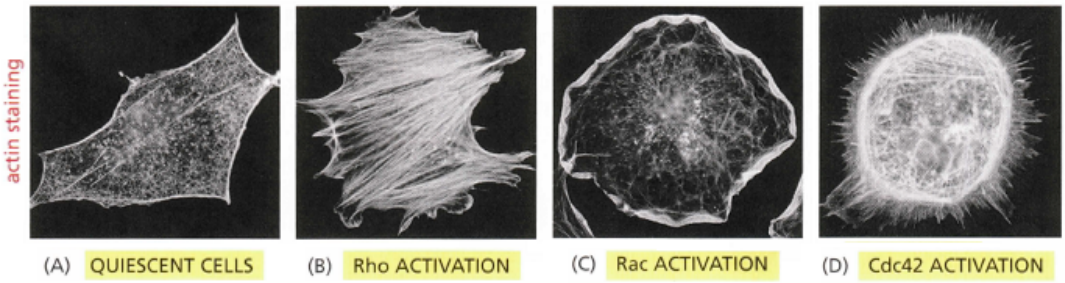

Figure 1.5: Selective Activation of RhoA, Rac1, or Cdc42 Produces Distinct Rearrangements in the Actin Cytoskeletons of Serum-Starved Swiss 3T3 Cells. For each of the conditions, actin was stained with rhodamine-labeled phalloidin. (**A**) A control serum-starved cell. (**B**) A cell that produced stress fibers in response to activation of RhoA. (**C**) A cell that produced a lamellipodium in response to activation of Rac1. (**D**) A cell that produced filopodia in response to activation of Cdc42. (These figures were taken from reference 3).

However, although these three Rho GTPases can induce rearrangements in the actin cytoskeleton, they do not directly interact with actin molecules. Rather, Rho GTPases are signaling molecules that indirectly influence actin dynamics.

1.3 Rho GTPase Signaling Activity is Regulated by GAPs and GEFs

Rho GTPases can exist in an "on" (GTP-bound) state and an "off" (GDP-bound) state. Therefore, these proteins are frequently referred to as molecular switches. When a Rho GTPase is in the "on" (GTP-bound) state, it can propagate a signal by interacting with downstream effector proteins. These effector proteins can, in turn, activate other proteins, such as actin nucleators that promote the formation of new filaments (Fig. 1.6)[10].

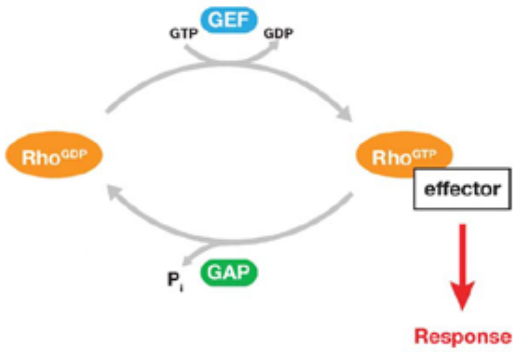

Figure 1.6: Rho GTPases Can Exist in an "on" (GTP-bound) State and an "off" (GDP-bound) State. When a Rho GTPase is in the "on" (GTP-bound) state, it can propagate a signal by interacting with downstream effector proteins. These effector proteins can, in turn, activate other proteins, such as actin nucleators that promote the formation of new filaments. Conversion between the "on" and "off" states is regulated by GAP and GEF enzymes. (This figure was taken from reference 10).

As their name suggests, Rho GTPases are enzymes that can bind and hydrolyze GTP. However, the intrinsic rates of hydrolysis for Rho GTPases are very slow. Hydrolysis of GTP proceeds much faster in the presence of a GTPase Activating Protein (GAP). A mechanism to explain how GAPs accelerate GTP hydrolysis has been proposed, based on crystallographic studies. In each of these studies, a Rho GTPase / GAP complex was crystallized in the presence of GDP and an inorganic fluoride salt in order to trap the complex in a structure that mimics the transition state of the hydrolysis reaction (Fig. 1.7A)[11-13]. These structures suggest that a water molecule is positioned near the γ-phosphate of GTP in the transition state (Fig. 1.7B)[11-13]. A new bond between this water molecule and the γ-phosphate appears to be forming as a P-O bond between the β- and γ-phosphate groups of GTP appears to be breaking (Fig. 1.7B)[13]. Interactions between the carbonyl group on the catalytic Arg85 residue in the GAP ($R85_{GAP}$, also referred to as the "arginine finger") and the side chain of Gln63 (Q63) in RhoA (or Gln61 in Cdc42) help to orient the water molecule within the transition state (Fig. 1.7A)[11-12]. These interactions stabilize the transition state and accelerate hydrolysis.

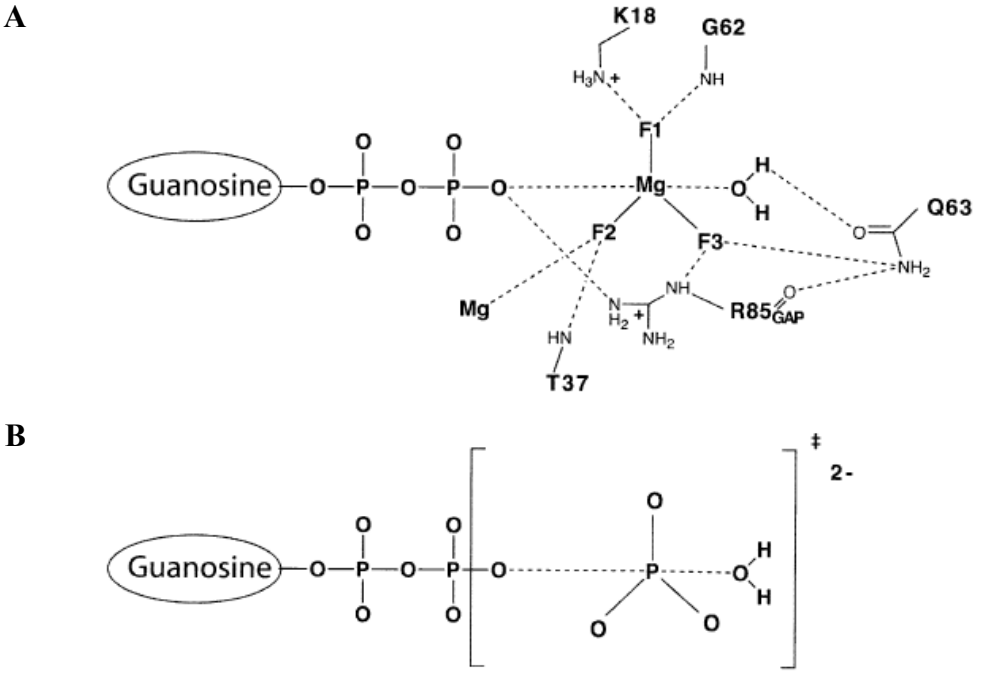

Figure 1.7: GTPase Activating Proteins (GAPs) Stabilize the Transition State of the GTP Hydrolysis Reaction. A RhoA / GAP complex was crystallized in the presence of GDP and an inorganic fluoride salt[13]. Within this structure, the nucleotide, inorganic salt, and a water molecule are arranged in a pattern that corresponds to the transition state of the GTP hydrolysis reaction. (**A**) Cartoon showing specific interactions that were observed between amino acids in RhoA, the catalytic Arg85 (R85) amino acid in the GAP ($R85_{GAP}$), and atoms in the GDP molecule, the inorganic salt, and the water molecule. (**B**) Cartoon showing a proposed transition state of the GTP hydrolysis reaction that is based on the experimentally determined structural data depicted in (A). (These figures were taken from reference 13).

While GAPs promote the conversion of Rho GTPases from the active (GTP-bound) state to the inactive (GDP-bound) state, another group of enzymes, called Guanine nucleotide Exchange Factors (GEFs), promote the reverse process. When a GEF binds to an inactive Rho GTPase, it causes conformational changes within the Rho GTPase that displace the bound GDP molecule and a Mg^{+2} cofactor (Fig. 1.8)[14]. In particular, a hydrophobic methyl group from Ala61 in RhoA displaces the Mg^{+2} cofactor, which lowers the affinity of RhoA for GDP[15]. Furthermore, in the RhoA/GEF structure, a hydrogen bond between the Lys18 side chain in RhoA and GDP is lost, which further lowers the affinity of RhoA for GDP[15]. Once the nucleotide is displaced, the Rho GTPase can bind to a new nucleotide. Although it is possible that the Rho GTPase will bind to another GDP molecule, it is more probable that it will bind to a GTP molecule, since this form of the nucleotide is present at a higher concentration within the cell[14].

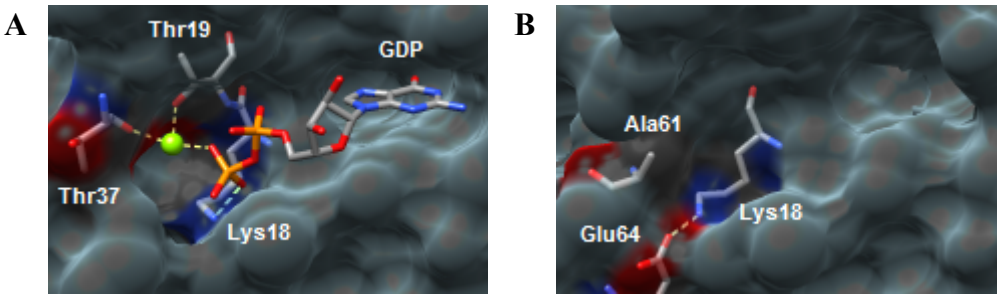

Figure 1.8: GEFs Bind to Rho GTPases and Promote Dissociation of the Bound Nucleotide. (**A**) This experimentally determined structure shows that RhoA can bind to GDP and a Mg^{+2} cofactor in the absence of a GEF. (PDB code 1FTN[16]). (**B**) When RhoA binds to Dbs, it undergoes conformational changes that displace both GDP and the Mg^{+2} cofactor (PDB code 1LB1[17]). In particular, a hydrophobic methyl group from Ala61 in RhoA displaces the Mg^{+2} cofactor, which lowers the affinity of RhoA for GDP[15]. Furthermore, in this structure, a hydrogen bond between the Lys18 side chain in RhoA and GDP is lost, which further lowers the affinity of RhoA for GDP[15].

It is important to note that, although the majority of the structural data for GEFs and GAPs have been acquired using soluble forms of these proteins, most of these enzymes have at least one domain that can interact with membranes[18]. And, this interaction can play an important role in the activity of the enzyme. For example, a Rac1-specific GAP called β2-chimaerin adopts a compact inactive conformation in the cytosol (Fig. 1.9A) and an elongated active structure when it is bound to acidic phospholipid membranes (Fig. 1.9B)[19]. The C1 domain of β2-chimaerin binds to the lipid second messenger molecule diacylglycerol or to phorbol esters and plays an important role in translocating the GAP to membranes.

Like β2-chimaerin, many GEFs and GAPs are capable of adopting an inactive autoinhibited conformation and most of these enzymes contain at least one domain that can interact with membranes[18]. Therefore, it is possible that membrane binding may promote structural rearrangement of these enzymes in a manner similar to that observed with β2-chimaerin. However, future studies are needed to determine whether this is the case.

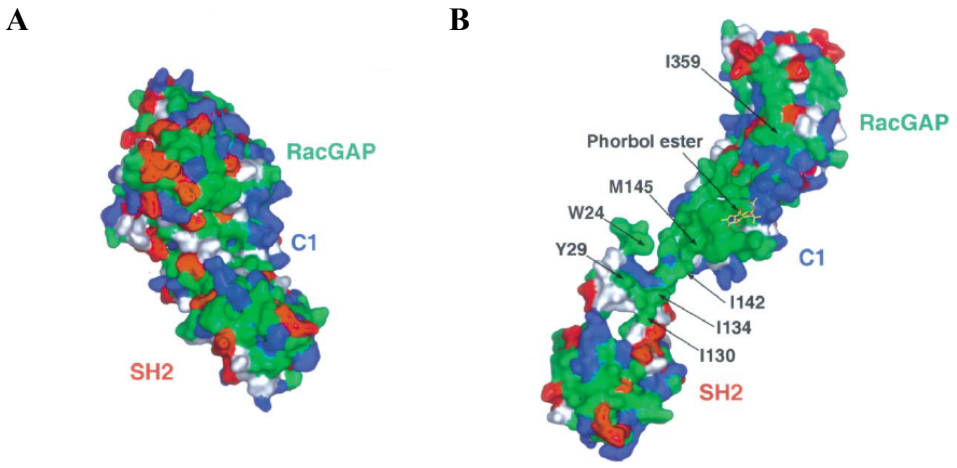

Figure 1.9: Membrane Binding Causes Conformational Changes in β2-Chimaerin. (**A**) Structure of the inactive cytosolic conformation of β2-chimaerin determined by x-ray crystallography. (**B**) Model of the active membrane-bound structure of β2-chimaerin. In these figures, green represents hydrophobic residues, blue represents basic residues, red represents acidic residues, and white represents uncharged polar residues. (These figures were taken from reference 19).

1.4 Prenylation Plays an Important Role in Rho GTPase Localization

Like most GEFs and GAPs, Rho GTPases can also interact with membranes. In the latter case, this is due to a series of post-translational modifications that add a hydrophobic lipid tail to the C-termini of the proteins.

Most of the human Rho GTPases have a series of four amino acids known as a "CAAX" box at their C-termini. In this abbreviation, C represents a cysteine amino acid, A represents an aliphatic amino acid, and X represents the terminal amino acid. The CAAX sequence of amino acids is recognized by specific enzymes within the cell (Fig. 1.10a)[20-21]. First, the cysteine is prenylated by either a geranylgeranyltranserase (GGTase) or a farnesyltransferase (FTase) in the cytosol. Although two of the ~20 mammalian Rho GTPases are able to undergo either farnesylation or geranylgeranylation[20],

approximately half of the remaining members of this family of proteins appear to be exclusively farnesylated while the other half appear to be exclusively geranylgeranylated[20]. The three most commonly studied Rho GTPases (Rac1, Cdc42, and RhoA) are geranylgeranylated[20]. The prenylation of a Rho GTPase appears to play an important role in its localization and its signaling activities[22-23].

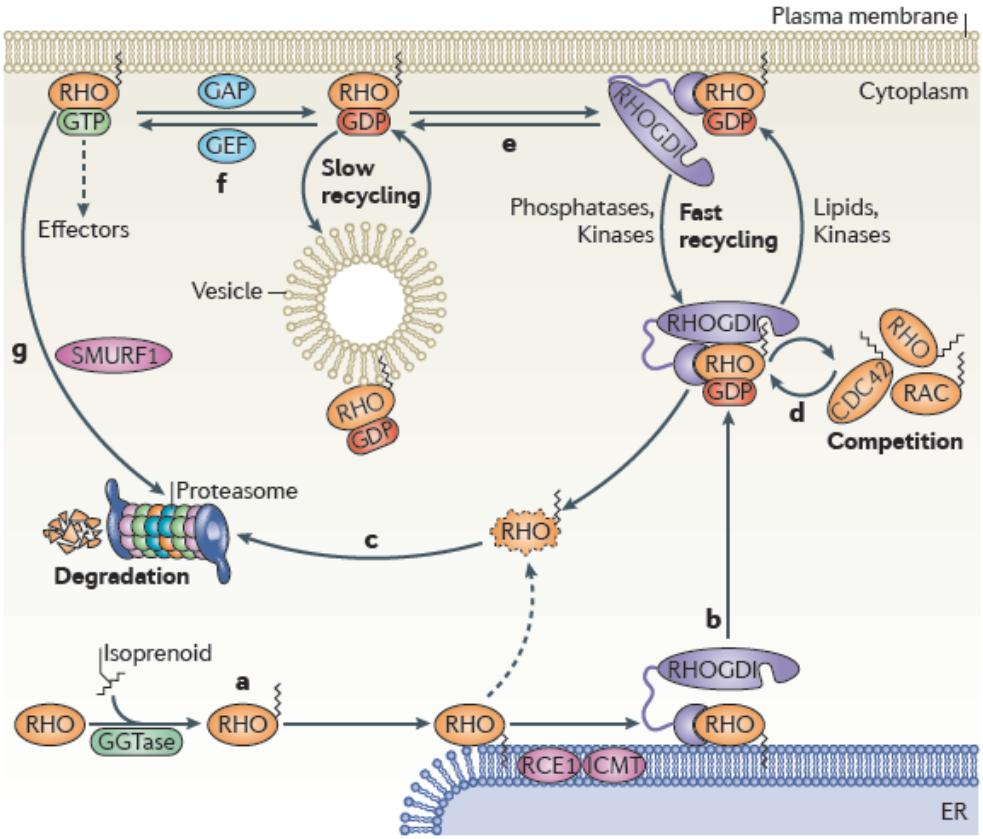

Figure 1.10: Prenylation Plays an Important Role in Rho GTPase Localization. (**a**) The CAAX sequence of amino acids is recognized by specific enzymes within the cell. First, the cysteine is prenylated. Then, the Rho GTPase is localized to the endoplasmic reticulum (ER), where it is further modified by two more enzymes. Ras-converting enzyme 1 (RCE1) removes the last 3 amino acids (-AAX) and isoprenylcysteine-*O*-carboxyl methyltransferase (ICMT) methylates the cysteine residue. (**b**) The Rho GTPase can be extracted from the ER by a Rho Guanine nucleotide Dissociation Inhibitor (RhoGDI). (**c**) In the absence of a RhoGDI, Rho GTPases can misfold and be targeted for degradation. (**d**) The concentration of RhoGDI within the cell is finite. Therefore, multiple Rho GTPases must compete with each other for the opportunity to bind to and be stabilized by a RhoGDI molecule. (**e**) Studies have shown that Rho GTPase mutants that are incapable of binding to RhoGDIs can still make their way to the plasma membrane. These mutants may be transported to the plasma membrane by vesicles. Similarly, vesicles may also be used to transport Rho GTPases away from the plasma membrane. (**f**) Conversion between the "on" and "off" states of the Rho GTPase is regulated by GAP and GEF enzymes. (**g**) Rho GTPases can be ubiquitinated by enzymes such as SMURF1 in order to target them for degradation. (This figure was taken from reference 21).

After a Rho GTPase is prenylated, it localizes to the endoplasmic reticulum (ER), where it is further modified by two additional enzymes. Ras-converting enzyme 1 (RCE1) removes the last 3 amino acids (-AAX) and isoprenylcysteine-*O*-carboxyl methyltransferase (ICMT) methylates the cysteine residue. At this point, the Rho GTPase can be extracted from the ER by a Rho Guanine nucleotide Dissociation Inhibitor (RhoGDI) (Fig. 1.10b). In fact, although the lipid tails of Rho GTPases can anchor them to membranes, the majority of Rho GTPases within a cell are bound to a RhoGDI in the cytosol[21].

There are three mammalian isoforms of RhoGDI that are referred to as RhoGDI1, RhoGDI2, and RhoGDI3 (or RhoGDIα, RhoGDIβ, and RhoGDIγ). However, only the RhoGDI1 isoform is ubiquitously expressed. Furthermore, Rho GTPases have a higher binding affinity for the RhoGDI1 isoform. Therefore, most studies have focused on this isoform.

As its name suggests, RhoGDI1 prevents dissociation of the nucleotide from the Rho GTPase. Similarly, RhoGDI1 prevents nucleotide exchange (e.g., from GDP to GTP). Moreover, RhoGDI1 inhibits hydrolysis of GTP by the Rho GTPase both in the absence and in the presence of a GAP[25]. Therefore, when a Rho GTPase is bound to RhoGDI1, it is effectively "locked" into one activity state. A helix-loop-helix motif referred to as the "regulatory arm" near the N-terminus of RhoGDI1 appears to be instrumental in inhibiting both nucleotide dissociation and GTP hydrolysis (Fig. 1.11).

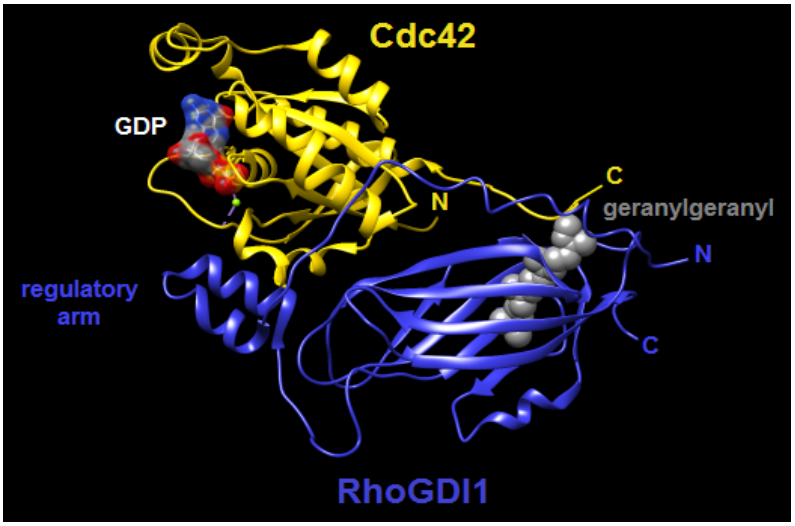

Figure 1.11: Structure of Cdc42 in Complex with RhoGDI1. Cdc42 is colored in gold and RhoGDI1 is colored in blue. A helix-loop-helix motif referred to as the "regulatory arm" near the N-terminus of RhoGDI1 appears to be instrumental in preventing nucleotide dissociation from Cdc42. The geranylgeranyl tail of Cdc42 inserts into a gap between two antiparallel β-sheets at the C-terminus of RhoGDI1. (PDB code 1DOA[24]).

When a Rho GTPase binds to RhoGDI1, its geranylgeranyl tail inserts into a gap between two antiparallel β-sheets at the C-terminus of RhoGDI1 (Fig. 1.11). By shielding this hydrophobic tail from the aqueous environment of the cytosol, RhoGDI1 helps to prevent misfolding and degradation of the RhoGTPase (Fig. 1.10c). However, the concentration of RhoGDI1 within the cell is finite. Therefore, multiple Rho GTPases must compete with each other for the opportunity to bind to and be stabilized by a RhoGDI1 molecule (Fig. 1.10d). This relatively recent finding suggests that overexpression of a Rho GTPase would disrupt this balance by introducing another pool of molecules that would compete with endogenous Rho GTPases for binding to RhoGDI1.

RhoGDI1 also helps to rapidly shuttle Rho GTPases between the cytosol and membranes (Fig. 1.10e). This shuttling provides an important mechanism to regulate Rho GTPase activity. In particular, by sequestering Rho GTPases away from membranes, RhoGDI1 prevents Rho GTPases from engaging in signaling activities. However, RhoGDI1 can also quickly release a Rho GTPase so that it can bind to a membrane, become activated by a GEF, and interact with downstream effectors (Fig. 1.10f). The fast recycling of Rho GTPases between the cytosol and membranes may be regulated by kinases, that phosphorylate the Rho GTPase or RhoGDI1 and alter the binding affinity between these two molecules, and phosphatases that remove these phosphate groups[21].

Although RhoGDI1 clearly plays an important role in shuttling Rho GTPases between the cytosol and membranes, the cell may employ other methods to shuttle Rho GTPases to membranes. This would explain certain experimental results that showed that Rho GTPase mutants that are incapable of binding to RhoGDIs can still make their way to the plasma membrane. These mutants may bind to vesicles and slowly be transported to the plasma membrane (Fig. 1.10e). Similarly, vesicles can be used to transport Rho GTPases away from the plasma membrane.

1.5 Crosstalk Between Rho GTPases

Many studies have shown that one RhoGTPase can influence the behavior of other Rho GTPases. This crosstalk can be the result of direct competition between the Rho GTPases for limited resources (e.g., RhoGDI1) or it can be indirect and involve activation or inactivation of an intermediate protein.

In general, Rho GTPases can influence each other at three different levels. First, the activity of one Rho GTPase (R1) can influence the activity of another Rho GTPase (R2). For example, when one Rho GTPase (R1) is activated, it could inactivate a GEF that is capable of activating a second Rho GTPase (R2) (Fig. 1.12a1). Alternatively, R1 could activate a GAP that is capable of inactivating R2 (Fig 1.12a2). Second, R1 can directly influence the stability of R2 by displacing it from RhoGDI (Fig 1.12a3). Finally, R1 can interfere with the downstream signaling of R2 by inactivating a shared effector protein (Fig. 1.12a4) or a shared target protein (Fig. 1.12a5). At each of these levels, the crosstalk may involve inhibition of R2 signaling by R1 (Fig. 1.12a). Alternatively, activation of R1 could also lead to enhancement of R2 signaling (Fig. 1.12b).

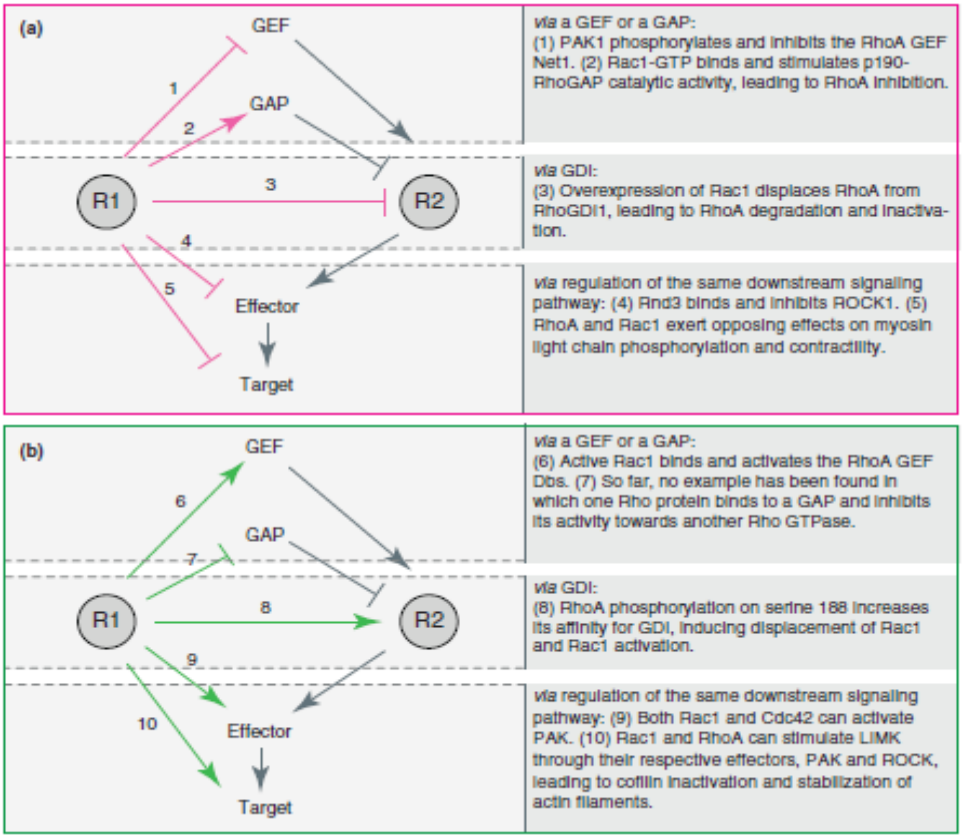

Figure 1.12: Possible Modes of Crosstalk Between Two Rho GTPases (R1 and R2). (**A**) Examples where activation of R1 leads to inhibition of R2 signaling. (**B**) Examples where activation of R1 leads to enhancement of R2 signaling. (These figures were taken from reference 26).

Many studies have highlighted the roles of various GEFs, GAPs, and downstream effectors in regulating the crosstalk between Rac1 and RhoA (Fig. 1.13)[26]. However, the extent to which each of these proteins regulates this crosstalk may vary, depending on the situation. Furthermore, for each of these situations, the factors that determine which of these proteins are predominantly responsible for regulating this crosstalk remain poorly understood.

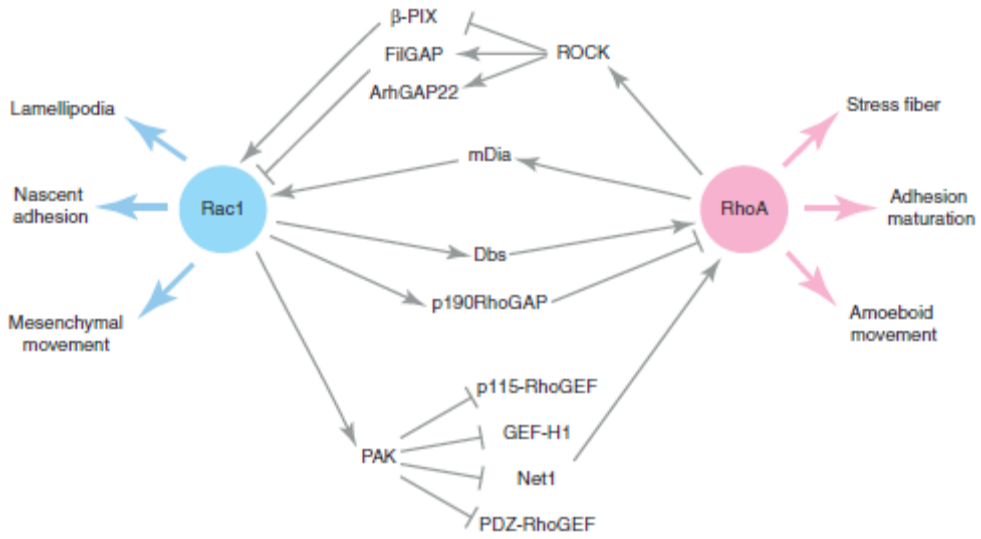

Figure 1.13: Proposed Modes of Crosstalk Between Rac1 and RhoA. (This figure was taken from reference 26).

Therefore, to directly measure the crosstalk between Rho GTPases, it would be best to develop a method to selectively perturb the activity of one Rho GTPase and to simultaneously measure how the activities of other Rho GTPases within the same cell respond to this perturbation (Fig. 1.14). Ideally, these experiments would be repeated multiple times to account for cell-to-cell variability.

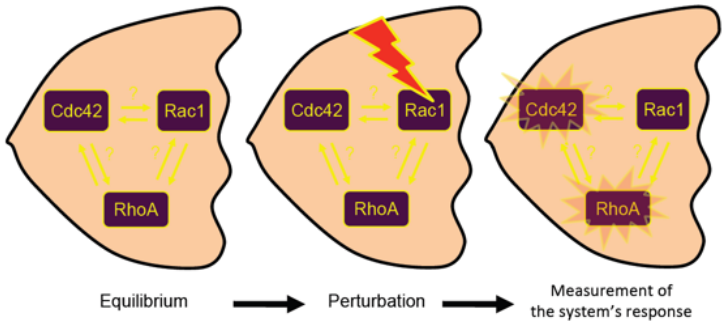

Figure 1.14: Acute Perturbation and Activity Measurement of Rho GTPases in Living Cells.

1.6 TIRF Microscopy

Although actin can be found throughout the cell, it is predominantly concentrated beneath the plasma membrane in a region known as the actin cortex (Fig. 1.4B). Furthermore, regulation of actin dynamics by Rho GTPases often involves events that occur at or near the plasma membrane (Fig. 1.10). Therefore, experimental techniques that focus on this region of the cell can be used to study actin dynamics and its regulation by Rho GTPase signaling networks. One such technique is that of Total Internal Reflection Fluorescence (TIRF) microscopy.

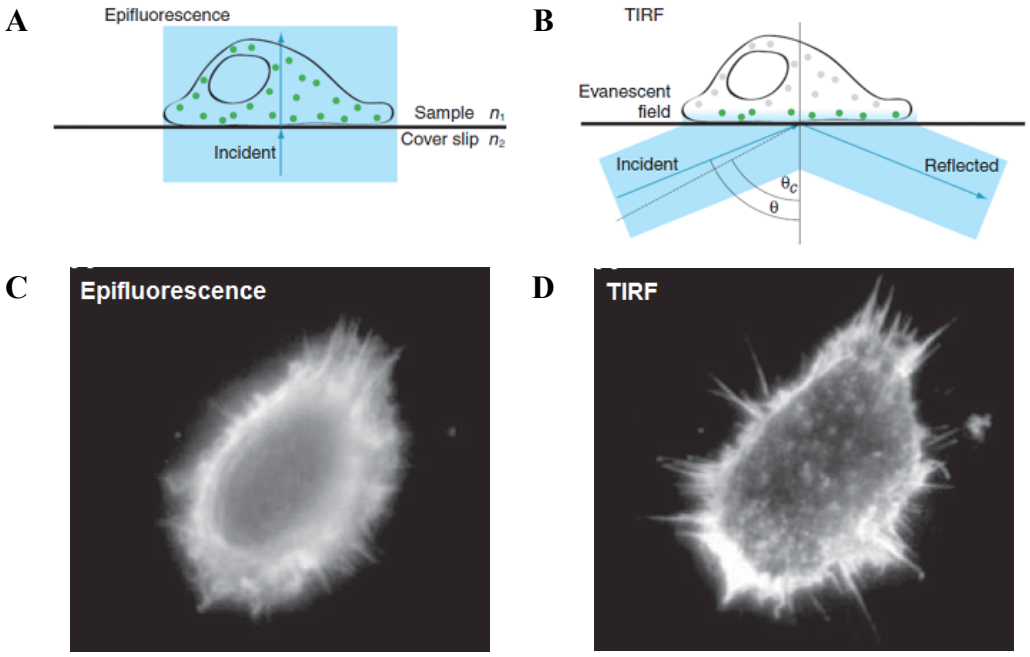

Figure 1.15: Total Internal Reflection Fluorescence (TIRF) Microscopy. (**A**) In epifluorescence microscopy, incident light excites fluorophores throughout a cell (green circles). (**B**) In TIRF microscopy, incident light is directed toward the interface formed by a glass cover slip and an aqueous sample such that the light undergoes total internal reflection (TIR)[27,28]. This produces an evanescent field that penetrates into the aqueous sample. However, the intensity of the evanescent field decreases exponentially with increasing distance from the glass/aqueous interface. Therefore, the evanescent field can be used to selectively excite fluorophores in a cell that are close (50-300 nm) to the cover slip (green circles)[27,28]. (**C**) A HeLa cell was fixed and the actin cytoskeleton of this cell was stained with a fluorescently labeled phalloidin. This image was acquired using traditional epifluorescence microscopy. (**D**) A TIRF image of the cell shown in (C). (These figures were taken from references 27 and 28).

In TIRF microscopy, incident light is directed toward the interface formed by a glass cover slip and an aqueous sample such that the light undergoes total internal reflection (TIR) (Fig. 1.15B)[27,28]. This produces an evanescent field that penetrates into the aqueous sample. However, the intensity of the evanescent field decreases exponentially with increasing distance from the glass/aqueous interface.

Therefore, the evanescent field can be used to selectively excite fluorophores in a cell that are close (50-300 nm) to the coverslip[28].

TIRF microscopy can reveal details about the actin cytoskeleton that are obscured in traditional epifluorescence microscopy (Fig. 1.5C and Fig. 1.5D).

2. MATERIALS AND METHODS

2.1 Materials

2.1.1 Equipment and Consumables

Table 2.1: Equipment and Consumables Used for Mammalian Cell Culture

Description		Catalogue Number / Model	Company
Biosafety Cabinet		NU-440-500E	Nuaire
Cell Culture Vessels	100 mm Dish	353003	BD Falcon
	4-well Lab-Tek™ I	155383	Thermo Scientific Nunc
	4-well Lab-Tek™ II	155382	
	8-well Lab-Tek™ I	155411	
	384-well Plate	781092	greiner bio-one
Centrifuge		5810	eppendorf
Centrifuge Rotor (swing-bucket)		A-4-81	eppendorf
Cryo 1°C Freezing Container		5100-0001	Thermo Scientific
Cryogenic Tube		366656	Thermo Scientific Nunc
Freezer (-152ºC)		MDF-1156	Sanyo
Hemacytometer		Z359629	Sigma-Aldrich
Incubator		HERAcell® 150	Thermo Scientific Heraeus
Microscope		Eclipse TE200	Nikon
Lid (for 384-well Plates)		3099	Costar
Vacuum Filter (500 mL)		83.1823	Sarstedt
Water Bath		3047	Köttermann

Table 2.2: Equipment and Consumables Used for Neurite Outgrowth Screens

Description	Catalogue Number / Model	Company
96-well Plate (sterile)	249946	Nalge Nunc
96-well Plate (sterile)	655 180	greiner bio-one
Disposable Reagent Reservoir, 100 mL (sterile)	HT71.1	Carl Roth GmbH & Co. KG
Microplate Sealing Film	60941-112	VWR
Multichannel Pipette, 850 µL	Impact 2	Matrix
Multichannel Pipette, 125 µL	Impact 2	Matrix
Pipette Tips, 1250 µL (sterile)	8042	Thermo Scientific Matrix
Pipette Tips, 1250 µL (non-sterile)	8046	Thermo Scientific Matrix
Pipette Tips, 125 µL (sterile)	7442	Thermo Scientific Matrix
Plate Reader	infinite M1000	Tecan
Plate Washer	ELx405 Select CW	BioTek

Table 2.3: Equipment and Consumables Used for Cloning

Description	Catalogue Number / Model	Company
Biological Shaker	New Brunswick™ I26	eppendorf
Burner	gasprofi 1 SCS micro	WLD-TEC GmbH
Butane	C206 super	Campingaz
Butane Gas Regulator	Typ 794	Cavagna Group
Camera (for gels)	EX1	Samsung
Centrifuge	5417R	eppendorf
	5424	eppendorf
Centrifuge Rotor (fixed angle)	F-45-30-11	eppendorf
	FA-45-24-11	eppendorf
Cuvette (disposable)	67.785	Sarstedt
Electrophoresis Chamber	Mini-Plus-Unit HU10	biostep GmbH
Heating Block	DB-3D	Techne
	252-2	PMC
	QBD4	Grant
Incubator	100-800	Memmert
PCR Thermocycler	mastercycler ep 5341	eppendorf
UV lamp	NU-6 KL	Benda
UV Transilluminator (for gels)	UST-20M-8E	biostep GmbH

Table 2.4: Equipment and Consumables Used for Live and Fixed Cell Imaging

Description	Catalogue Number / Model / Details	Company
Immersion Oil Type-F	IMMOIL-F30CC	Olympus
Lens Cleaning Tissue	2105 841	Whatman
Microscope (widefield)	Olympus IX81, Hamamatsu ORCA ER C4742-80-12AG Camera, Objective = UPlans APO 10x NA, Filters: BFP/GFP/RFP, Software: Scanˆ R	Olympus
Microscope (widefield/TIRF)	Olympus IX81F-3, Hamamatsu Image EM CCD-C9100-13 Camera, Objective = PlanApo 60xOil TIRF (NA = 1.45), Lasers: 405 nm, 445 nm, 488 nm/514 nm, 561 nm, Filters: BFP/GFP/RFP, YFP/CFP, TBFP/TGFP/TRFP, TBFP/TCFP/TYFP/TRFP, Software: Cellˆ R	Olympus
Microscope (confocol)	LSM 510 Meta Objective = 40x water	Zeiss

Table 2.5: General Equipment and Consumables

Description		Catalogue Number / Model	Company
Aspiration Tool (for Vacuum Pump)		VACUBOY	Integra Biosciences
Balance		PA114	Ohaus Corp.
Filter (for Vacuum Pump)		158015	Integra Biosciences
Freezer (-80ºC)		New Brunswick™ U725-86	eppendorf
Gloves (Nitrile)		1280M	Meditrade
Kimwipes		34155	Kimberly Clark
Parafilm® M		H666.1	Carl Roth GmbH & Co. KG
pH Meter		SevenEasy™	Mettler-Toledo GmbH
pH Sensor		InLab® Expert Pro	Mettler-Toledo GmbH
Pipette Controller		accu-jet® pro	Brand
Pipette (1 mL, 100 µL, 10 µL)		Research	eppendorf
Pipette Tips	1 mL	70.762	Sarstedt
	200 µL	70.760.002	Sarstedt
	20 µL	70.1114	Sarstedt
Serological Pipettes	25 mL	612-1245	VWR
	10 mL	612-1248	VWR
	5 mL	612-1270	VWR
Tubes	50 mL	62.547.254	Sarstedt
	15 mL	62.554.502	Sarstedt
	2 mL	72.695	Sarstedt
	1.5 mL	72.704	Sarstedt
	0.5 mL	72.706	Sarstedt
	0.2 mL	72.737.002	Sarstedt
Vacuum Pump		VACUSAFE comfort	Integra Biosciences
Vortex Mixer		G560E	Scientific Industries

2.1.2 Reagents

Table 2.6: Reagents Used for Mammalian Cell Culture

Description	Catalogue Number	Company
DMSO	A994.1	Carl Roth GmbH & Co. KG
FBS	3302-P100309	PAN-Biotech GmbH
L-glutamine	P04-80100	PAN-Biotech GmbH
MEM Eagle (for transfection)	P04-00507	PAN-Biotech GmbH
MEM Eagle (for N2a cells)	P04-08050	PAN-Biotech GmbH
Penicillin/Streptomycin	P06-07100	PAN-Biotech GmbH
Sodium Pyruvate	P04-43100	PAN-Biotech GmbH
Trypsin-EDTA	P10-023100SP	PAN-Biotech GmbH
X-tremeGENE 9	06 365 787 001	Roche Diagnostics GmbH

Table 2.7: Reagents Used for Neurite Outgrowth Screens

Description	Catalogue Number	Company
Chondramide C	-	Max Planck Institute of Molecular Physiology – Dortmund
DMSO	A994.1	Carl Roth GmbH & Co. KG
Jasplakinolide	sc-202191A	Santa Cruz Biotechnology
Taxol	T7402	Sigma-Aldrich
WST-1 Cell Proliferation Reagent	11 644 807 001 or 05 015 944 001	Roche Diagnostics GmbH

Table 2.8: Reagents and Kits Used for Cloning

Description		Catalogue Number	Company
Acetic Acid		45726	Sigma-Aldrich
Agarose		T846.2 or T846.3	Carl Roth GmbH & Co. KG
Antibiotics	Ampicillin	K029.1	Carl Roth GmbH & Co. KG
	Kanamycin	T832.1	Carl Roth GmbH & Co. KG
Big Dye Terminator Mix		06112-1	Max Planck Institute of Molecular Physiology – Dortmund
Buffers	NEBuffer 1	B7001S	New England Biolabs
	NEBuffer 2	B7002S	New England Biolabs
	NEBuffer 3.1	B7203S	New England Biolabs
	NEBuffer 4	B7004S	New England Biolabs
	NEBuffer EcoRI	B0101S	New England Biolabs
	Phusion® HF Reaction Buffer (5x)	B0519S	Ambion
	T4 DNA Ligase Buffer (10x) with 10 mM ATP	B0202S	New England Biolabs
	TAE Buffer (1x)	40 mM Tris-acetate (pH 8.0), 1 mM EDTA	-
Culture Tubes (sterile)		T406-2A	Simport
dNTP Mix (10 mM each)		-	Max Planck Institute of Molecular Physiology – Dortmund
$Na_2EDTA \bullet 2H_2O$		E5134	Sigma-Aldrich
Enzymes	AgeI	R0552S	New England Biolabs
	Antarctic Phosphatase	M0289L or M0289S	New England Biolabs
	AseI	R0526S	New England Biolabs
	BamHI	R0136S	New England Biolabs
	BsrGI	R0575S	New England Biolabs
	EcoRI	R0101L	New England Biolabs
	MfeI	R0589S	New England Biolabs
	MluI	R0198S	New England Biolabs
	NgoMIV	R0564S	New England Biolabs
	NheI-HF	R3131S	New England Biolabs

Table 2.8: Reagents and Kits Used for Cloning (continued)

Description		Catalogue Number	Company
Enzymes	Phusion® DNA Polymerase	F530S or F530L	Finnzymes
	T4 DNA Ligase	M0202S	New England Biolabs
	XbaI	R0145L	New England Biolabs
	XhoI	R0146S	New England Biolabs
Ethidium Bromide (0.025%)		HP47.1	Carl Roth GmbH & Co.KG
Gene Ruler™ 1kb DNA Ladder		SM0311 or SM0314	Fermentas
Glycerol		G2025	Sigma-Aldrich
Isopropanol		6752.1	Carl Roth GmbH & Co.KG
Kits	Plasmid Purification Kit	27106	Qiagen
	Gel Extraction Kit	28706	Qiagen
	PCR Purification Kit	28106	Qiagen
Loading Dye (5x, Gel Pilot)		239901	Qiagen
LB (Luria-Bertani) medium		-	Max Planck Institute of Molecular Physiology – Dortmund
LB agar plates		-	Max Planck Institute of Molecular Physiology – Dortmund
Scalpel		5518091	B. Braun
Sodium Acetate		0258	J.T. Baker
Sodium Chloride (NaCl)		71376	Sigma-Aldrich
Sodium Hydroxide		71689	Sigma-Aldrich
Trizma Base		T6066	Sigma-Aldrich

Table 2.9: Reagents Used for Live and Fixed Cell Imaging

Description		Catalogue Number	Company
Alexa Fluor® 488 Phalloidin		A12379	Invitrogen
Antibodies	Anti-α-Tubulin Antibody Produced in Mouse	T5168	Sigma-Aldrich
	Alexa Fluor® 568 Goat Anti-Mouse IgG (H+L) Antibody	A-11004	Invitrogen
BSA		11930.03	SERVA Electrophoresis GmbH
DMEM (for imaging media)		P04-01163	PAN-Biotech GmbH
FBS		3302-P100309	PAN-Biotech GmbH
Formaldehyde Solution (37 wt. % in H_2O)		533998	Sigma-Aldrich
Hoechst 33342		B2261	Sigma-Aldrich
Potassium Phosphate Monobasic		P9791	Sigma-Aldrich
Potassium Choride		P9541	Sigma-Aldrich
Sodium Chloride		71376	Sigma-Aldrich
Sodium Phosphate Dibasic Heptahydrate		X987.1	Carl Roth GmbH & Co.KG
Triton® X-100		37240	SERVA Electrophoresis GmbH

Table 2.10: General Reagents

Description		Catalogue Number	Company
Absolute Ethanol		20821.265	AnalaR Normapur
Buffer Solution	pH = 4.01	340-1000040240	Mercateo
	pH = 7.00	340-1000072640	Mercateo
	pH = 10.00	340-1000103840	Mercateo
Hydrochloric acid (HCl)		H1758	Sigma-Aldrich
Nuclease-free Water		AM9932	New England Biolabs

2.1.3 Cell Lines

Table 2.11: Cell Lines Used for Mammalian Cell Culture

Cell Line	Species	Cell Type	Morphology	DSMZ Nr.
Neuro-2a	Mouse	Embryo	Neuroblast	ACC 148

Table 2.12: Cell Lines Used for Cloning

Cell Line	Genotype	Company
Top 10	F^- mcrA Δ(mrr-hsdRMS-mcrBC) Φ80lacZΔ M15 Δ lacX74 recA1 araD139 Δ(ara-leu) 7697 galU galK rpsL (Str^R) endA1 nupG Λ-	Invitrogen
XL10Gold	TetR Δ(mcrA)183 Δ(mcrCB-hsdSMR mrr) 173 endA1 supE44 thi-1 recA1 gyrA96 relA1 lac Hte [F' proAB lacIqZ Δ M15 Tn10(TetR) Amy CamR]	Stratagene

2.1.4 Primers and Plasmids

Table 2.13: Primers Used for Cloning (ordered from Sigma-Aldrich)

Name	Type[a]	Sequence[b]
PAK1_forward	For	5'-TAGGCTGGGAATTCCAAGAAAGAGAAAGAGCGGCC-3'
PAK1_reverse	Rev	5'-TCGGCGCGGGATCCCTATGACTTATCTGTAAAGC3'
RBD_forward	For	5'-CTCAGATCGAATTCCCTGGAGGACCTCAATATGC-3'
RBD_reverse	Rev	5'-CCCGCGGTGGATCCCTAGCCTGTCTTCTCCAGC -3'
rGBD_forward	For	5'-CTCAGATCGAATTCCATCCTGGAGGACCTC-3'
rGBD_reverse	Rev	5'-CTCACTATGGATCCCTAGCCTGTCTTCTCCAGC-3'
p67phox aa1-203 forward	For	5'-CAAGCTTCGAATTCCATGTCCCTGGTGGAGGCC-3'
p67phox aa1-203 reverse	Rev	5'-GATCCGGTGGATCCCTACGTCGCCTTGCCTAGG-3'
WASP-GBD_forward	For	5'-GCCCCCTTGAATTCCGACATCCAGAACCCTGAC-3'
WASP-GBD_reverse	Rev	5'-GATGCATGGGATCC**CTA**TCGAGATGGCGGTGG-3'
BsrGI-Start-Rac	For	5'-GGAGGTGTACAAGTCC**ATG**CAGGCCATCAAGTGTG-3'
Rac-XhoI	Rev	5'-AATTCTACTCGAGGCAGGGATTTTCTCTTCCTCTTC-3'
XbaI-Start-Rac	For	5'-GGAGGAGTCTAGATCC**ATG**CAGGCCATCAAGTGTG-3'
Rac-Stop-MfeI	Rev	5'-AATTCTCAATTGAG**TTA**GGATTTTCTCTTCCTCTTC-3'
NheI-Start-Rac	For	5'-GGAGGAGCTAGCATCC**ATG**CAGGCCATCAAGTGTG-3'
Rac-NgoMIV	Rev	5'-AATTCTGCCGGCAGCAGGGATTTTCTCTTCCTCTTC-3'
NheI-linker	For	5'-TCAGTTGCTAGCCTCAAGCTTCGAATTCTG-3'
NES-BsrGI[c]	Rev	5'-AGAGTCAGCTCGAGATATCTTGTACGAGTCCAG-3'
XbaI-Cdc42	For	5'-CTGTACTCTAGATCC**ATG**CAGACAATTAAGTG-3'
Cdc42-S-Stop	Rev	5'-TCGAGTCAATTGAG**TTA**GGACCTGCGGCTCTTC-3'
FW-XbaI-RhoA-Q63L	For	5'-GGAATTCTAGATCC**ATG**GCTGCCATCCGGAAG-3'
RhoA-S-Stop2	Rev	5'-CGAGTCAATTGAG**TTA**GGAACCAGATTTTTTC-3'
Xho-linker	For	5'-AGCTGTCTCGAGGTTCTGGAAGTGGATCC-3'
MfeI-linker	Rev	5'-GTGGTGCAATTGATCCTCGGGGTCTTC-3'

a) For = forward, Rev = reverse
b) Restriction sites are highlighted in brown; extra bases added to ensure insertion into the proper reading frame are highlighted in yellow; start and stop codons are shown in **bold**
c) Although the name of this primer implies that it has a BsrGI restriction site, it actually has a XhoI restriction site.

Table 2.14: Primers Used for Sequencing (ordered from Sigma-Aldrich)

Name	Type	Sequence
Seqmyctag	Forward	5'-GAACAAAAACTCATCTCAGAAGAGGATCTG-3'
T7forward	Forward	5'-TAATACGACTCACTATAGGG-3'
mCherryC	Forward	5'-GCCCGGCGCCTACAACGTC-3'
N1-delCMV	Forward	5'-TCCGCGTTACATAACTTACGG-3'
SeqUb_833_s	Forward	5'-CACATGAAGCAGCACGACTT-3'
pEGFP-C11266s	Forward	5'-CATGGTCCTGCTGGAGTTCGTG-3'
pEGFP-N1500F	Forward	5'-TAACAACTCCGCCCCATTGAC-3'
delCMVseq	Forward	5'-ATATATGGAGTTCCGCGTTA-3'
pEGFP-C11266F	Forward	5'-CATGGTCCTGCTGGAGTTCGTG-3'
LOV-F	Forward	5'-AGAGAGAGGGAGTCATGCTGAT-3'
hRac1-F	Forward	5'-AACCAATGCATTTCCTGGAG-3'
pBABE_3_rev	Reverse	5'-ACCCTAACTGACACACATTCC-3'
Terminator reverse	Reverse	5'-AGTGGCACCTTCCAGGGTCAA-3'
NotI-EGFP-concat	Reverse	5'-CTAGAGTCGCGGCCGCTTTACTTG-3'
mCherryN	Reverse	5'-GCCCTCGCCCTCGATCTCG-3'
pEGFP-N1771R	Reverse	5'-GACACGCTGAACTTGTGGC-3'
pEGFP-N11548R	Reverse	5'-GTAACCATTATAAGCTGCAATAAAC-3'
GFPseq_141as	Reverse	5'-GAACTTCAGGGTCAGCTTGCCGT-3'
hRac1-R	Reverse	5'-GATACCACTTTGCACGGACA-3'

Table 2.15: Mammalian Expression Plasmids

Name	Description of the Expressed Protein	Source[Reference]
pmCherry-N1	mCherry	Max Planck Institute of Molecular Physiology (Dortmund)
delCMV-mCherry	mCherry	This thesis
pmCitrine-N1	mCitrine	Max Planck Institute of Molecular Physiology (Dortmund)
delCMV-mCitrine	mCitrine	This thesis
pmCherry-actin-UB	mCherry labeled actin	Melanie Gräßl/Verena Hannak (Technical University of Dortmund)
pmCherry-actin-delCMV	mCherry labeled actin	Verena Hannak (Technical University of Dortmund)
pΔSV40-PAK-GBD-mCherry (pAL197)	The GTPase binding domain (GBD) of PAK1 linked to mCherry	Christopher A. Voigt (University of California, San Fransicso)[29]
pΔSV40-mCherry-WASP-GBD (pAL198)	mCherry linked to the GTPase binding domain (GBD) of WASP	Christopher A. Voigt (University of California, San Fransicso)[29]
mCherry-Rhotekin(8-89)-mCherry-C1	The GTPase binding domain (GBD) of Rhotekin flanked by mCherry tags at the N-terminus and the C-terminus	Ryohei Yasuda (Duke University Medical Center, Durham, North Carolina)[30]
GFP-rGBD	GFP linked to the GTPase binding domain (GBD) of Rhotekin	William M. Bement (University of Wisconsin-Madison)[31]
pGEX-4T-I-p67^{phox}-aa1-203	The Rac1 GTPase binding domain (GBD) of p67^{phox}	Mohammad Reza Ahmadian (Heinrich–Heine-University, Düsseldorf)
delCMV-mCherry-p67^{phox} (aa1-203)	mCherry linked to the Rac1 GTPase binding domain (GBD) of p67^{phox}	Djamschid Solouk (Ruhr University, Bochum)[32]
delCMV-mCherry-PAK-GBD	mCherry linked to the Rac1/Cdc42 GTPase binding domain (GBD) of PAK1	This thesis
delCMV-mCherry-RBD	mCherry linked to the GTPase binding domain (GBD) of Rhotekin	This thesis
delCMV-mCherry-rGBD	mCherry linked to the GTPase binding domain (GBD) of Rhotekin	This thesis
delCMV-mCherry-WASP-GBD	mCherry linked to the Cdc42 GTPase binding domain (GBD) of WASP	This thesis
C1-EGFP-DNIC2-delCMV	EGFP linked to dynein intermediate chain 2 (DNIC2)	Anja Biesemann (Ruhr University, Bochum)[33]
delCMV-EGFP-tubulin	EGFP linked to tubulin	Julia Arens (Technical University of Dortmund)[34]
delCMV-EGFP-p67^{phox} (aa1-203)	EGFP linked to the Rac1 GTPase binding domain (GBD) of p67^{phox}	This thesis

Table 2.15: Mammalian Expression Plasmids (continued)

Name	Description of the Expressed Protein	Source[Reference]
PA-Cdc42Q61L-Venus	A Venus labeled photoactivatable (PA) Cdc42	Klaus Hahn (University of North Carolina, Chapel Hill)[35]
PA-Cdc42Q61L-mCherry	An mCherry labeled photoactivatable (PA) Cdc42	Klaus Hahn (University of North Carolina, Chapel Hill)[35]
mCerulean-PA-Cdc42Q61L	An mCerulean labeled photoactivatable (PA) Cdc42	Johannes Koch (University of Duisburg-Essen)
PA-Rac1Q61L-Venus	A Venus labeled photoactivatable (PA) Rac1	Klaus Hahn (University of North Carolina, Chapel Hill)[35]
PA-Rac1Q61L-mCherry	An mCherry labeled photoactivatable (PA) Rac1	Klaus Hahn (University of North Carolina, Chapel Hill)[35]
mCerulean-PA-Rac1Q61L	An mCerulean labeled photoactivatable (PA) Rac1	Klaus Hahn (University of North Carolina, Chapel Hill)[35]
delCMV-mTurquoise2-NES-PA-Rac1Q61L	mTurquoise2 linked to a nuclear export sequence (NES) and a photoactivatable (PA) Rac1	This thesis
TagBFP-2×eDHFR-CAAX	TagBFP linked to 2 copies of *E. coli* dihydrofolate reductase (eDHFR) and the C-terminus of Kras (KRC)	Yao-Wen Wu (Chemical Genomics Centre of the Max Planck Society, Dortmund/Max-Planck-Institute of Molecular Physiology, Dortmund)
pEGFP-2×FKBP'	EGFP linked to 2 copies of the F36V mutant of FK506-binding protein (FKBP)	Yao-Wen Wu (Chemical Genomics Centre of the Max Planck Society, Dortmund/Max-Planck-Institute of Molecular Physiology, Dortmund)
Rac1Q61L	A constitutively active mutant of Rac1	Gary Bokoch (The Scripps Research Institute, CA)
pcDNA3-EGFP-Cdc42Q61L	An EGFP labeled constitutively active mutant of Cdc42	Gary Bokoch (The Scripps Research Institute, CA)
pcDNA3-EGFP-RhoA-Q63L	An EGFP labeled constitutively active mutant of RhoA	Gary Bokoch (The Scripps Research Institute, CA)
Rac1Q61LΔCAAX-EGFP-2×FKBP'	A constitutively active mutant of Rac1 linked to EGFP and 2 copies of the F36V mutant of FK506-binding protein (FKBP)	This thesis
EGFP-Rac1Q61LΔCAAX-2×FKBP'	EGFP linked to a constitutively active mutant of Rac1 and 2 copies of the F36V mutant of FK506-binding protein (FKBP)	This thesis
EGFP-2×FKBP'-Rac1Q61LΔCAAX	EGFP linked to 2 copies of the F36V mutant of FK506-binding protein (FKBP) and a constitutively active mutant of Rac1	This thesis

Table 2.15: Mammalian Expression Plasmids (continued)

Name	Description of the Expressed Protein	Source[Reference]
delCMV-EGFP-2×FKBP'-Rac1Q61LΔCAAX	EGFP linked to 2 copies of the F36V mutant of FK506-binding protein (FKBP) and a constitutively active mutant of Rac1	This thesis
pmTurquoise2-C1	mTurquoise2	Max Planck Institute of Molecular Physiology (Dortmund)
pmTurquoise2-NES	An mTurquoise2 labeled nuclear export sequence (NES)	Theodorus W.J. Gadella Jr (University of Amsterdam) and Antoine Royant (Institute of Structural Biology, Grenoble)[36]
mTurquoise2-NES-2×FKBP'	mTurquoise2 linked to a nuclear export sequence (NES) and 2 copies of the F36V mutant of FK506-binding protein (FKBP)	This thesis
delCMV-mTurquoise2-NES-2×FKBP'	mTurquoise2 linked to a nuclear export sequence (NES) and 2 copies of the F36V mutant of FK506-binding protein (FKBP)	This thesis
mTurquoise2-2×FKBP'-Rac1Q61LΔCAAX	mTurquoise2 linked to 2 copies of the F36V mutant of FK506-binding protein (FKBP) and a constitutively active mutant of Rac1	This thesis
delCMV-mTurquoise2-2×FKBP'-Rac1Q61LΔCAAX	mTurquoise2 linked to 2 copies of the F36V mutant of FK506-binding protein (FKBP) and a constitutively active mutant of Rac1	This thesis
mTurquoise2-NES-2×FKBP'-Rac1Q61LΔCAAX	mTurquoise2 linked to a nuclear export sequence (NES), 2 copies of the F36V mutant of FK506-binding protein (FKBP), and a constitutively active mutant of Rac1	This thesis
delCMV-mTurquoise2-NES-2×FKBP'-Rac1Q61LΔCAAX	mTurquoise2 linked to a nuclear export sequence (NES), 2 copies of the F36V mutant of FK506-binding protein (FKBP), and a constitutively active mutant of Rac1	This thesis
mTurquoise2-NES-2×FKBP'-Cdc42Q61LΔCAAX	mTurquoise2 linked to a nuclear export sequence (NES), 2 copies of the F36V mutant of FK506-binding protein (FKBP), and a constitutively active mutant of Cdc42	This thesis
delCMV-mTurquoise2-NES-2×FKBP'-Cdc42Q61LΔCAAX	mTurquoise2 linked to a nuclear export sequence (NES), 2 copies of the F36V mutant of FK506-binding protein (FKBP), and a constitutively active mutant of Cdc42	This thesis

Table 2.15: Mammalian Expression Plasmids (continued)

Name	Description of the Expressed Protein	Source[Reference]
mTurquoise2-NES-2×FKBP'-RhoAQ63LΔCAAX	mTurquoise2 linked to a nuclear export sequence (NES), 2 copies of the F36V mutant of FK506-binding protein (FKBP), and a constitutively active mutant of RhoA	This thesis
delCMV-mTurquoise2-NES-2×FKBP'-RhoAQ63LΔCAAX	mTurquoise2 linked to a nuclear export sequence (NES), 2 copies of the F36V mutant of FK506-binding protein (FKBP), and a constitutively active mutant of RhoA	This thesis

2.2 Methods

2.2.1 Mammalian Cell Culture and Transfection

All procedures involving direct handling of Neuro-2a (N2a) cells were performed in a biosafety cabinet (Nuaire). Some reagents (e.g., N2a medium, Trypsin-EDTA, etc.) were pre-warmed in a 37°C water bath (Köttermann). Other reagents (e.g., X-tremeGENE 9 transfection reagent) were used at room temperature (RT).

N2a cells were seeded onto a 100 mm culture dish (BD Falcon) containing 10 mL of warm N2a medium (Table 2.16). Then, the cells were incubated at 5% CO_2 and 37°C.

Table 2.16: Preparation of 500 mL of N2a Medium[a]

Component	Company	Volume (mL)
FBS	PAN-Biotech GmbH	50
Penicillin/Streptomycin	PAN-Biotech GmbH	5
L-glutamine	PAN-Biotech GmbH	5
Sodium Pyruvate	PAN-Biotech GmbH	5
MEM Eagle	PAN-Biotech GmbH	435

a) After the medium was prepared, it was passed through a sterile vacuum filter (Sarstedt)

Whenever the cells were deemed to be ~70-80% confluent (typically every 2-3 days), the cells were detached from the culture dish and ~400 – 600 µL of the re-suspended cells was seeded onto a new 100 mm culture dish (BD Falcon) containing 10 mL of warm N2a medium. Detachment was performed in three steps. In the first step, the cells were washed with 1 mL of warm Trypsin-EDTA (PAN-Biotech GmbH). In the second step, the cells were incubated with 2 mL of warm Trypsin-EDTA (PAN-Biotech GmbH) at 5% CO_2 and 37°C for ~6 minutes. Finally, 5 mL of warm N2a medium was added to the dish and the cells were re-suspended using a 10 mL serological pipette.

For long-term storage, re-suspended N2a cells from 5-10 dishes were combined and centrifuged at 1000 rpm and 4°C for 5 minutes. Then, the supernatant was discarded and the pellet was re-suspended in 5-10 mL of cold N2a medium containing 10% DMSO. The re-suspended cells were aliquoted into 1 mL cryotubes (Thermo Scientific Nunc) and transferred to a Cryo 1°C Freezing Container (Thermo Scientific). The Container was stored overnight at -80°C. Then, the cryotubes were transferred to a -152°C freezer (Sanyo).

For microscopy experiments, re-suspended N2a cells were seeded onto an appropriate cell culture vessel (e.g., a 4-well Lab-Tek™ I, a 4-well Lab-Tek™ II, an 8-well Lab-Tek™ I, or a 384-well Plate).

For certain microscopy experiments, N2a cells were transfected with one or more mammalian expression plasmids (Table 2.15). Transfection of N2a cells was performed with the X-tremeGENE 9 transfection reagent (Roche). First, 3 µL of transfection reagent was diluted with 100 µL of MEM Eagle (PAN-Biotech). Then, the diluted transfection reagent was added to the plasmid DNA to a final ratio of 1 µg of DNA/3 µL of transfection reagent. While the DNA/transfection reagent solution incubated at RT for ~30 minutes, fresh, warm N2a medium was added to the cells. Then, the DNA/transfection reagent solution was added to the cells.

2.2.2 Neurite Outgrowth Screens and Proliferation Assays

For neurite outgrowth screens, 5 µL of warm N2a medium was added to each well of a 384-well plate (greiner bio-one). Then, the plate was centrifuged at 1000 rpm for 1 minute. Re-suspended N2a cells were diluted with warm N2a medium to a final density of 37,500 cells/mL. And, 80 µL of the diluted cells was added to each well of the 384-well plate (~3000 cells/well). The cells were incubated overnight at 5% CO_2 and 37°C.

DMSO solutions of synthetic analogues and reference compounds were supplied by chemists at the Max Planck Institute of Molecular Physiology. These solutions were serially diluted with warm N2a medium containing taxol (Sigma-Aldrich) and the diluted solutions were added to the cells. Serially diluted DMSO solutions were used as controls. For each well containing a compound or DMSO, the final concentration of taxol was 1 µM. The compounds were initially tested at the following concentrations: 15.00 µM, 5.00 µM, 1.67 µM, 555.56 nM, 185.19 nM, 61.73 nM, 20.58 nM, 6.86 nM, 2.29 nM, 762.08 pM, 254.03 pM, and 84.68 pM. However, selected experiments were also performed at the following concentrations: 28.23 pM, 9.41 pM, 3.14 pM, 1.05 pM, 348.46 fM, 116.15 fM, 38.72 fM, 12.91 fM, 4.30 fM, 1.43 fM, 0.48 fM, and 0.16 fM. The cells were incubated in the presence of the compounds or DMSO for 2 hours at 5% CO_2 and 37°C. Each experiment was performed in triplicate. For reference, some wells contained cells without any compound or DMSO.

Then, the cells were fixed by replacing the N2a medium in each well of the plate with warm 4 % formaldehyde in 1x PBS (Table 2.17) and incubating the cells at 37°C for 20 minutes.

Table 2.17: Preparation of 1 L of 1x PBS

Component	Company	Quantity
Sodium Chloride (NaCl)	Sigma-Aldrich	8.00 g
Potassium Chloride (KCl)	Sigma-Aldrich	0.20 g
Potassium Phosphate Monobasic (KH_2PO_4)	Sigma-Aldrich	2.68 g
Sodium Phosphate Dibasic Heptahydrate ($Na_2HPO_4 \cdot 7H_2O$)	Sigma-Aldrich	0.24 g
Hydrochloric Acid (HCl)	Sigma-Aldrich	enough to adjust the pH to 7.4
ddH_2O	Milipore	enough to adjust the volume to 1L

The procedure described in Table 2.18 was used to stain the actin filaments, microtubules, and nuclei of the cells.

For the proliferation assays, re-suspended N2a cells were diluted with warm N2a medium to a final density of 10,000 cells/mL. And, 200 µL of the diluted cells was added to each well of a 96-well plate (Nalge Nunc). The cells were incubated overnight at 5% CO_2 and 37°C.

Table 2.18: Procedure Used to Stain the Fixed N2a cells

Step	Description	Solution	Temperature (°C)[a]	Duration
1.	Wash the cells 5 times	1x PBS containing 0.01% Triton® X-100	RT	-
2.	Permeabilization	1x PBS containing 0.25% Triton® X-100	RT	15 min.
3.	Wash the cells 5 times	1x PBS containing 0.001% Triton® X-100	RT	-
4.	Blocking	10% BSA in 1x PBS	37	30 min.
5.	Primary staining of microtubules	1:5000 dilution of anti-α-tubulin antibody (mouse) in 1% BSA/PBS	37	1 hour
6.	Wash the cells 5 times	1x PBS containing 0.001% Triton® X-100	RT	-
7.	Secondary staining of microtubules, staining of the nuclei, staining of actin	1:1000 dilution of Alexa-568 anti-mouse antibody, 1:1000 dilution of Hoechst stock solution, 1:1000 dilution of Alexa-488-phalloidin in 1% BSA/PBS to the rinsed media reservoir.	37	1 hour
8.	Wash the cells 5 times	1x PBS containing 0.001% Triton® X-100	RT	-

a) RT = room temperature

DMSO solutions of synthetic analogues were supplied by chemists at the Max Planck Institute of Molecular Physiology. Each of these solutions was serially diluted with DMSO to prepare a series of ten 100x stock solutions. Then, each of the 100x stock solutions was diluted to 1x with warm N2a medium and the diluted solutions were added to the cells. For each well containing a compound, the final concentration of DMSO was 1% (v/v). The compounds were tested at the following concentrations: 60.00 µM, 20.00 µM, 6.67 µM, 2.22 µM, 740.74 nM, 246.91 nM, 82.30 nM, 27.43 nM 9.14 nM, 3.05 nM . Each experiment was performed in quadruplicate.

The cells were incubated in the presence of the compounds for 3 days at 5% CO_2 and 37°C. Then, 10 µL of WST-1 Cell Proliferation Reagent (Roche) was added to each of the wells. And, the cells were incubated for 1.5-2 hours at 5% CO_2 and 37°C. Finally, for each well, the absorbance at 450 nm (A_{450}) and the absorbance at 650 nm (A_{650}) was measured using a plate reader (Tecan).

2.2.3 Cloning

In general, a new plasmid was constructed by combining two DNA fragments together (Fig. 2.1).

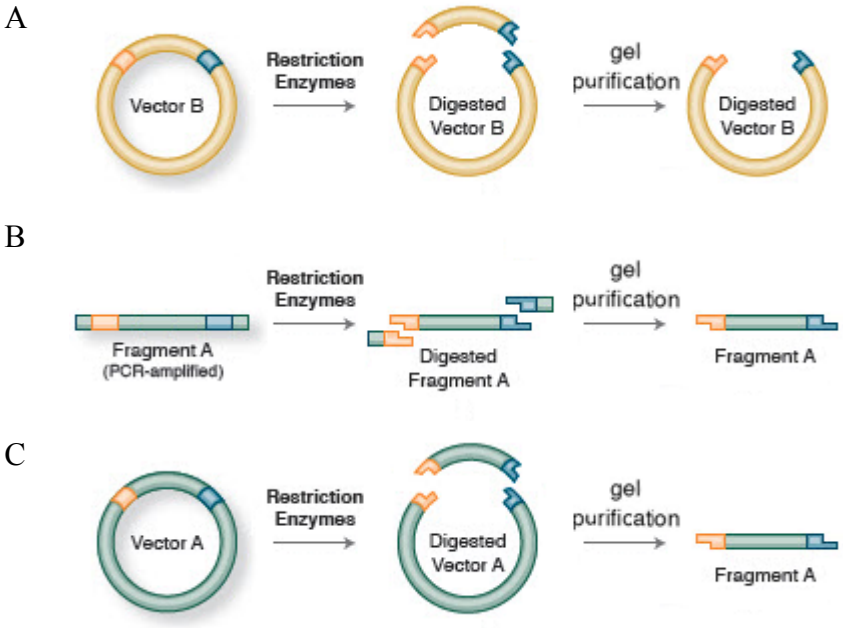

Figure 2.1: Isolation of DNA Fragments Used for Cloning. (A) Isolation of the "backbone" fragment. **(B)** Isolation of the "insert" fragment by PCR amplification. **(C)** Isolation of the "insert" fragment by digestion of an existing plasmid. (These figures were taken from the New England Biolabs website, https://www.neb.com).

One of the fragments, hereafter referred to as the "backbone" fragment, was generated by digesting an existing mammalian expression plasmid with two unique restriction enzymes (Fig. 2.1A). For each µg of plasmid, 5 U of each enzyme was used (Table 2.19). And, the digestions were incubated for 2 hours at 37°C. Whenever possible, the restriction enzymes were heat inactivated according the the manufacturer's instructions. Then, the 5' phosphates of the DNA were removed by addition of 1 µL of Antarctic Phosphatase (New England Biolabs) followed by 1 hour of incubation at 37°C. The Antarctic Phosphatase was also heat inactivated according the the manufacturer's instructions. Then, the DNA was purified by electrophoresis using a 1% agarose gel (Table 2.20) and the fragment of interest was isolated using a QIAquick Gel Extraction Kit (Qiagen).

Table 2.19: Example of Double Digestion Conditions

Component	Volume	Initial Concentration	Final Concentration
Nuclease-free Water	2.5 µL	-	-
Buffer = NEBuffer EcoRI	1.5 µL	10x	1x
DNA= delCMV-mCherry-actin	9.0 µL	0.442 µg/µL	0.265 µg/µL
BamHI	1.0 µL	20,000 U/mL	1333 U/mL
EcoRI	1.0 µL	20,000 U/mL	1333 U/mL

The second fragment, hereafter referred to as the "insert" fragment, was frequently prepared using polymerase chain reaction (PCR) amplification (Fig. 2.1B, Table 2.21, Table 2.22). A plasmid containing the sequence of interest was used as the template DNA. And, forward and reverse primers (Table 2.13) were designed so that the amplified DNA would contain the sequence of interest, flanked by restriction sites that matched those used to prepare the backbone fragment.

Table 2.20: Example of Gel Electrophoresis Conditions

Gel Volume	Gel Composition	Running Buffer	Loading Dye	Voltage	Duration
100 mL	1% agarose in 1x TAE with 4 drops of ethidium bromide	1x TAE	GelPilot (Qiagen)	~85V	1 hour

Table 2.21: Example of Polymerase Chain Reaction (PCR) Amplification Conditions

Component	Volume	Initial Concentration	Final Concentration
Nuclease-free Water	32.5 µL	-	-
Phusion® HF Reaction Buffer	10.0 µL	5x	1x
dNTPs	1.0 µL	10 mM each	200 µM each
Forward Primer	2.5 µL	10 µM	0.5 µM
Reverse Primer	2.5 µL	10 µM	0.5 µM
Template DNA	1.0 µL	10 ng/µL	200 pg/µL
Phusion® DNA Polymerase	0.5 µL	2 U/µL	0.02 U/µL

The following PCR program was used:

Table 2.22: PCR Program Used for Amplification

Repetitions	T (°C)	Time
1	98	3 min.
20	98	10 sec.
	68	30 sec.
	72	15 sec.[a]
1	72	8 min.
1	8	∞

a) For amplification of mTurquoise2-NES and PA-Rac1, 1 minute was used.

The amplified insert DNA was purified using a QIAquick PCR Purification Kit (Qiagen). Then, the insert DNA was digested with appropriate restriction enzymes (Table 2.19). The digested insert fragment was purified by electrophoresis using a 1% agarose gel (Table 2.20) and the fragment of interest was isolated using a QIAquick Gel Extraction Kit (Qiagen).

On rare occasions, it was not necessary to use PCR to isolate the insert fragment. In these instances, it was possible to directly digest an existing plasmid to produce an insert fragment that could be ligated with the backbone fragment (Fig. 2C).

Once the backbone and insert fragments were prepared and purified, they were ligated together. For each ligation, the backbone fragment and the insert fragment were combined in a roughly 1:1 molar ratio and 500 U of T4 DNA Ligase (New England Biolabs) was used (Table 2.23). Ligations were typically incubated overnight at 16°C.

Table 2.23: Example of Conditions Used for a Ligation

Component	Volume (µL)	Initial Concentration	Final Concentration
PCR Product (~619 bp)	14.6	32 ng/µL	11.68 ng/µL
Backbone Fragment (~4247 bp)	20.2	162 ng/µL	81.81 ng/µL
T4 Ligase Buffer (with ATP)	4.00	10x	1x
T4 Ligase	1.25	400,000 U/mL	12,500 U/mL

The following table summarizes the fragments that were ligated together to produce new mammalian expression plasmids:

Table 2.24: Summary of New Mammalian Expression Plasmids

New Plasmid	Isolation of the Backbone Fragment	Isolation of the Insert Fragment
delCMV-mCherry	Double Digestion (AseI, BsrGI) of pmCherry-N1	Double Digestion (AseI, BsrGI) of delCMV-mCherry-actin
delCMV-mCherry-PAK-GBD	Double Digestion (BamHI, EcoRI) of delCMV-mCherry-actin	PCR amplification of the PAK GBD (template = pΔSV40-PakGBD-mCherry, forward primer = PAK1_forward, reverse primer = PAK1_reverse)
delCMV-mCherry-RBD	Double Digestion (BamHI, EcoRI) of delCMV-mCherry-actin	PCR amplification of the Rhotekin GBD (template = mCherry-Rhotekin(8-89)-mCherry-C1, forward primer = RBD_forward, reverse primer = RBD_reverse)
delCMV-mCherry-rGBD	Double Digestion (BamHI, EcoRI) of delCMV-mCherry-actin	PCR amplification of the Rhotekin GBD (template = GFP-rGBD, forward primer = rGBD_forward, reverse primer = rGBD_reverse)
delCMV-mCherry-WASP-GBD	Double Digestion (BamHI, EcoRI) of delCMV-mCherry-actin	PCR amplification of the WASP GBD (template = pΔSV40-mCherry-WASP-GBD, forward primer = WaspGBD_forward, reverse primer = WaspGBD_reverse)
delCMV-mCitrine	Double Digestion (AseI, BsrGI) of pmCitrine-N1	Double Digestion (AseI, BsrGI) of delCMV-mCitrine-RBD
delCMV-EGFP-p67^{phox} (aa1-203)	Double Digestion (BamHI, EcoRI) of delCMV-EGFP-DNIC2	PCR amplification of the p67^{phox} GBD (template = pGEX-4T-I-p67^{phox}-aa1-203, forward primer = p67phox aa1-203 forward, reverse primer = p67phox aa1-203 reverse)
Rac1Q61LΔCAAX-EGFP-2×FKBP'	Double Digestion (AgeI, NheI-HF) of pEGFP-2×FKBP'	PCR amplification of Rac1Q61LΔCAAX (template = Rac1Q61L, forward primer = NheI-Start-Rac, reverse primer = Rac-NgoMIV)
EGFP-Rac1Q61LΔCAAX-2×FKBP'	Double Digestion (BsrGI, XhoI) of pEGFP-2×FKBP'	PCR amplification of Rac1Q61LΔCAAX (template = Rac1Q61L, forward primer = BsrGI-Start-Rac, reverse primer = Rac-XhoI)
EGFP-2×FKBP'-Rac1Q61LΔCAAX	Double Digestion (MfeI,XbaI) of pEGFP-2×FKBP'	PCR amplification of Rac1Q61LΔCAAX (template = Rac1Q61L, forward primer = XbaI-Start-Rac, reverse primer = Rac-Stop-MfeI)

Table 2.24: Summary of New Mammalian Expression Plasmids (continued)

New Plasmid	Isolation of the Backbone Fragment	Isolation of the Insert Fragment
delCMV-EGFP-2×FKBP'-Rac1Q61LΔCAAX	Double Digestion (AseI, BglII) of delCMV-EGFP-tubulin	Double Digestion (AseI, BsrGI) of EGFP-2×FKBP'-Rac1Q61LΔCAAX
mTurquoise2-2×FKBP'-Rac1Q61LΔCAAX	Double Digestion (BsrGI, NheI-HF) of EGFP-2×FKBP'-Rac1Q61LΔCAAX	Double Digestion (BsrGI, NheI-HF) of pmTurquoise2-N1
mTurquoise2-NES-2×FKBP'-Rac1Q61LΔCAAX	Double Digestion (NheI-HF, XhoI) of mTurquoise2-2×FKBP'-Rac1Q61LΔCAAX	PCR amplification of mTurquoise2-NES (template = pmTurquoise2-NES, forward primer = NheI-linker, reverse primer = NES-BsrGI)
mTurquoise2-NES-2×FKBP'-Cdc42Q61LΔCAAX	Double Digestion (MfeI, XbaI) of mTurquoise2-NES-2×FKBP'-Rac1Q61LΔCAAX	PCR amplification of Cdc42Q61LΔCAAX (template = pcDNA3-EGFP-Cdc42Q61L, forward primer = XbaI-Cdc42, reverse primer = Cdc42-S-Stop)
mTurquoise2-NES-2×FKBP'-RhoAQ63LΔCAAX	Double Digestion (MfeI, XbaI) of mTurquoise2-NES-2×FKBP'-Rac1Q61LΔCAAX	PCR amplification of RhoAQ63LΔCAAX (template = pcDNA3-EGFP-RhoA-Q63L, forward primer = FW-XbaI-RhoA-Q63L, reverse primer = RhoA-S-Stop2)
mTurquoise2-NES-2×FKBP'	Double Digestion (NheI-HF, XhoI) of pEGFP-2×FKBP'	Double Digestion (NheI-HF, XhoI) of mTurquoise2-NES-2×FKBP'-Rac1Q61LΔCAAX
delCMV-mTurquoise2-2×FKBP'-Rac1Q61LΔCAAX	Double Digestion (BsrGI, NheI-HF) of delCMV-EGFP-2×FKBP'-Rac1Q61LΔCAAX	Double Digestion (BsrGI, NheI-HF) of pmTurquoise2-N1
delCMV-mTurquoise2-NES-2×FKBP'-Rac1Q61LΔCAAX	Double Digestion (NheI-HF, XhoI) of delCMV-mTurquoise2-2×FKBP'-Rac1Q61LΔCAAX	PCR amplification of mTurquoise2-NES (template = pmTurquoise2-NES, forward primer = NheI-linker, reverse primer = NES-BsrGI)
delCMV-mTurquoise2-NES-2×FKBP'-Cdc42Q61LΔCAAX	Double Digestion (Mlu, BsrGI) of delCMV-mTurquoise2-NES-2×FKBP'-Rac1Q61LΔCAAX	Double Digestion (MluI, BsrGI) of mTurquoise2-NES-2×FKBP'-Cdc42Q61LΔCAAX
delCMV-mTurquoise2-NES-2×FKBP'-RhoAQ63LΔCAAX	Double Digestion (Mlu, BsrGI) of delCMV-mTurquoise2-NES-2×FKBP'-Rac1Q61LΔCAAX	Double Digestion (MluI, BsrGI) of mTurquoise2-NES-2×FKBP'-RhoAQ63LΔCAAX
delCMV-mTurquoise2-NES-2×FKBP'	Double Digestion (AseI, BsrGI) of delCMV-mTurquoise2-NES-2×FKBP'-Rac1Q61LΔCAAX	Double Digestion (AseI, BsrGI) of mTurquoise2-NES-2×FKBP'

Table 2.24: Summary of New Mammalian Expression Plasmids (continued)

New Plasmid	Isolation of the Backbone Fragment	Isolation of the Insert Fragment
delCMV-mTurquoise2-NES-PA-Rac1Q61L	Double Digestion (MfeI, XhoI) of delCMV-mTurquoise2-NES-2×FKBP'-Rac1Q61LΔCAAX	PCR Amplification of PA-Rac1Q61L (template = mCerulean-PA-Rac1Q61L, forward primer = Xho-linker, reverse primer = MfeI-linker)

A small amount (1-5 µL) of the ligation solution was used to transform competent *E. coli* cells (Table 2.25).

Table 2.25: Heat Shock Protocol for Transforming Competent *E. coli* cells.

Step	Description
1.	Pre-warm an LB agar plate (with the appropriate antibiotic) in the 37°C incubator.
2.	Add 1-5 µL of the ligation to competent *E. coli* cells and thaw the cells on ice for ~10 min.
3.	Incubate the cells at 42°C for 2 min.
4.	Cool the cells on ice for 2 min.
5.	Add 1 mL of sterile LB medium to the cells.
6.	Shake the cells at 37°C for ~1 hour.
7.	Centrifuge the cells at 5000 rpm for 5 min. Discard most of the supernatant.
8.	Use the remainder of the supernatant to re-suspend the cells.
9.	Plate the cells on the pre-warmed LB agar plate.
10.	Incubate the LB agar plate overnight at 37°C.

Individual colonies (typically 3-6) were selected from the LB agar plate for further characterization. Each colony was used to inoculate 5 mL of sterile Luria-Bertani (LB) medium containing the appropriate antibiotic (e.g., ampicillin or kanamycin). The inoculated cultures were incubated overnight at 37°C with shaking. For each of the overnight cultures, a glycerol stock solution was prepared by combining 700 µL of the overnight culture and 300 µL of sterile 50% glycerol. The glycerol stock solutions were stored at -80°C. Plasmid DNA was isolated from the remainders of each of the overnight cultures using a QIAprep Spin Miniprep Kit (Qiagen).

Plasmid DNA was subjected to sequencing analysis (Table 2.26 and Table 2.27).

Table 2.26: Preparing Plasmid DNA for Sequencing Analysis

Component	Volume	Initial Concentration	Final Concentration
Plasmid DNA	0.5 µL	0.500 µg/µL	0.025 µg/µL
Sequencing Primer	0.5 µL	10 µM	0.5 µM
Nuclease-free Water	7.0 µL	-	-
Big Dye Terminator Mix	2.0 µL	-	-

Table 2.27: PCR Program Used for Sequencing

Repetitions	T (°C)	Time (sec)
1	96	30
25	96	30
	50	15
	60	240
1	8	∞

2.2.4 Live and Fixed Cell Imaging

Widefield images of the fixed and stained cells of the neurite outgrowth screens were obtained on an Olympus IX81 microscope equipped with a 10x objective and a Hamamatsu ORCA ER C4742-80-12AG Camera. Light for excitation of the fluorophores was produced with an MT20 light source (Olympus). The procedure of image acquisition was automated with the Scanˆ R software (Olympus). For each well of the plate, images were taken at 6 positions. For each position, images were taken of the nuclei (DAPI), the microtubules (RFP), and the actin filaments (GFP).

Widefield and Total Internal Reflection Fluorescence (TIRF) images of live or fixed N2a cells were obtained on an Olympus IX81F-3 microscope equipped with a 60x objective and a Hamamatsu Image EM CCD-C9100-13 Camera. Light for excitation of the fluorophores was produced with an MT20 light source (Olympus). For certain photoactivation experiments, neutral density filters from Thor Labs (NDUV510B, NDUV520B, and NDUV530B) were used to reduce the intensity of light produced by the MT20. For TIRF images, four lasers (405 nm, 445 nm, 488 nm/514 nm, and 561 nm) were used to selectively excite fluorphores within a limited distance (90-200 nm) of the glass substrate. The procedure of image acquisition was automated with the Cellˆ R software (Olympus). For live cell imaging, the N2a medium was removed and replaced with warm imaging medium [10% v/v FBS (PAN-Biotech), 90% v/v DMEM (PAN-Biotech)] prior to imaging.

Confocal images of fixed N2a cells were obtained on an LSM 510 Meta microscope equipped with a 40x objective. Light for excitation of the fluorophores was produced with an LSM 510 Laser Module (Zeiss). The procedure of image acquisition was automated with the LSM Software (Zeiss).

2.2.5 Software

The following software was used for data analysis and preparation of figures.

Table 2.28: Software

Name	Organization(s)
ApE (A plasmid Editor)	University of Utah
CellProfiler[37]	Broad Institute
ImageJ[38]	National Institutes of Health (NIH)
NeuriteQuant[39]	Max-Planck-Institute (MPI) of Molecular Physiology, Dortmund University of Technology, University of California, San Diego (UCSD) National Chiao Tung University
Office (Excel, Word, PowerPoint)	Microsoft
Paint	Microsoft
PRISM	GraphPad

3. RESULTS

3.1 Neurite Outgrowth Screens and Proliferation Assays

In cells, actin molecules can exist as independent entities or they can combine together to form filaments (Fig. 1.2). Interconversion between the monomeric and filamentous forms of actin is crucial for proper cellular function. Interestingly, several natural products that interfere with this interconversion have been identified. Three such molecules are phalloidin, jasplakinolide, and chondramide C (Fig. 3.1A). And, methods for synthetic preparation of these molecules have been reported in the literature[40-48]. Furthermore, chemists at the Max Planck Institute of Molecular Physiology have reported a strategy to synthesize a library of small molecules based on these natural products[5].

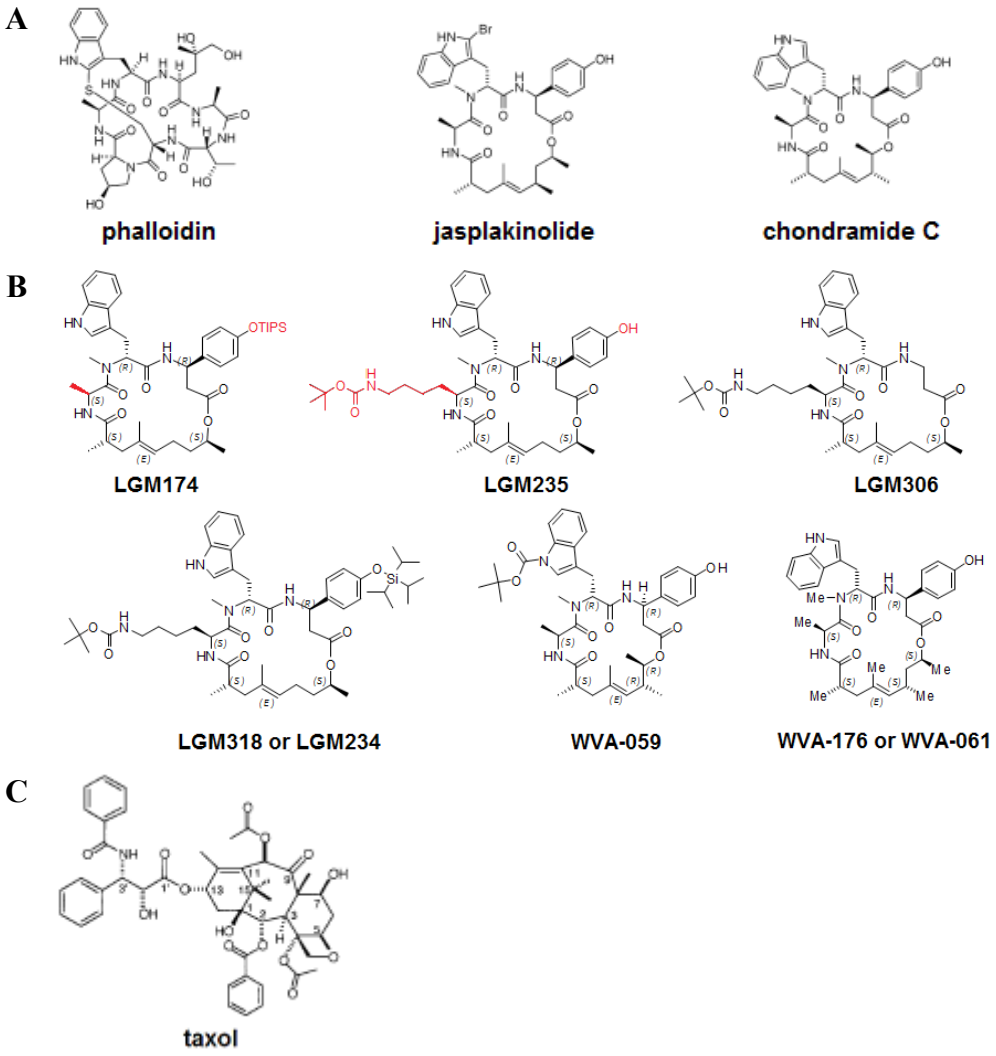

Figure 3.1: Small Molecules Used in the Neurite Outgrowth Screens. (A) Natural products known to stabilize actin filaments. **(B)** Synthetic analogues of the natural products shown in (A). **(C)** Structure of taxol.

Synthetic analogues from this library were screened for their ability to perturb actin dynamics. This screen is based upon the idea that disruptions to the balance between protrusive and contractile forces associated with microtubules and actin filaments, respectively, can lead to changes in cell morphology[49-51]. Therefore, each of the compounds was combined with taxol, a natural product known to stabilize microtubules[52] and added to N2a cells. Jasplakinolide and chondramide C, which are known to induce the formation of neurites in the presence of taxol, were used as positive controls.

Neurite formation was only observed in the presence of three of the analogues tested (WVA-176, LGM174, and LGM235). And, for two of these analogues (WVA-176 and LGM174), neurites were only observed at the two highest concentrations tested (Fig. 3.2A and Fig. 3.2B). However, cells treated with 5 μM LGM174 produced fewer neurites than cells treated with the same concentration of WVA-176. Rather, at 5 μM, LGM174 was more likely to cause the accumulation of actin in the perinuclear regions of the cells (Fig. 3.2B). This effect was still observable at 1.67 μM of LGM174. However, when the concentration of LGM174 was reduced to 555.56 nM, this effect was no longer prominent (Fig. 3.2B).

LGM235 behaved similar to the positive controls (jasplakinolide and chondramide C), producing neurites over a much larger concentration range than WVA-176 or LGM174 (Fig. 3.3A). LGM235 also demonstrated similarities to LGM174, since lower concentrations of the compound produced an accumulation of actin in the perinuclear region (Fig. 3.3B). However, for LGM235, this effect was observed over a far broader range of concentrations (Fig. 3.3C). Interestingly, although LGM235 clearly disrupts normal actin dynamics at lower concentrations, it does not affect cell proliferation at these concentrations (Fig. 3.4A).

Fluorescent analogues of LGM235 were synthesized by adding TAMRA or BODIPY moieties to the lysine side chain (Fig. 3.4B and Fig 3.4C). These compounds were generated as possible alternatives to fluorescently labeled phalloidins that are routinely used to stain actin structures in fixed and permeabilized cells. Both 21C and 21D successfully labeled actin structures in fixed and permeabilized cells[8]. However, only 21D was capable of staining static, long-lived actin filaments in live N2a cells. In contrast to LGM235 (Fig. 3.4A), neither 21C nor 21D impeded cell proliferation at high concentrations (Fig. 3.4B and Fig. 3.4C).

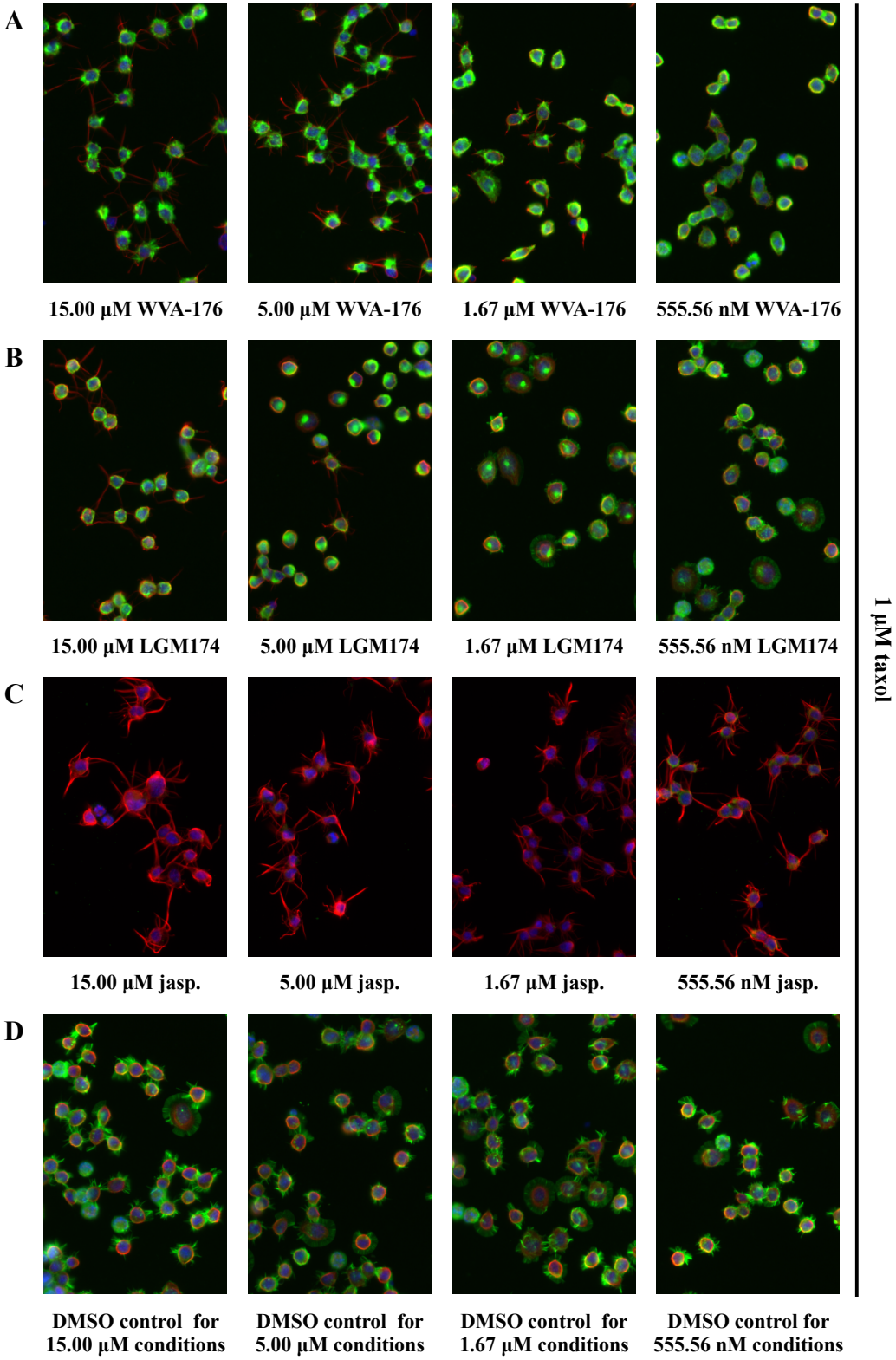

Figure 3.2: Rearrangements of the Actin Cytoskeleton in N2a Cells Induced by WVA-176 and LGM174. These are composite images showing the microtubules (red), actin filaments (green), and nuclei (blue) of N2a cells treated with various concentrations of WVA-176 **(A)**, LGM174 **(B)**, jasplakinolide (jasp.) **(C)**, or DMSO **(D)**.

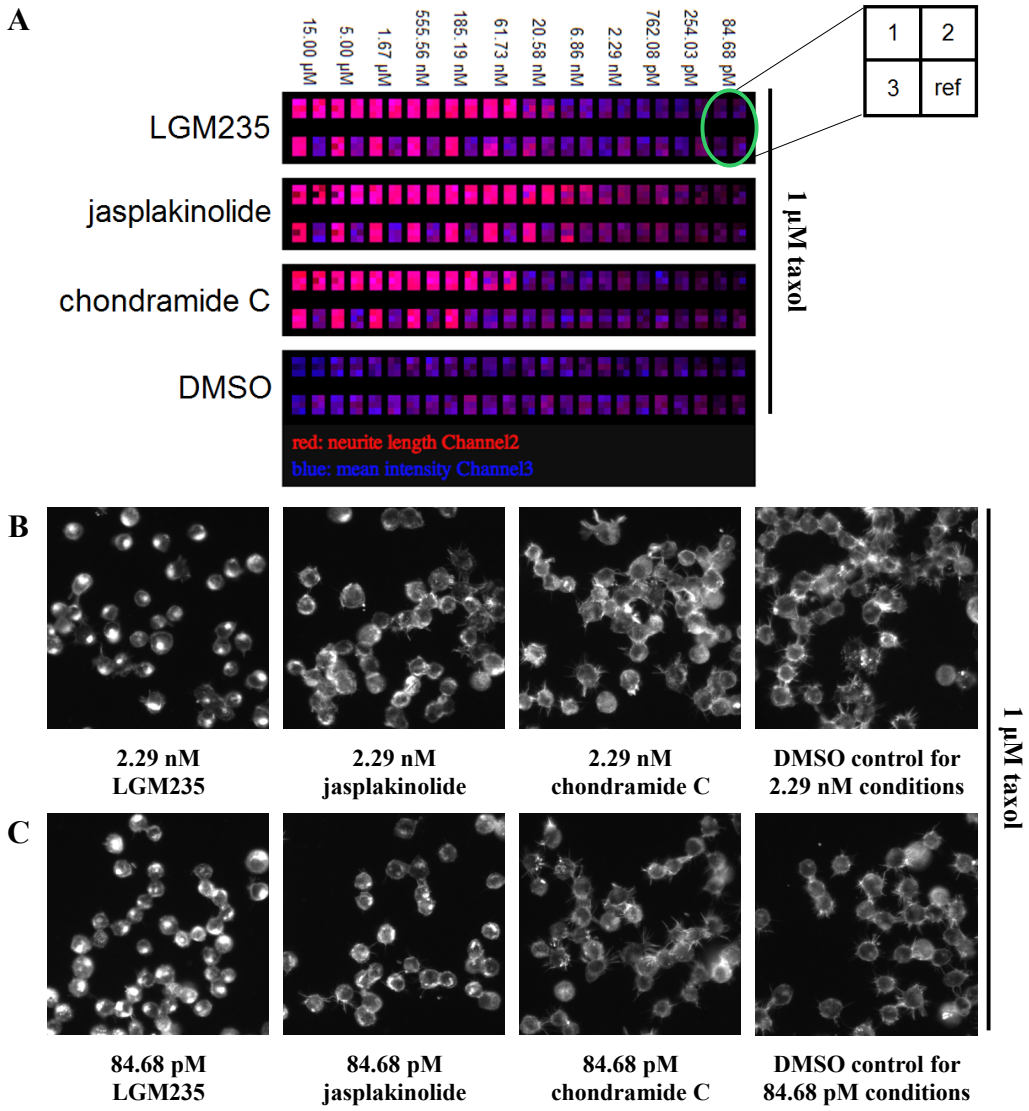

Figure 3.3: Rearrangements of the Actin Cytoskeleton in N2a Cells Induced by LGM235. (A) Heat maps generated by NeuriteQuant[39] to highlight conditions where neurites were observed. For each concentration, 3 wells of cells were treated with the compound and one well was left as a reference (ref). The arrangement of these 4 wells is depicted in the schematic shown on the right. **(B and C)** Widefield images showing the localization of actin in N2a cells treated with 1 µM taxol and LGM235, jasplakinolide, chondramide C, or DMSO.

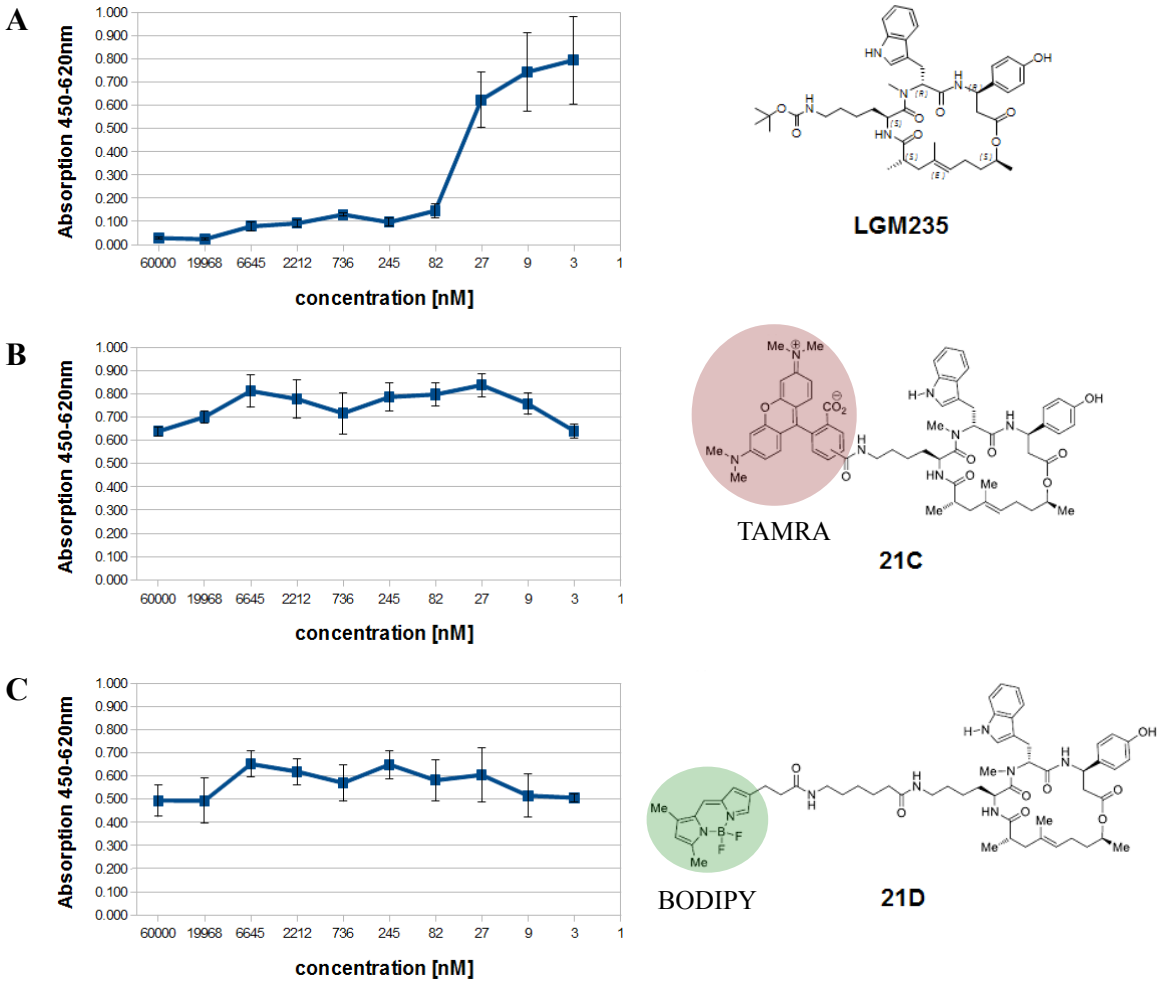

Figure 3.4: Cell Proliferation of N2a Cells in the Presence of LGM235, 21C, and 21D. Cells were incubated in the presence of LGM235 **(A)**, 21C **(B)**, or 21D **(C)** for 3 days at 5% CO_2 and 37°C. Then, 10 µL of WST-1 Cell Proliferation Reagent (Roche) was added to each of the wells and the cells were incubated for 1.5-2 hours at 5% CO_2 and 37°C. For each well, the absorbance at 450 nm and the absorbance at 650 nm was measured.

3.2 TIRF-based Biosensors for Measuring Rho GTPase Activity

Rho GTPases are a group of signaling molecules that regulate various cellular processes. Because of their ability to exist in an "on" (GTP-bound) state and an "off" (GDP-bound) state, Rho GTPases are frequently referred to as molecular switches. When a Rho GTPase is in the active (GTP-bound) state, it can interact with downstream effector proteins. Therefore, since effector proteins selectively bind to the active forms of Rho GTPases, they can be used as the basis for the design of Rho GTPase activity biosensors.

The approach used here is similar to previous methods published in the literature[29-31] and involves the construction of a mammalian expression plasmid that encodes a fluorescent protein linked to the GTPase-binding domain (GBD) of an effector protein (Fig. 3.5A). A truncated CMV promoter (delCMV)[53] was used to ensure that expression of the protein would be weak, thereby minimizing disruption of normal cellular processes by the biosensor. Low-level expression of the biosensor should also result in a lower background fluorescence signal, making changes in localization of the biosensor easier to detect.

Each biosensor should accumulate in regions of the cell where its corresponding Rho GTPase is highly active. And, since Rho GTPases such as Rac1, Cdc42, and RhoA are frequently activated by membrane-bound GEFs[14,18], one would expect the activation of these Rho GTPases to be accompanied by recruitment of their corresponding biosensors to the plasma membrane. Total Internal Reflection Fluorescence (TIRF) microscopy can be used to monitor this recruitment in the region of the cell nearest to the glass substrate (Fig. 3.5B).

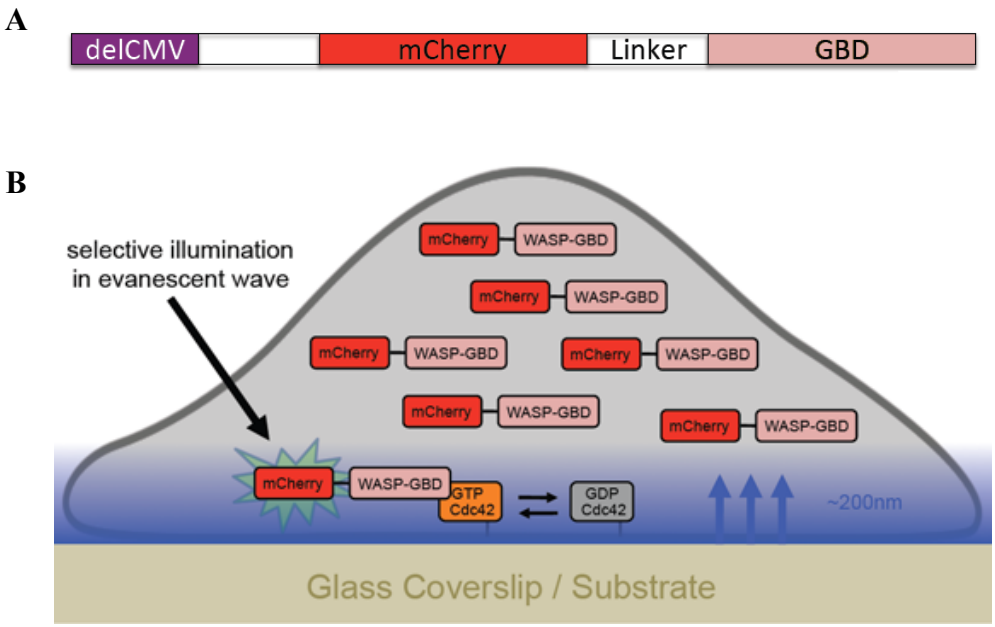

Figure 3.5: TIRF-based Biosensors for Measuring Rho GTPase Activity. (A) Essential features (promoter, fluorescent protein sequence, and GBD sequence) of a mammalian expression plasmid that encodes a biosensor. **(B)** Representation of a cell on a glass substrate. When Cdc42 becomes activated at the plasma membrane, it should recruit its corresponding biosensor from the cytosol to the plasma membrane. TIRF microscopy, which measures fluorescence intensity in the region nearest to the glass substrate, can be used to monitor recruitment of the biosensor.

Two previously published plasmids and new plasmids developed as part of the work described here that encode biosensors for measuring Rho GTPase activity are summarized in Table 3.1 and Figure 3.6.

Table 3.1: Plasmids Encoding TIRF-based Rho GTPase Activity Biosensors

Plasmid Name	Description of the GBD	Corresponding Rho GTPase
pΔSV40-mCherry-WASP-GBD	WASP (amino acids 201-231)	Cdc42
pΔSV40-PAK-GBD-mCherry	PAK1 (amino acids 67-129)	Rac1/Cdc42
delCMV-mCherry-WASP-GBD	WASP (amino acids 201-231)	Cdc42
delCMV-mCherry-PAK-GBD	PAK1 (amino acids 67-129)	Rac1/Cdc42
delCMV-mCherry-RBD	Rhotekin (amino acids 8-89)	RhoA
delCMV-mCherry-rGBD	Rhotekin (amino acids 7-89)	RhoA
delCMV-EGFP-p67^{phox}-aa1-203	p67^{phox} (amino acids 1-203)	Rac1
delCMV-mCherry	-	-
delCMV-mCitrine	-	-

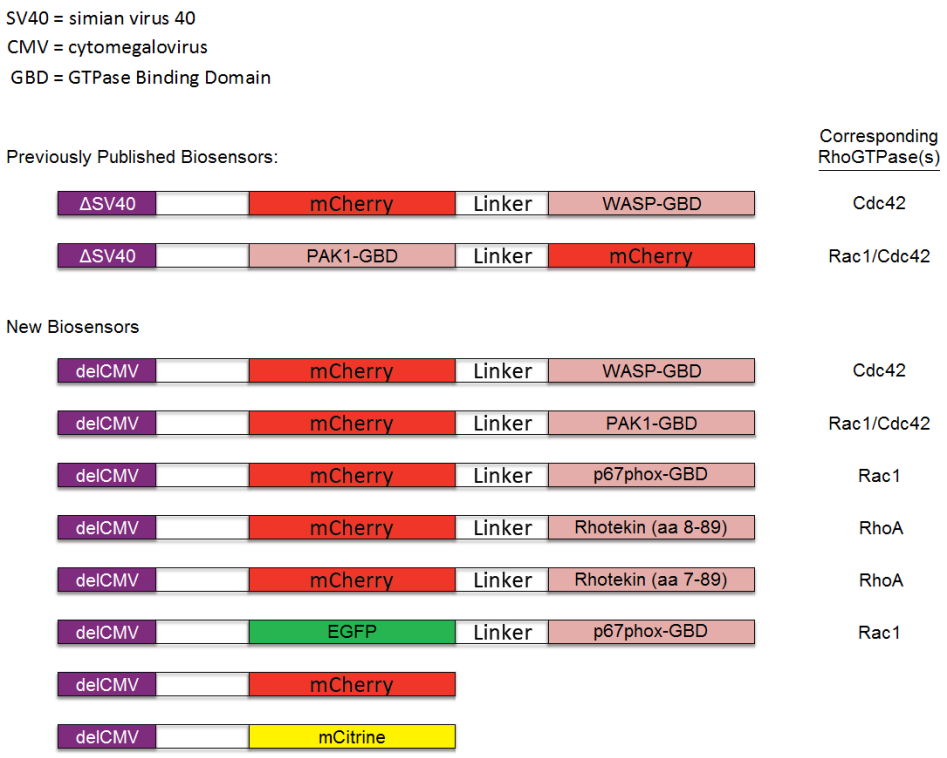

Figure 3.6: Essential Features of Plasmids Encoding TIRF-based Biosensors for Measuring Rho GTPase Activity. This figure highlights the differences between the plasmids encoding the biosensors: promoter, fluorescent tag, GBD, and corresponding Rho GTPase(s).

3.3 Acute Photoactivation of Rac1

3.3.1 Photoactivation of Rac1 Induces Lamellipodia Formation in N2a Cells

Phototropins are a class of protein kinases that become activated upon exposure to light. These proteins are sometimes referred to as light switches, since they adopt one conformation in the dark and another conformation when they are illuminated with light of an appropriate wavelength.

In phototropin1, the kinase domain is located next to a light-oxygen-voltage 2 (LOV2) domain that acts as a photosensor. NMR studies suggest that the LOV2 domain sterically blocks the kinase domain in the "dark" state and that light leads to structural rearrangements that remove this steric block. In particular, a Jα helix at the C-terminus of the LOV2 domain appears to unravel in the "lit" state[54-56].

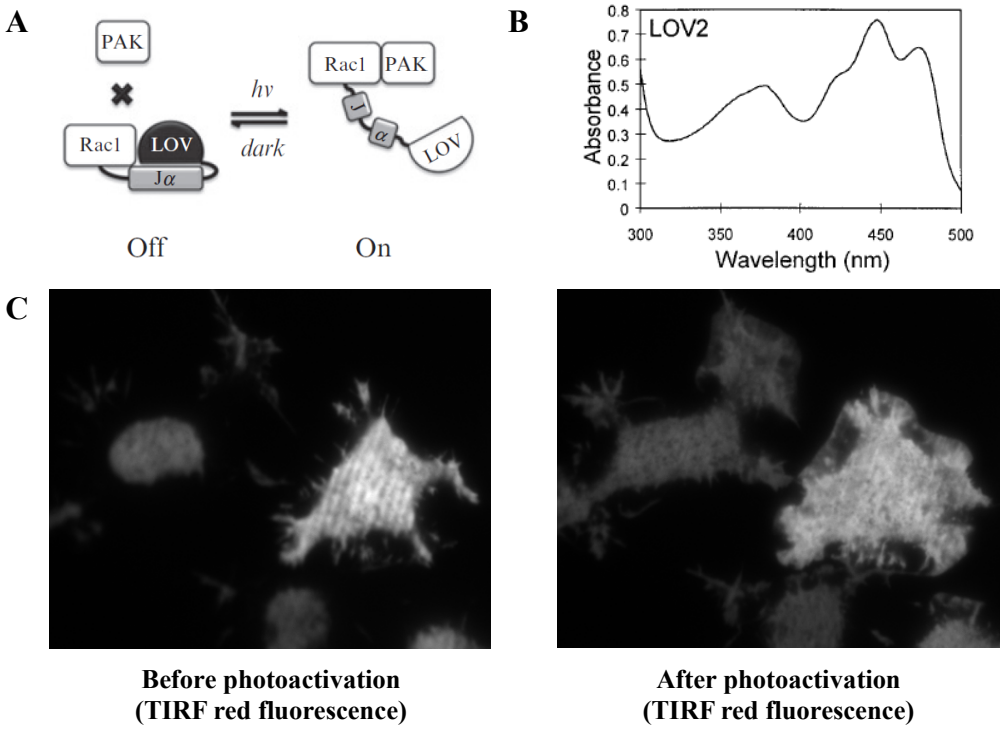

Figure 3.7: Acute Photoactivation of Rac1 Induces Lamellipodia Formation in N2a Cells. (A) Cartoon illustrating the proposed conformational change that PA-Rac1 undergoes upon exposure to light. In the "dark" state, the LOV2 domain sterically blocks Rac1 from interacting with downstream effector proteins, such as PAK1. However, upon illumination, the Jα helix unravels and releases the Rac1, allowing it to bind to its downstream effector proteins. (This figure was taken from reference 57). **(B)** Absorption spectrum of the LOV2 domain from *Avena sativa* phototropin1 (This figure was taken from reference 58). **(C)** N2a cells expressing PA-Rac1-Venus and mCherry before (left) and after (right) photoactivation [63 (1-sec.) pulses of blue light (~420-434 nm) applied at 4-sec. Intervals]. Acute photoactivation of Rac1 produced lamellipodia at the periphery of many cells.

Wu et al. have proposed that the LOV2 domain can be used to "cage" other proteins so that their behavior can be controlled by exposure to light. As an example of this, they fused the LOV2 domain from *Avena sativa* (oat) phototropin1 to the N-terminus of a human Rac1 mutant[35] (Fig. 3.7A). This fusion protein was referred to as photoactivatable Rac1 (PA-Rac1). Unlike wild-type Rac1, where activity is determined by the state of the bound nucleotide (GTP or GDP), the activity of PA-Rac1 should be solely determined by the conformation of the adjacent LOV2 domain. Therefore, a Q61L mutation was introduced to lock Rac1 in the active state and to lower its affinity for RhoGDI and for GEFs. Also, E91H and N92H mutations were introduced to reduce the likelihood that PA-Rac1 would sequester GAPs and indirectly activate endogenous Rac1 proteins.

The LOV2 domain absorbs light over a very broad range of wavelengths[58] (Fig. 3.7B), including those typically used to excite blue, cyan, and green fluorescent proteins. Wu et al. also warn that certain wavelengths that are used to excite yellow fluorescent proteins might also be capable of activating PA-Rac1[57]. Based on this information, studies involving acute photoactivation of Rac1 were performed primarily in combination with red fluorescent proteins, such as mCherry. As a further precaution, to minimize pre-activation, cells were transferred to foil-covered containers immediately after transfection and great care was taken to avoid exposing the cells to light prior to microscopy experiments.

As a preliminary experiment, N2a cells expressing a Venus-labeled PA-Rac1 and mCherry were exposed to 1 second pulses of blue light (~420-434 nm) at 4 second intervals. After ~5 minutes of this photoactivation protocol, many cells developed lamellipodia (Fig. 3.7C), a phenotype commonly observed upon activation of Rac1.

3.3.2 Optimization of a Reversible Photoactivation Protocol

Wu et al. report that photoactivation is a reversible process, with a dark recovery half-life of ~43 seconds[35]. Therefore, a reversible photoactivation protocol was developed (Fig. 3.8A) consisting of three phases: "pre-activation", "photoactivation", and "post-activation". Throughout all three phases, red TIRF images were acquired at 5 second intervals. However, during the "photoactivation" phase of the protocol, the cells were constantly illuminated with blue light in between these intervals. Constant blue light illumination was used instead of pulses to minimize dark recovery between TIRF measurements.

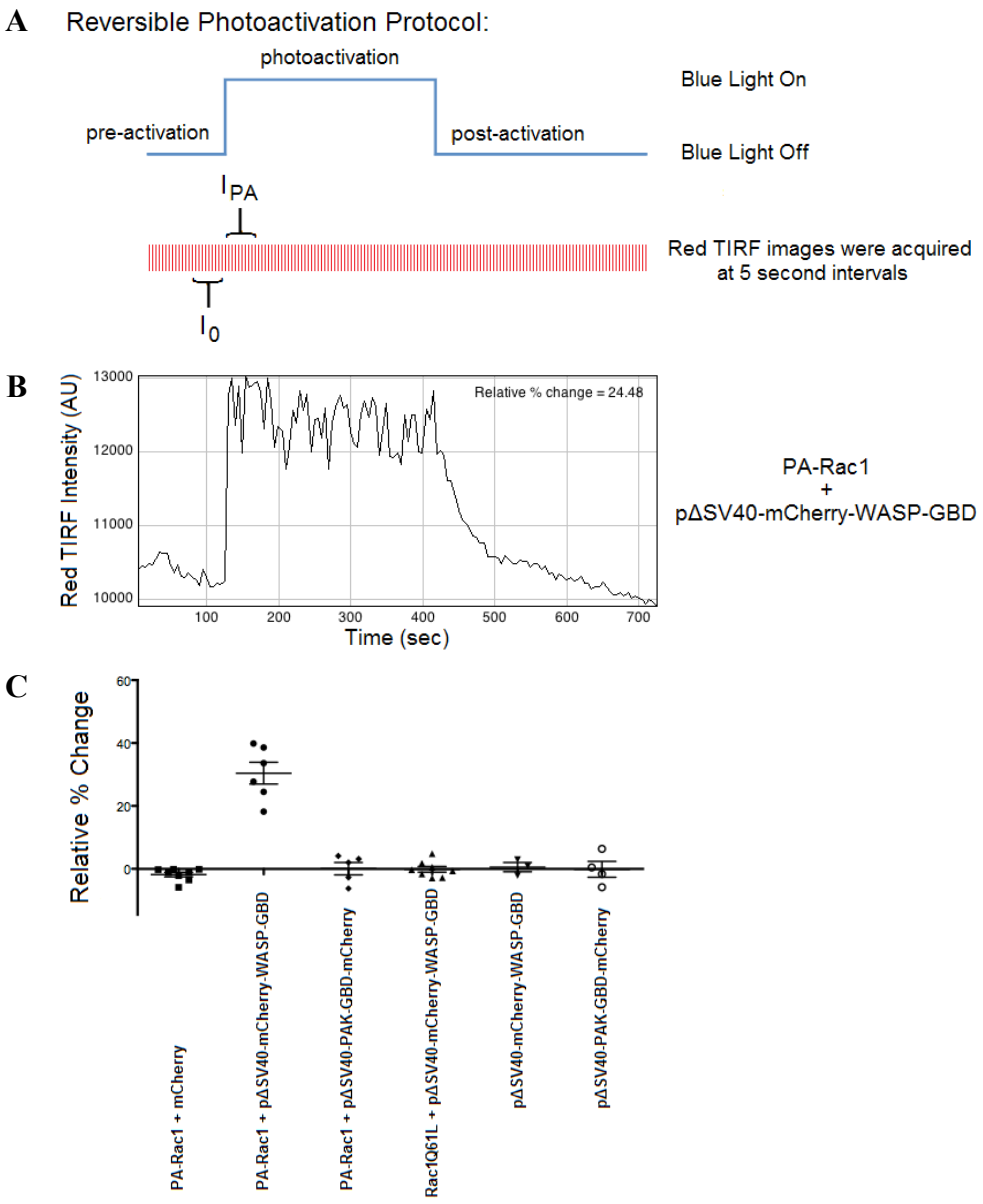

Figure 3.8: Responses of Previously Published Biosensors to Reversible Photoactivation of Rac1. (A) Cartoon illustrating the protocol used to reversibly photoactivate Rac1. Throughout all 3 phases of the protocol ("pre-activation", "photoactivation", and "post-activation"), red TIRF images were acquired at 5 second intervals. However, during the "photoactivation" phase of the protocol, the cells were constantly illuminated with blue light in between these intervals. **(B)** Graph showing the changes in red TIRF intensity that were observed when an N2a cell expressing PA-Rac1 and the previously published WASP biosensor was subjected to the protocol shown in (A). **(C)** Plot comparing the relative % changes observed for different experimental conditions. Cells expressing the previously published WASP biosensor showed a dramatic increase in intensity upon photoactivation of Rac1. Conversely, cells expressing the previously published PAK1 biosensor or mCherry (control) did not show any significant changes in intensity upon photoactivation of Rac1. Biosensor recruitment was also not observed in control experiments where a constitutively active Rac1 mutant (Rac1Q61L) was substituted for PA-Rac1 or where PA-Rac1 was omitted. (Note: For these experiments, the level of FBS in the medium was lowered to 2% approximately 4 hours after transfection. However, similar results were observed when this step was omitted).

This protocol was used to test the effect of acute photoactivation of Rac1 on the localization of 2 previously published Rho GTPase biosensors (Fig. 3.6)[29]. One of these biosensors was based on the GBD of PAK1, which binds to both active Rac1 and active Cdc42. The other biosensor was based on the GBD of WASP, which only binds to active Cdc42. Each of these biosensors was encoded by a plasmid containing a truncated SV40 promoter (ΔSV40) and each of these biosensors was labeled with mCherry.

Relative % change in TIRF intensity of the biosensor upon photoactivation of Rac1 was used to measure the extent of recruitment of the biosensor to the plasma membrane.

$$\text{relative \% change} = \frac{I_{PA} - I_0}{I_0} \times 100$$

In this equation, I_{PA} represents the average, background subtracted, TIRF intensity of the biosensor within a cell during initial photoactivation and I_0 represents the average, background subtracted, TIRF intensity of the biosensor within a cell immediately prior to photoactivation (Fig. 3.8A).

Photoactivation of Rac1 led to recruitment of the WASP biosensor to the plasma membrane (Fig. 3.8B and Fig. 3.8C). This suggests that activation of Rac1 leads to activation of Cdc42, which is consistent with other published data[59]. Furthermore, after photoactivation, the intensity of this biosensor quickly returned to a value that was similar to that observed prior to photoactivation, demonstrating that activation of Cdc42 is reversible.

Photoactivation of Rac1 did not lead to recruitment of the PAK1 biosensor (Fig. 3.8C). This result was surprising, since PAK1 has been shown to bind to active Rac1. However, Wu et al. report that they were not able to directly measure binding between PA-Rac1 and PAK1, since measurements performed under ambient light ("room light") conditions produced inconsistent results[57]. Instead, they generated "dark" and "lit" mutants of PA-Rac1 in order to estimate the binding affinities of PAK1 for PA-Rac1 in these two states[57]. Nevertheless, experiments with the WASP (Fig. 3.8B and 3.8C) suggest that photoactivation of Rac1 leads to activation of Cdc42. So, even if the PAK1 biosensor is unable to bind directly to PA-Rac1, it should be recruited to the plasma membrane by the activated Cdc42. However this was not observed. Therefore, only the WASP biosensor was selected for use in experiments to optimize the reversible photoactivation protocol.

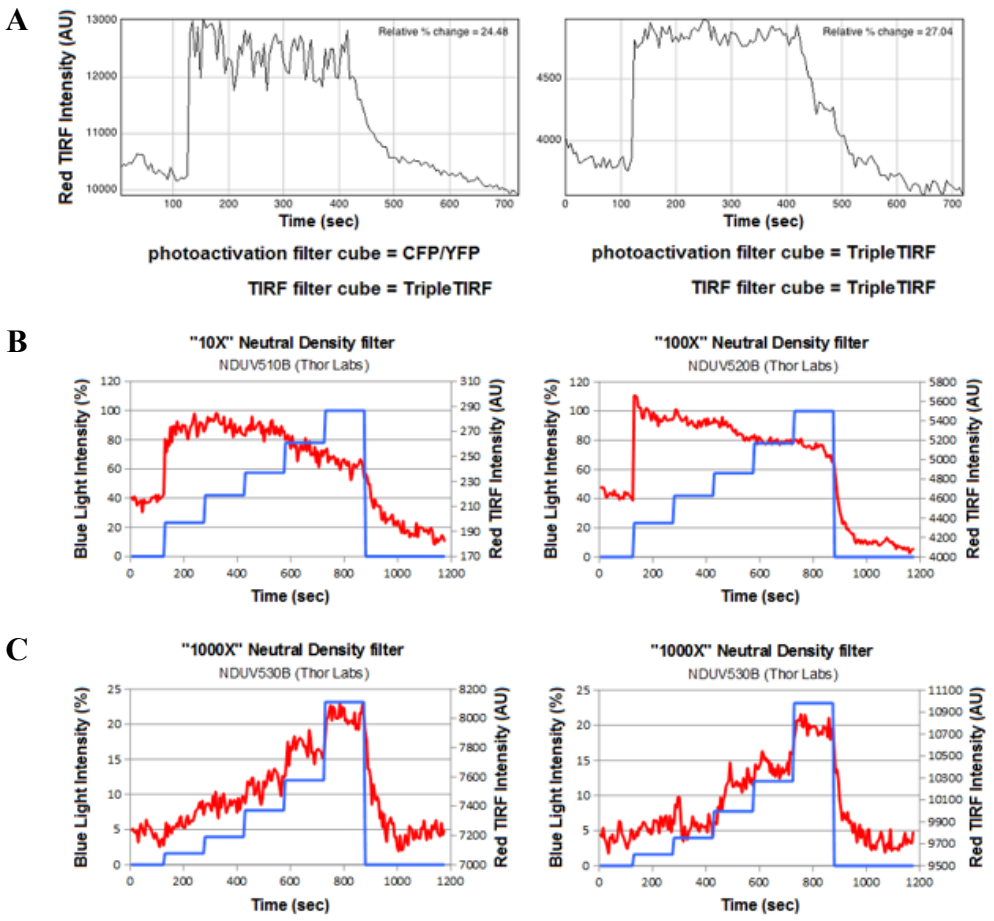

Figure 3.9: Optimization of the Reversible Photoactivation Protocol. All experiments shown here were performed with N2a cells Expressing a Venus-labeled PA-Rac1 and the previously published WASP biosensor (Fig. 3.6). **(A)** Comparison of results obtained when photoactivation and measurements of recruitment were performed using different filter cubes (left) or the same filter cube (right). The modified protocol (right) produces less noise during the photoactivation phase without affecting the magnitude of the relative % change. **(B)** Light titrations using "10X" and "100X" neutral density filters. In these experiments there is no correlation between the intensity of blue light and the level of biosensor recruitment. (**C**) Light titrations using a "1000X" neutral density filter. In these experiments, increasing the intensity of the blue light leads to increases in the level of biosensor recruitment.

First, attempts were made to reduce the noise that appears during the photoactivation phase of the protocol (Fig. 3.8B and Fig. 3.9A). It was reasoned that this noise might come from the repetitive switching from a CFP/YFP filter cube (for global photoactivation) to a TripleTIRF filter cube (for monitoring recruitment of the biosensor) and back again; imperfect repositioning of the filters caused by this repetitive switching might lead to variations in the TIRF intensity. Therefore, the protocol was modified so that the TripleTIRF filter cube was used for both of these processes. There was a possibility that this modification would reduce the intensity of the blue light to a level that would no longer produce photoactivation. However, the modified protocol produced relative % changes similar

to those observed with the original protocol while simultaneously reducing the noise that appeared with the original protocol (Fig. 3.9A).

Light titrations were also performed to determine whether the level of biosensor recruitment could be controlled by varying the intensity of the blue light. Initial attempts to modulate the level of photoactivation using NDUV510B and NDUV520B neutral density filters (Thor Labs), which reduced the intensity of the light by 10-fold and 100-fold, respectively, were unsuccessful (Fig. 3.9B). Rather, the level of biosensor recruitment remained relatively constant during these experiments, suggesting that even the minimum dose of light tested was sufficient to produce the maximum level of photoactivation. However, light titrations performed with the NDUV530B neutral density filter (Thor Labs), which reduced the intensity of the light by 1000-fold, showed a clear correlation between the intensity of the light used and the level of biosensor recruitment (Fig. 3.9C).

All subsequent photoactivation experiments were performed using an optimized protocol that included using the NDUV530B neutral density filter (Thor Labs) to reduce the intensity of the blue light. Furthermore, in this optimized protocol, a single filter cube (TripleTIRF) was used for both photoactivation and for monitoring recruitment of the biosensor.

3.3.3 Comparison of TIRF-based Biosensors Used to Measure Rac1 Activity

It is important to note that the GBD of PAK1 binds to both active Rac1 and active Cdc42. Consequently, biosensors based on this GBD will not be able to distinguish between these two Rho GTPases. Therefore, a new biosensor (delCMV-mCherry-p67^{phox}-GBD) based on the GBD of p67^{phox}, which selectively binds to active Rac1, was prepared by Djamschid Solouk (a Master's student under my supervision)[32].

For comparison, a new PAK1-based biosensor (delCMV-mCherry-PAK-GBD) was also prepared. There are two important features that distinguish the new PAK1-based biosensor from the previously published PAK1-based biosensor (Fig. 3.6). First, the plasmid encoding the new biosensor has a delCMV promoter to ensure low-level expression of the protein. Second, for the new biosensor, the fluorescent tag (mCherry) is fused to the N-terminus of the GBD, rather than the C-terminus.

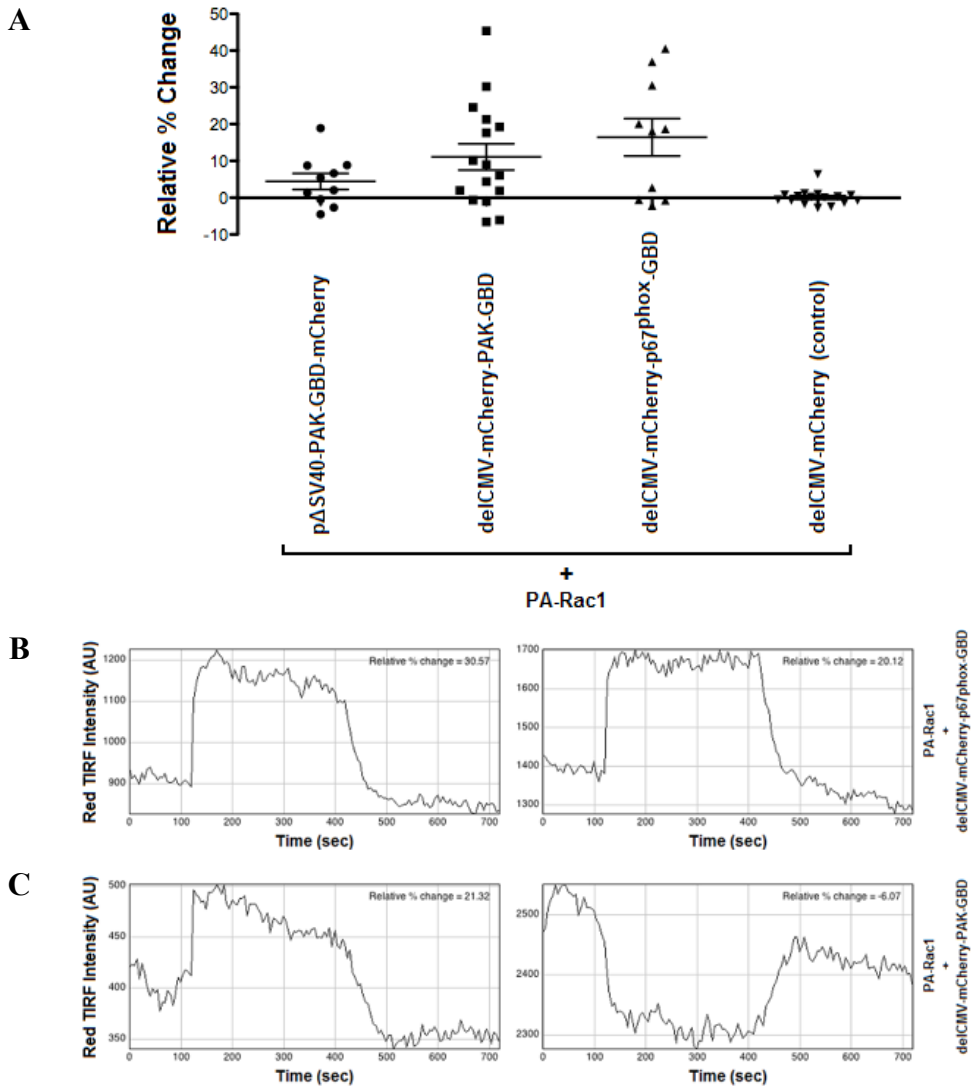

Figure 3.10: Comparison of Biosensors Used to Measure Rac1 Activity. N2a cells expressing PA-Rac1 and a biosensor were subjected to the optimized reversible photoactivation protocol. **(A)** On average, the new Rac1 biosensor (delCMV-mCherry-p67^{phox}-GBD) produced the largest relative % change, the previously published Rac1/Cdc42 biosensor (pΔSV40-PAK-GBD-mCherry) produced the smallest relative % change, and the new Rac1/Cdc42 biosensor (delCMV-mCherry-PAK-GBD) produced an intermediate value. However, the new Rac1/Cdc42 biosensor also produced the largest range of values, including negative values that were larger in magnitude than those observed for the other conditions. Graphs of N2a cells expressing PA-Rac1 and the new Rac1 biosensor **(B)** or the new Rac1/Cdc42 biosensor **(C)** are shown for comparison to each other.

The optimized reversible photoactivation protocol was used to examine the responses of different biosensors used to measure Rac1 activity (Fig. 3.10A). Consistent with the data shown in Figure 3.8C, the previously published PAK1 biosensor (pΔSV40-PAK-GBD-mCherry) showed the weakest response to photoactivation of Rac1. On average, the biosensor based on the GBD of p67^{phox} (delCMV-mCherry-p67^{phox}-GBD) showed the largest relative % change in response to reversible photoactivation of Rac1

(Fig. 3.10A and Fig. 3.10B). And, the new PAK1-based biosensor (delCMV-mCherry-PAK-GBD) showed an average relative % change intermediate between the other two biosensors. However, this biosensor also produced the broadest range of values, including negative values that were larger in magnitude than those observed with the other biosensors (Fig. 3.10C).

3.3.4 Measuring the Crosstalk Between Rac1, Cdc42, and RhoA

In addition to the published Cdc42 biosensor (pΔSV40-mCherry-WASP-GBD) and the new Rac1 biosensor (delCMV-mCherry-p67^{phox}-GBD) described above, a new RhoA biosensor (delCMV-mCherry-RBD), based on the Rhotekin GBD (RBD), was developed as part of the work described here. And, light titrations similar to those shown in Figure 3.9C were used to examine the responses of these three biosensors to acute photoactivation of Rac1 in N2a and HeLa cells[32].

On average, each of the biosensors showed an increase in activity of the corresponding GTPase upon acute photoactivation of Rac1 (Fig. 3.11 and Fig. 3.12). This was somewhat surprising, since there have been many studies showing that activation of Rac1 leads to inhibition of RhoA[26]. However, closer inspection of the data revealed that one of the N2a cells did indeed show a decrease in RhoA activity upon acute photoactivation of Rac1 (Fig. 3.13A). Interestingly, this was not observed for experiments with HeLa cells. Similarly, Wu et al. noted that MEF, HEK293, and HeLa cells displayed different responses to photoactivation of Rac1[35]. And, they concluded that the pathways that regulate these responses may vary among different cell lines[35]. However, the data shown here also suggest that the crosstalk between Rac1 and RhoA may vary within a population of N2a cells.

In a series of experiments performed by, Aline Timmermann (another Master's student under my supervision) N2a cells expressing PA-Rac1 and the RhoA biosensor were exposed to three short pulses of 100% blue light at two time point (0 hrs and 9.5 hrs)[60]. The results of these experiments were similar to those shown in Figure 3.11, with the majority of cells showing an increase in RhoA activity upon photoactivation of Rac1. However, a small number of cells showed a decrease in RhoA activity upon photoactivation of Rac1. Cells expressing high levels of PA-Rac1 or moderate to high levels of the biosensor were more likely to show a decrease in RhoA activity (Fig. 3.13B). Surprisingly, one of these cells actually changed its behavior over time (Fig. 3.13C). However, this appears to be a rare occurrence.

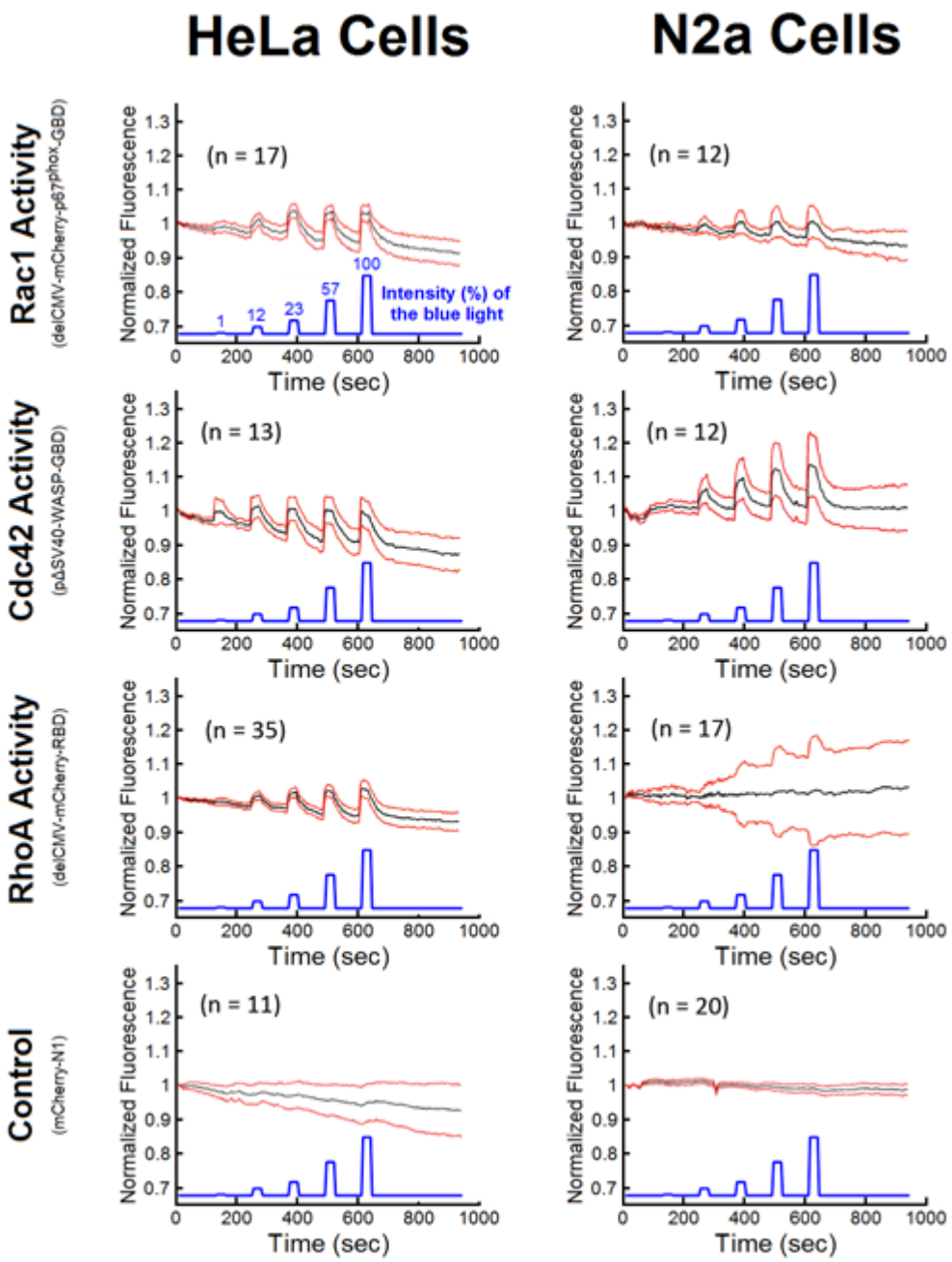

Figure 3.11: Measurement of Rac1, Cdc42, and RhoA Activities in Response to Photoactivation of Rac1. Cells expressing a Venus-labeled PA-Rac1 and one of the biosensors or mCherry-N1 (control) were subjected to pulsed light titrations using the "1000X" neutral density filter. For each graph, the number of cells studied (n) is indicated. Black lines show the average response for all of the cells studied. Red lines show the average plus (above) or minus (below) one standard deviation. [These data were acquired during the MPI Systems Biology Practical (2012) under the supervision of Djamschid Solouk. Dr. Leif Dehmelt and Dr. Tomàš Mazel oversaw the data analysis.]

The relationship between Rac1 activity and RhoA activity in N2a cells remains unclear. And, alternative approaches to study this relationship (described below) have been developed.

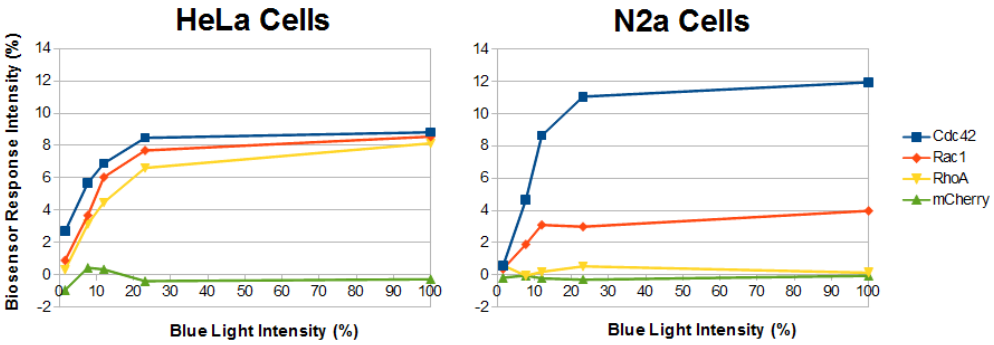

Figure 3.12: Blue Light Dose-Response Curves for the Data Shown in Figure 3.11.

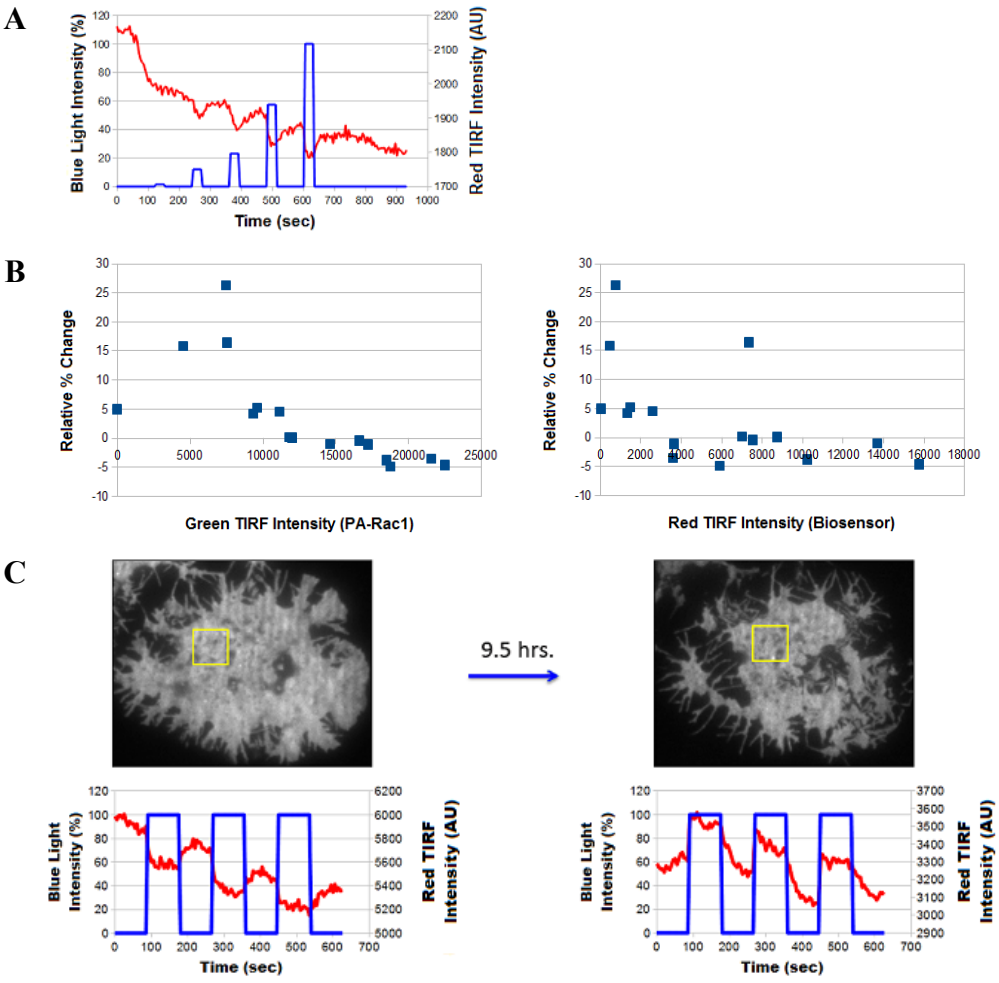

Figure 3.13: Photoactivation of Rac1 Leads to RhoA Inhibition in a Limited Number of N2a Cells. (A) An example from the experiments described in Figure 3.11. **(B)** Graphs showing that cells expressing high levels of PA-Rac1 or moderate to high levels of the RhoA biosensor (at 0 hrs) are more likely to show RhoA inhibition upon photoactivation of Rac1. **(C)** Images (above) and graphs (below) of an N2a cell that initially showed RhoA inhibition (left) and later activation (right) in response to photoactivation of Rac1. Yellow boxes indicate the regions used to make the graphs. [The data in B and C were acquired by Aline Timmermann]

3.3.5 Localization of PA-Rac1 in N2a and HeLa Cells

Finally, confocal microscopy experiments were performed (by Johannes Koch, a PhD student at the University of Duisburg-Essen) to examine the localization of PA-Rac1 in N2a cells. Surprisingly, a large fraction of PA-Rac1 was found to localize to the nuclei of N2a cells (Fig. 3.14A and Fig. 3.14B). And, similar results were observed in HeLa cells (Fig. 3.14C and Fig. 3.14D), demonstrating that this behavior is not specific to N2a cells.

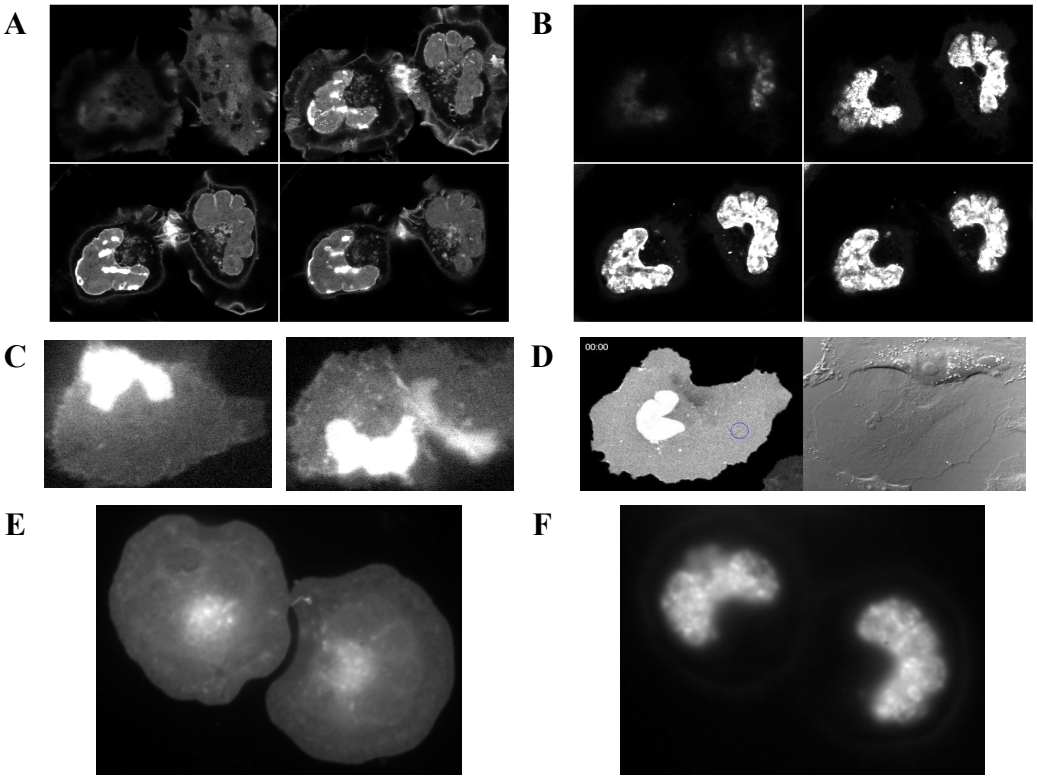

Figure 3.14: Localization of PA-Rac1 in N2a and HeLa cells. (A) Confocal images showing the localization of PA-Rac1 in N2a cells. **(B)** Confocal images [corresponding to those in (A)] showing the nuclei of N2a cells expressing PA-Rac1. **(C)** Widefield images showing the localization of PA-Rac1 in HeLa cells. **(D)** Image from a supplementary movie published by Wu et al.[35] showing the localization of PA-Rac1 in a HeLa cell. (**E**) Widefield image showing the localization of EGFP-Rac1Q61L in N2a cells. (**F**) Widefield image [corresponding to the image in (E)] showing the nuclei of N2a cells expressing EGFP-Rac1Q61L. (Images in A, B, E, and F were provided by Johannes Koch. Images in C were provided by Djamschid Solouk)

This behavior is very different from that typically observed for wild-type Rac1, which is predominantly found in the cytosol in complex with RhoGDI[21]. However, the Q61L mutation in PA-Rac1 greatly reduces its affinity for RhoGDI[35]. Nevertheless, the nuclear localization of PA-Rac1 does not appear to be related to the Q61L mutation, since EGFP-Rac1Q61L was not usually observed in the nuclei of N2a

cells (Fig. 3.14E and Fig. 3.14F).

Wild-type Rac1 also undergoes post-translational prenylation, which allows it to interact with membranes. And, since no mutations were made to PA-Rac1 to prevent this modification, PA-Rac1 might also be expected to localize to membranes. And, indeed, PA-Rac1 does appear to localize to the plasma membrane (Fig. 3.14A). However, it is unclear why a significant fraction of PA-Rac1 is also found in the nucleus.

It is worth noting that the nuclei of N2a cells expressing PA-Rac1 appear to be deformed (Fig. 3.14B), suggesting that PA-Rac1 can interfere with normal cellular function, even in the absence of blue light. This effect appears to be related to the Q61L mutation, since N2a cells expressing EGFP-Rac1Q61L frequently displayed the same phenotype (Fig. 3.14F). Furthermore, Wu et al. report that they also observed residual pre-activation of PA-Rac1 in the dark and they propose different methods to reduce this effect by optimizing the expression level of PA-Rac1.

3.3.6 Design and Preparation of an Optimized PA-Rac1

Based on the observations described above, a new photoactivatable Rac1 construct was designed and prepared. The plasmid for this construct (delCMV-mTurquoise2-NES-PA-Rac1Q61L) has a delCMV promoter to ensure low-level expression of the protein. This should minimize disruption of normal cellular processes by PA-Rac1. It may also minimize residual pre-activation of PA-Rac1 in the dark. Furthermore, since previous experiments showed that the response of the RhoA biosensor depends upon the level of PA-Rac1 (Fig. 3.13B), experiments with this new construct might help to clarify the relationship between Rac1 activity and RhoA activity in N2a cells. A nuclear export sequence (NES)[36] was also added between the fluorophore and the LOV2 domain to prevent accumulation of PA-Rac1 within the nucleus.

Preliminary experiments have shown that this optimized PA-Rac1 localizes primarily to the plasma membrane (Fig. 3.15). And, the nuclear deformations observed with the original PA-Rac1 construct appear largely absent in N2a cells expressing the new PA-Rac1 construct.

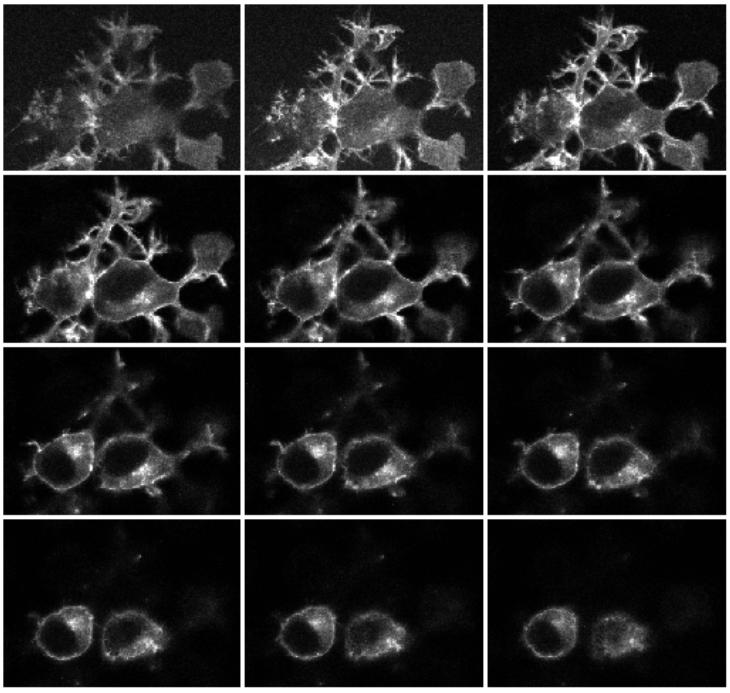

Figure 3.15: Localization of an Optimized PA-Rac1 in N2a cells. N2a cells expressing an optimized PA-Rac1 were fixed and confocal images of these cells were taken.

3.4 Recruitment of Active Rho GTPases to the Plasma Membrane

3.4.1 A Novel Bioorthogonal and Reversible CID System

The approach described by Wu et al. to photoactivate Rac1 has many attractive features. For example, this approach is relatively simple to implement. Also, photoactivation of Rac1 is rapid and reversible (Fig. 3.8B). Furthermore, the amount of light required to activate PA-Rac1 is extremely small (Fig. 3.9C).

However, this approach also suffers from certain limitations. For example, because the LOV2 domain absorbs light over a very broad range of wavelengths, including those typically used to excite blue, cyan, and green fluorescent proteins, these proteins cannot be monitored without activating PA-Rac1. Also, unlike wild-type Rac1 or the Rac1Q61L mutant, PA-Rac1 frequently localizes to the nuclei of N2a and HeLa cells (Fig. 3.14). Moreover, expression of PA-Rac1 often induces nuclear deformations, even in the absence of blue light (Fig. 3.14).

It should be noted here that Wu et al. also prepared a photoactivatable Cdc42 construct (PA-Cdc42)[35]. However, an additional mutation (F56W) had to be introduced in Cdc42 in order to stabilize the caged conformation of PA-Cdc42[35]. Although this mutation lowered the affinity of PA-Cdc42 for the PAK1 effector protein in the dark state[35], it is unclear whether this mutation also affects Cdc42 function in other ways. According to Wu et al., photoactivation of this construct in HEK293 and HeLa cells led to the formation of filopodia[35]. However, photoactivation experiments with this construct, performed as part of the work described here, did not lead to membrane recruitment of the biosensors described above or to morphological changes in N2a cells (data not shown).

It should also be noted that, although the PA-Rac1 and PA-Cdc42 constructs were originally reported over 4 years ago[35], Wu et al. have not developed a photoactivatable RhoA construct. This may suggest that their approach is not easily applied to other Rho GTPases.

In light of these observations, an alternative approach to control Rho GTPase activity, based on chemically induced dimerization (CID) was developed. In this approach, a small molecule (referred to as a "dimerizer") binds simultaneously to two distinct protein modules to form a heterodimeric protein complex. The dimerizer presented here was designed (by members of Dr. Yaowen Wu's group at the Chemical Genomics Centre of the Max Planck Society) to contain one moiety (SLF') that binds to the F36V mutant of FKBP (FKBP') and another moiety (TMP) that binds to *E. coli* dihydrofolate reductase (eDHFR) (Fig. 3.16A). These two protein modules were selected because neither is endogenous to mammalian cells. Therefore, unlike other dimerizers (e.g., rapamycin), SLF'-TMP should not interact with endogenous proteins (e.g., wild-type FKBPs) or produce off-target effects.

Aliquots of dimerizer (Fig. 3.16A), competitor (Fig. 3.16B), and two mammalian expression plasmids, one encoding a fusion protein consisting of EGFP linked to two copies of the FKBP' module (pEGFP-2×FKBP') and another encoding a fusion protein consisting of TagBFP linked to two copies of the eDHFR module and the C-terminal plasma membrane targeting sequence of K-Ras (TagBFP-2×eDHFR-CAAX), were provided by Dr. Yaowen Wu. N2a cells were transfected with both of these plasmids and the dimerizer (SLF'-TMP) was added to the cells, producing rapid recruitment of EGFP-2×FKBP' to the plasma membrane (Fig. 3.16C). Subsequent addition of the competitor (TMP) produced rapid dissociation of EGFP-2×FKBP' from the plasma membrane (Fig. 3.16C). A cartoon summarizing these observations is shown in Figure 3.16D.

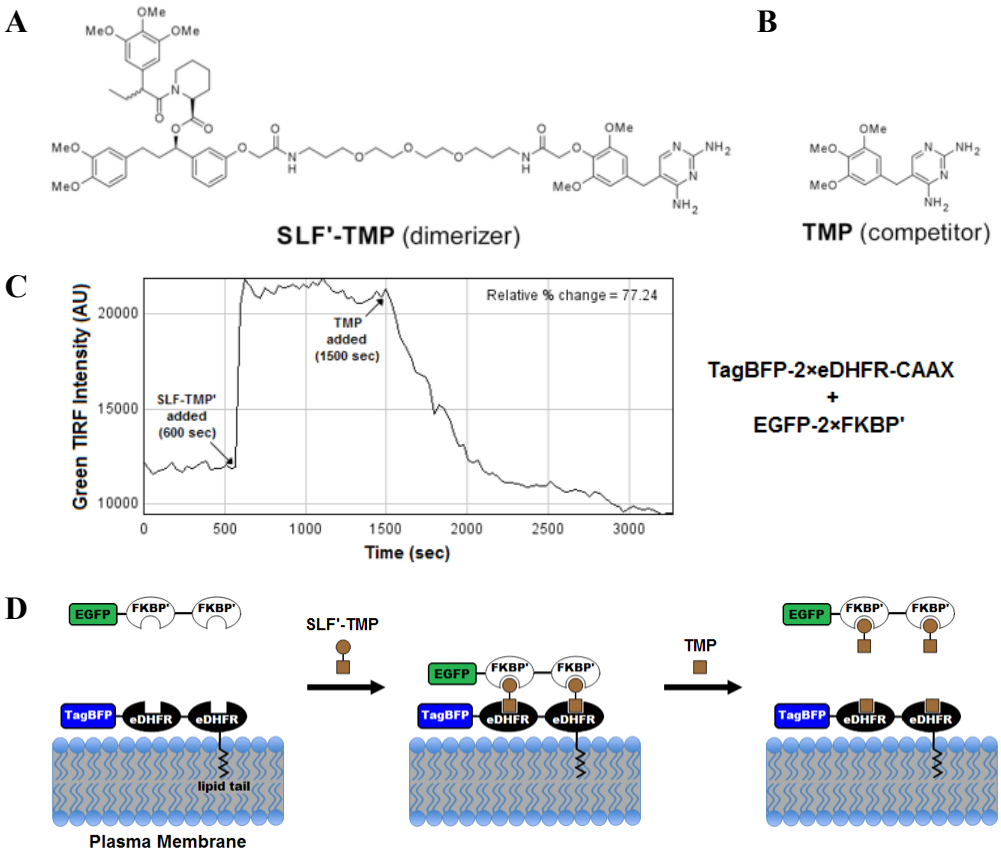

Figure 3.16: A Novel Bioorthogonal and Rapidly Reversible CID system. (A) Structure of the dimerizer. **(B)** Structure of the competitor. **(C)** An N2a cell expressing TagBFP-2×eDHFR-CAAX and EGFP-2×FKBP' was treated with 10 μM SLF'-TMP, causing rapid recruitment of EGFP-2×FKBP' to the plasma membrane. Subsequent addition of 10 μM TMP caused rapid dissociation of EGFP-2×FKBP' from the plasma membrane. **(D)** A cartoon summarizing the experiment shown in (C)

3.4.2 Recruitment of Constitutively Active Rac1 to the Plasma Membrane

The reversible CID system presented above can be used to mimic the cycling of Rac1 between the cytosol and the plasma membrane (Fig. 1.10). Therefore, three variants of the original pEGFP-2×FKBP' plasmid were prepared, each containing a sequence encoding a constitutively active Rac1 mutant (Rac1Q61L). The prenylation site of Rac1 was removed from these variants (ΔCAAX), in order to allow the localization of these proteins to be controlled using the CID system described above (Fig. 3.17B and Fig. 3.17C).

Although each of the fusion proteins shown in Figure 3.17C was successfully recruited to the plasma membrane using the CID system described above, only the proteins with the Rac1 mutant at the N-

terminus or the C-terminus produced lamellipodia in response to recruitment (Fig. 3.17D). Of these two proteins, lamellipodia formation was most frequently observed with the variant containing the Rac1 mutant at the C-terminus (EGFP-2×FKBP'-Rac1Q61LΔCAAX) (Fig. 3.17D). Moreover, this phenotype was rapidly reversed upon addition of competitor (Fig. 3.18).

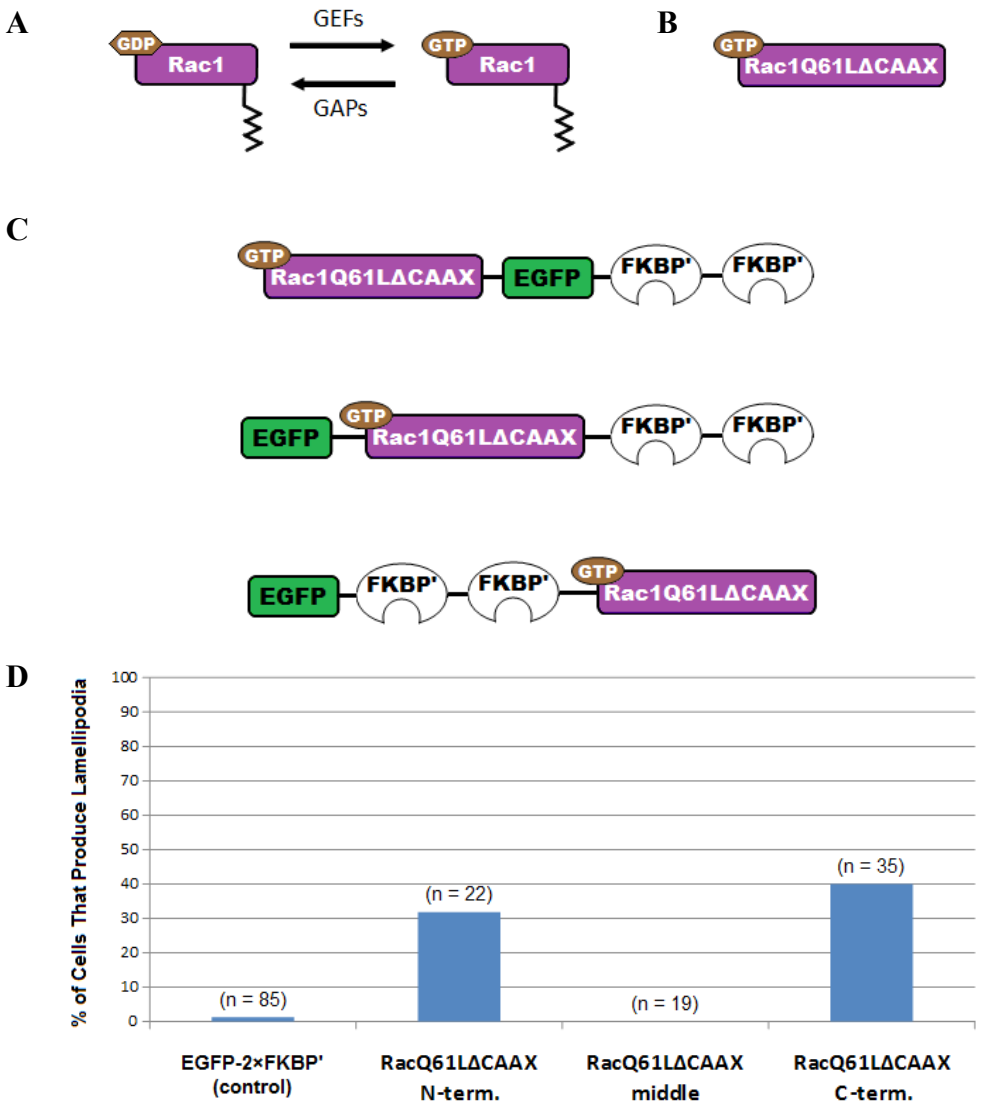

Figure 3.17: Recruiting a Constitutively Active Rac1 to the Plasma Membrane. (A) Regulation of wild-type Rac1 activity by GEFs and GAPs. **(B)** A constitutively active Rac1 mutant lacking the prenylation site (Rac1Q61LΔCAAX). **(C)** Three variants of EGFP-2×FKBP' with Rac1Q61LΔCAAX at the N-terminus (N-term.), between EGFP and the two FKBP' domains (middle), or at the C-terminus (C-term.). **(D)** N2a cells expressing TagBFP-2×eDHFR-CAAX and one of the proteins shown in (C) or EGFP-2×FKBP' (control) were treated with 10 μM SLF'-TMP. Then, the % of cells that formed lamellipodia was determined. For each condition, the number of cells studied (n) is indicated.

These results suggest that, even though the Rac1 mutant used in these studies is constitutively active, the protein must be properly localized within the cell in order to participate in signaling. This is in

agreement with other published data[22-23]. Furthermore, these results suggest that the approach described here can be used to control Rac1 activity in living cells.

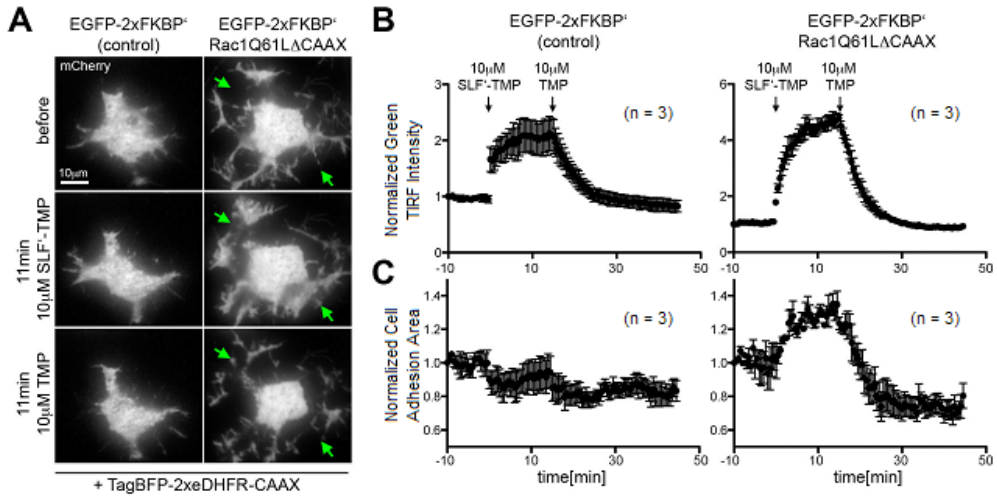

Figure 3.18: Reversible Recruitment of a Constitutively Active Rac1 Mutant to the Plasma Membrane Induces Reversible Lamellipodia Formation. (A) Red TIRF images of an N2a cell expressing TagBFP-2×eDHFR-CAAX, mCherry-N1, and EGFP-2×FKBP' (left) or EGFP-2×FKBP'-Rac1Q61LΔCAAX (right) at different time points during a reversible recruitment experiment. Green arrows indicate regions of reversible lamellipodium formation. **(B)** Changes in green TIRF intensity observed during the reversible recruitment experiments shown in (A).**(C)** Changes in cell adhesion area observed during the reversible recruitment experiments shown in (A). [For each of the graphs in (C) and (D), the number of cells studied (n) is indicated. Graphs in (C) and (D) were provided by Dr. Soumya Banerjee.]

3.4.3 Localization of EGFP-2×FKBP'-Rac1Q61LΔCAAX in N2a Cells

Widefield images of N2a cells expressing EGFP-2×FKBP' revealed that a large fraction of this protein is localized to the nucleus (Fig. 3.19A). In fact, this localization was frequently visible in the corresponding TIRF images (Fig. 3.19A), making it difficult to determine changes in fluorescence intensity at the plasma membrane. Notably, during CID-based recruitment experiments, addition of SLF'-TMP often led to a dramatic redistribution of EGFP-2×FKBP' from the nucleus to the plasma membrane (Fig. 3.16C and Fig. 3.19A), suggesting that EGFP-2×FKBP' can rapidly cycle between the nucleus and the cytosol.

Constructs containing the Rac1Q61LΔCAAX mutant displayed even higher levels of nuclear localization than EGFP-2×FKBP'. However, during CID-based recruitment experiments, addition of the dimerizer did not produce significant changes in nuclear localization of these proteins (Fig. 3.19B). This may suggest that cycling between the nucleus and the cytosol is slower for these proteins.

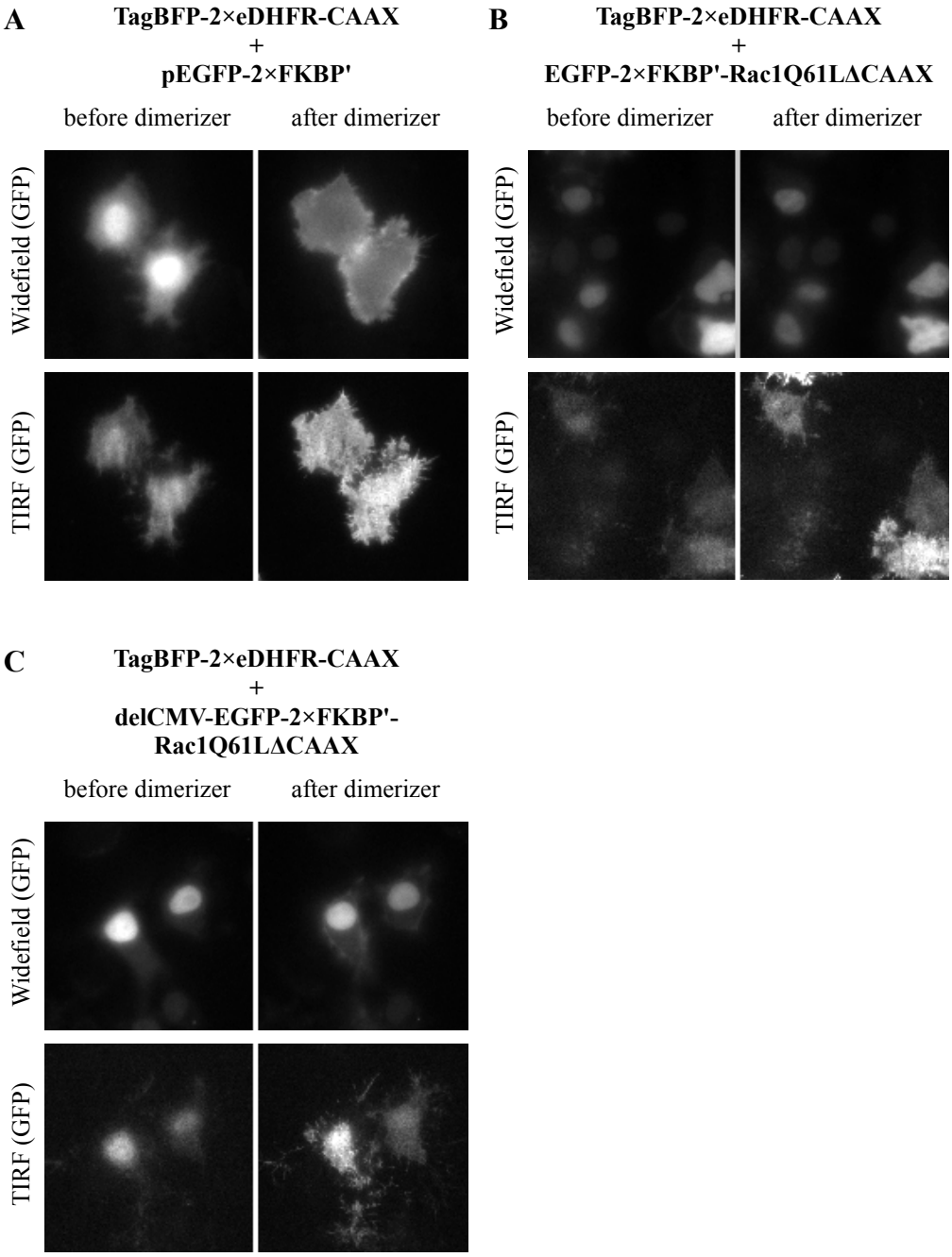

Figure 3.19: Localization of EGFP-2×FKBP' Constructs in N2a Cells. Widefield (top) and TIRF (bottom) images of N2a cells transfected with TagBFP-2×eDHFR-CAAX and pEGFP-2×FKBP' **(A)**, EGFP-2×FKBP'-Rac1Q61LΔCAAX **(B)**, or delCMV-EGFP-2×FKBP'-Rac1Q61LΔCAAX **(C)** plasmids were taken before (left) and after (right) addition of the dimerizer.

Alternatively, it may also suggest that these proteins are actively maintained within the nucleus. Occasionally, minor nuclear deformations were observed with these constructs (Fig. 3.19B). However, these deformations were not as frequent nor as pronounced as those observed with PA-Rac1 (Fig. 3.14).

To examine the effect of expression level on the nuclear localization of EGFP-2×FKBP'-Rac1Q61LΔCAAX, a new plasmid was prepared (delCMV-EGFP-2×FKBP'-Rac1Q61LΔCAAX) that contained a delCMV promoter to ensure low-level expression of the protein. However, experiments with this new plasmid (Fig. 3.19C) produced results similar to those observed with the original plasmid (Fig. 3.19B).

3.4.4 Optimization of the Rac1Q61LΔCAAX Construct

In addition to the mCherry biosensors presented here, mCitrine variants of these biosensors have also been prepared. This makes it possible to simultaneously measure two Rho GTPase activities within the same cell. However, these biosensors cannot be used in combination with the recruitment system described above, due to the spectral overlap between EGFP and mCitrine. Therefore, a new version of the Rac1Q61LΔCAAX construct, labeled with mTurquoise2, was prepared. A nuclear export sequence (NES)[36] was also added between the fluorophore and the two FKBP' domains of this construct to prevent accumulation of this protein within the nucleus (Fig. 3.20A). Notably, the nuclei of N2a cells expressing this protein appear similar to those of non-transfected cells (Fig. 3.20A).

This optimized recruitment system can be used in combination with both mCitrine and mCherry biosensors (Fig. 3.20B). And, these experiments are currently in progress. Preliminary data suggest

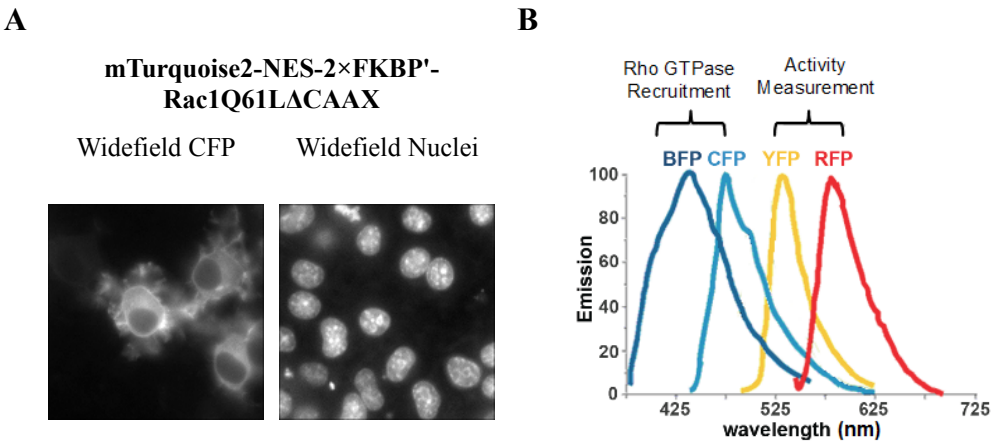

Figure 3.20: Optimization of the Rac1Q61LΔCAAX Construct. (A) Widefield image showing the localization of mTurquoise2-NES-2×FKBP'-Rac1Q61LΔCAAX in N2a cells (left). For comparison, a widefield image of the nuclei is shown (right). **(B)** Emission spectra of BFP, CFP, YFP, and RFP.

that recruitment of constitutively active Rac1 to the plasma membrane causes increases in Cdc42 and RhoA activities (data not shown). Although these results are similar to those observed with PA-Rac1 (Fig. 3.11), additional repetitions of these experiments are needed to confirm these results.

3.4.5 Reversible Recruitment of Active Cdc42 and RhoA to the Plasma Membrane

In addition to the Rac1Q61LΔCAAX construct described above, analogous constructs for Cdc42 (Cdc42Q61LΔCAAX) and RhoA (RhoAQ63LΔCAAX) were also prepared. And, each of these constructs was reversibly recruited to the plasma membrane in order to study how the localization of these proteins influences cell morphology and the actin cytoskeleton.

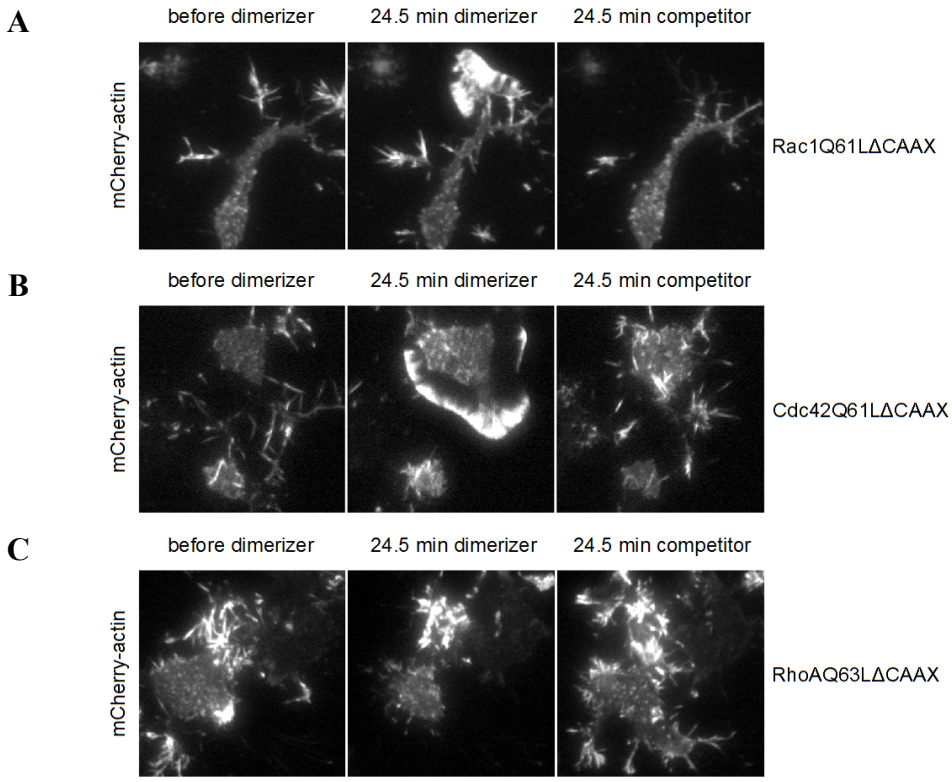

Figure 3.21: Changes in Cell Morphology and the Actin Cytoskeleton Induced by Acute and Reversible Recruitment of Constitutively Active Rho GTPases to the Plasma Membrane. TIRF images showing rearrangements of the actin cytoskeletons of N2a cells induced by acute and reversible recruitment of constitutively active Rho GTPases to the plasma membrane. Recruitment of Rac1Q61LΔCAAX (**A**) or Cdc42Q61LΔCAAX (**B**) to the plasma membrane led to the formation of actin-rich protrusions at the cell periphery while recruitment of RhoAQ63LΔCAAX (**C**) to the plasma membrane caused cell contraction. Addition of competitor caused rapid reversal of these phenotypes.

As expected, recruitment of constitutively active Rac1 or Cdc42 to the plasma membrane produced actin-rich protrusions at the cell periphery (Fig. 3.21A and Fig. 3.21B) and recruitment of constitutively active RhoA to the plasma membrane caused cell contraction (Fig. 3.21C). And, in each case, addition of competitor caused rapid reversal of the observed phenotype (i.e., loss of actin-rich protrusions for Rac1 and Cdc42 and cell expansion for RhoA).

3.4.6 Long-term Recruitment of Rho GTPases to the Plasma Membrane

Experiments described above showed that acute and reversible recruitment of constitutively active mutants of Rac1, Cdc42, or RhoA to the plasma membrane resulted in acute and reversible changes in cell morphology and the actin cytoskeleton (Fig. 3.21). However, it was not clear whether similar results would also be observed for long-term recruitment experiments. Moreover, for the experiments described above, the prenylation sites of Rac1, Cdc42, and RhoA were removed so that each of these proteins could be recruited to the plasma membrane using CID. Therefore, it was also not clear whether long-term recruitment experiments would produce results similar to those observed with overexpression of the full-length constitutively active forms of these three Rho GTPases.

To clarify these matters, N2a cells were first transfected with DNA encoding mCherry-actin and EGFP-labeled full-length Rac1Q61L, Cdc42Q61L, or RhoAQ63L. Consistent with the acute recruitment results described above (Fig. 3.21), cells overexpressing full-length Rac1Q61L or Cdc42Q61L predominantly showed lamellipodia and filopodia at the cell periphery, while cells expressing full-length RhoAQ63L predominantly formed filopodia (Fig. 3.22A). Moreover, cells expressing full-length RhoAQ63L were often smaller than control cells expressing mCherry-actin alone (Fig. 3.22B and Fig. 3.22C). This is consistent with the observation that acute recruitment of RhoAQ63LΔCAAX to the plasma membrane led to cell contraction (Fig. 3.21C). Interestingly, the % of cells displaying stress fibers was similar for all three of the full-length Rho GTPases (Fig. 3.22A).

Next, N2a cells expressing mCherry-actin, mCitrine-N1, TagBFP-2×eDHFR-CAAX, and one of the mTurquoise2-labeled Rho GTPase constructs described above were incubated overnight in the presence or the absence of dimerizer. When these long-term “recruitment” experiments were performed without dimerizer, the cells behaved similar to control cells expressing mCherry-actin alone (Fig. 3.22A and Fig. 3.23A). However, when these experiments were repeated in the presence of dimerizer, cells

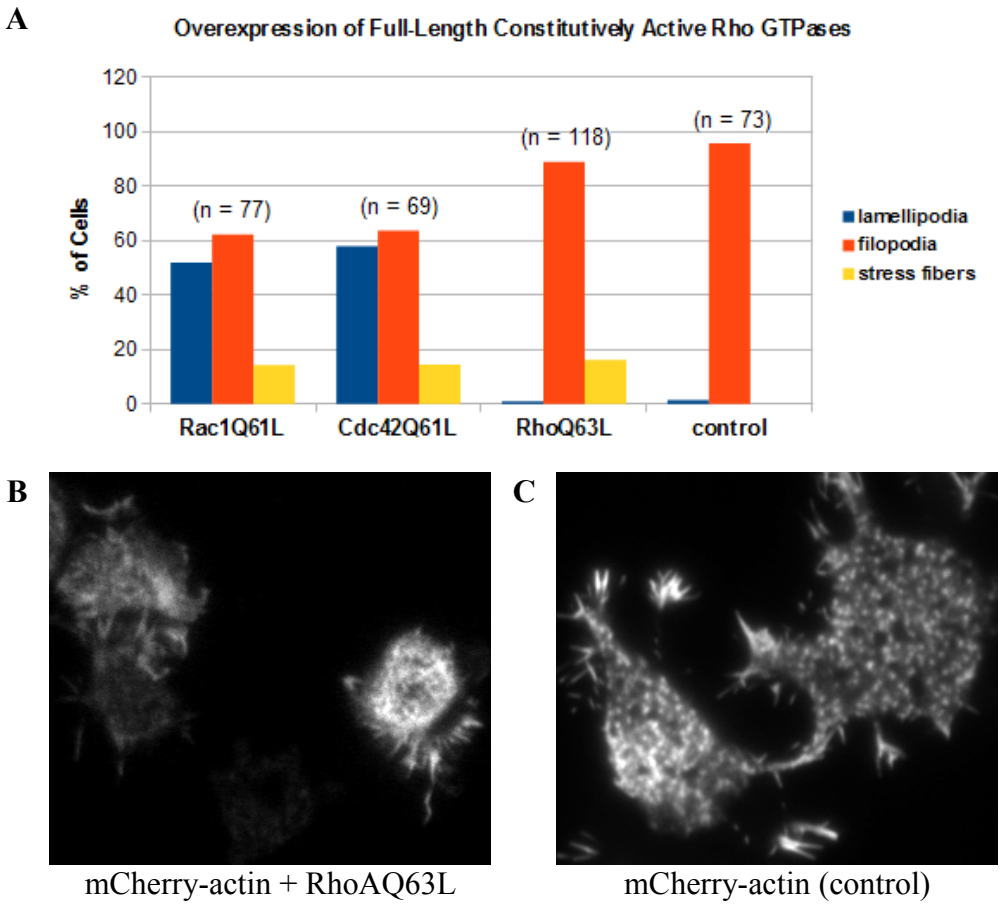

Figure 3.22: Changes in Cell Morphology and the Actin Cytoskeleton Induced by Overexpression of Full-length Constitutively Active Rho GTPases. (**A**) N2a cells overexpressing mCherry-actin and EGFP-labeled full-length Rac1Q61L, Cdc42Q61L, or RhoAQ63L were observed using TIRF microscopy. N2a cells overexpressing mCherry-actin alone were used as controls. Cells overexpressing full-length Rac1Q61L or Cdc42Q61L predominantly showed lamellipodia and filopodia at the cell periphery, while cells expressing full-length RhoAQ63L predominantly formed filopodia. Interestingly, the % of cells displaying stress fibers was similar for all three of the full-length Rho GTPases. For each condition, the number of cells studied (n) is indicated. (**B**) TIRF image of N2a cells expressing mCherry-actin and EGFP-labeled full-length RhoAQ63L. (**C**) TIRF image of N2a cells expressing mCherry-actin alone (control).

expressing the RhoAQ63LΔCAAX construct tended to be smaller than cells expressing this construct in the absence of dimerizer (Fig. 3.23C and Fig. 3.23D). These results were similar to those observed during short-term recruitment of RhoAQ63LΔCAAX to the plasma membrane (Fig. 3.21C) and during long-term overexpression of full-length RhoAQ63L (Fig. 3.22B and Fig. 3.22C). Furthermore, long-term recruitment of Rac1Q61LΔCAAX or Cdc42Q61LΔCAAX to the plasma membrane led to an increase in lamellipodia formation (Fig. 3.23B). These results were similar to those observed during short-term recruitment of Rac1Q61LΔCAAX and Cdc42Q61LΔCAAX to the plasma membrane (Fig. 3.21A and Fig 3.21B) and during long-term overexpression of full-length Rac1Q61L and Cdc42Q61L (Fig. 3.22A).

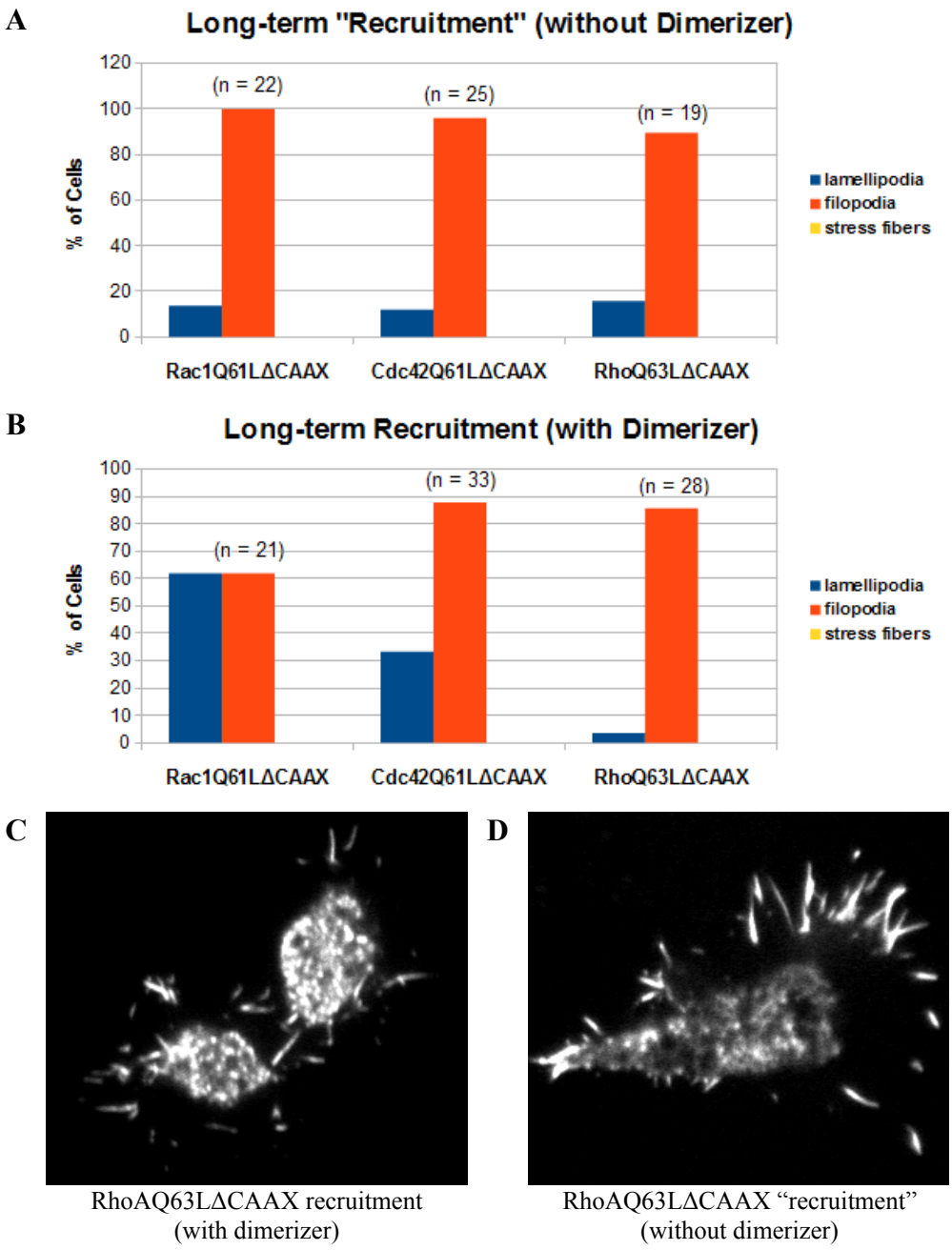

RhoAQ63LΔCAAX recruitment (with dimerizer)

RhoAQ63LΔCAAX "recruitment" (without dimerizer)

Figure 3.23: Changes in Cell Morphology and the Actin Cytoskeleton Induced by Long-term Recruitment of Constitutively Active Rho GTPases to the Plasma Membrane. N2a cells expressing mCherry-actin, mCitrine-N1, TagBFP-2×eDHFR-CAAX, and one of the mTurquoise2-labeled Rho GTPase constructs described above were incubated overnight in the absence (**A**) or the presence (**B**) of dimerizer. (**C**) TIRF image showing N2a cells from the long-term recruitment experiment performed with the RhoAQ63LΔCAAX construct in the presence of dimerizer. (**D**) TIRF image showing an N2a cell from the long-term "recruitment" experiment performed with the RhoAQ63LΔCAAX construct in the absence of dimerizer.

Therefore, long-term recruitment experiments produced results similar to those observed during acute and reversible recruitment of Rho GTPases to the plasma membrane. These experiments also produced results similar to those observed during overexpression of the full-length Rho GTPases. However, it should be noted that, although a small fraction of cells (14-16%) was observed to form stress fibers when the full-length constitutively active Rho GTPases were overexpressed (Fig. 3.22A), stress fibers were not observed during the long-term recruitment experiments (Fig. 3.23B). The reason for this remains unclear and further experiments are needed to clarify these results.

4. DISCUSSION

4.1 Natural Products Can Be Used As Templates to Develop Tools to Study Actin in Living Cells

Interconversion between the monomeric and filamentous forms of actin is crucial for proper cellular function. For example, during cell division, actin filaments at the leading edge of a motile cell disassemble and reassemble (along with the motor protein myosin) into a structure called the contractile ring that separates a mother cell into two daughter cells[3]. Similarly, the actin cytoskeleton of a white blood cell called a neutrophil must constantly rearrange as this cell searches for bacteria that gain access to the body[3].

Interestingly, small molecules that disrupt actin dynamics have been isolated from various natural sources (Table 1.1)[3,5-8]. Three of these molecules (phalloidin, jasplakinolide, and chondramide C) (Fig. 3.1A) have been shown to bind to and stabilize actin filaments[3,5]. In fact, structural studies have shown that phalloidin appears to bind to a pocket formed at the interface formed by three subunits of an actin filament (Fig. 4.1)[61].

Chemists at the Max Planck Institute of Molecular Physiology used this structural information to develop a strategy to synthesize a library of small molecules based on phalloidin, jasplakinolide, and chondramide C[5]. And, these analogues were screened for their ability to disrupt actin dynamics in living cells.

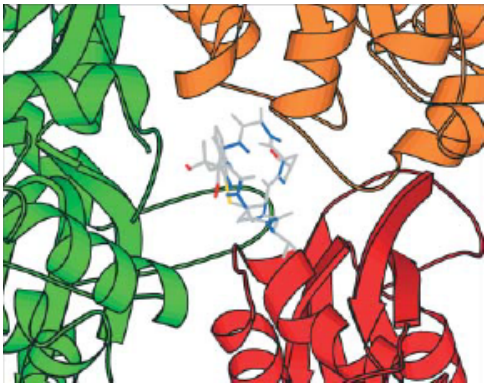

Figure 4.1: Phalloidin Binds to Actin Filaments at the Interface Formed by Three Subunits. (This figure was taken from reference 61).

At high concentrations, three of these analogues (WVA-176, LGM174, and LGM235) produced results similar to those observed with the parent molecules (jasplakinolide and chondramide C) (Fig. 3.2 and Fig. 3.3). However, for two of these analogues (LGM174, and LGM235), a new phenotype was observed at intermediate and/or lower concentrations (Fig. 3.2 and Fig. 3.3). In particular, these compounds caused actin to accumulate in the perinuclear region of N2a cells. Furthermore, additional screening experiments have shown that another analogue (LGM163) produces the same phenotype[62].

The three analogues that produce this new phenotype share many structural similarities (Fig. 4.2). In fact, LGM174 is simply a TIPS protected analogue of LGM163. Furthermore, LGM235 and LGM163 are nearly identical. However, the alanine in LGM163 has been replaced with an ε-Boc-protected lysine in LGM235.

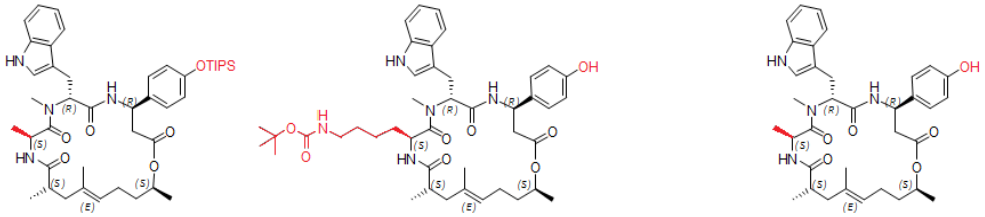

Figure 4.2: Structural Similarities Between LGM174, LGM235, and LGM163.

Currently, the mechanism by which these analogues perturb actin dynamics remains unclear. However, these three analogues could be used as templates to expand this new class of natural-product analogues. Furthermore, structural studies might reveal important information about how these analogues interact with actin.

Interestingly, although LGM235 was observed to induce perinuclear accumulation of actin over a broad range of concentrations (Fig. 3.3), this new phenotype was not observed during preliminary screening experiments of the fluorescently labeled analogues of LGM235 (data not shown). Nevertheless, these analogues were capable of binding to actin in fixed and permeabilized cells[8]. Furthermore, one of these fluorescently labeled analogues (21D) was found to be cell permeable and non-toxic, making it a useful new tool to study static, long-lived actin filaments in live N2a cells[8].

4.2 Biosensors for Measuring Rho GTPase Activity

Rho GTPases are a group of signaling molecules that regulate various cellular processes, including rearrangement of the actin cytoskeleton (Fig. 1.5). When a Rho GTPase is in the active (GTP-bound) state, it can interact with downstream effector proteins. Therefore, since effector proteins selectively bind to the active forms of Rho GTPases, they can be used as the basis for the design of Rho GTPase activity biosensors.

One of the simplest Rho GTPase activity biosensors consists of a fluorescent protein linked to the GTPase-binding domain (GBD) of an effector protein (Fig. 3.5A). And, this type of biosensor was used for the work presented here. There are multiple advantages to using this type of biosensor rather than FRET-based biosensors (Fig. 4.3). First, each biosensor presented here is entirely encoded by a single plasmid. However, for the approach shown in Figure 4.3A, two separate proteins must be overexpressed, each encoded by a separate plasmid. Second, in the approach described here, each Rho GTPase activity is measured using a single fluorescent protein. However, both of the approaches shown in Figure 4.3 require two fluorescent proteins to measure the activity of a single Rho GTPase. Third, the biosensors described here do not contain a prenylation site. Therefore, they should not compete with endogenous Rho GTPases for binding to RhoGDI (Fig. 1.10d). However, each of the approaches shown in Figure 4.3 would introduce a pool of prenylated proteins into the cell that would compete with endogenous Rho GTPases for binding to RhoGDI. Finally, the biosensors described here can be used to measure the activities of endogenous proteins, while the approaches shown in Figure 4.3 rely on activation of an overexpressed Rho GTPase.

Initially, two published biosensors[29], based on the PAK1 and WASP effector proteins were tested (Fig. 3.8C). However, only the WASP biosensor was recruited to the plasma membrane in response to photoactivation of Rac1. Therefore, a new PAK1-based biosensor (delCMV-mCherry-PAK-GBD) was prepared. There are two important features that distinguish the new PAK1-based biosensor from the previously published PAK1-based biosensor (Fig. 3.6). First, the plasmid encoding the new biosensor has a delCMV promoter to ensure low-level expression of the protein. Second, for the new biosensor, the fluorescent tag (mCherry) is fused to the N-terminus of the GBD, rather than the C-terminus.

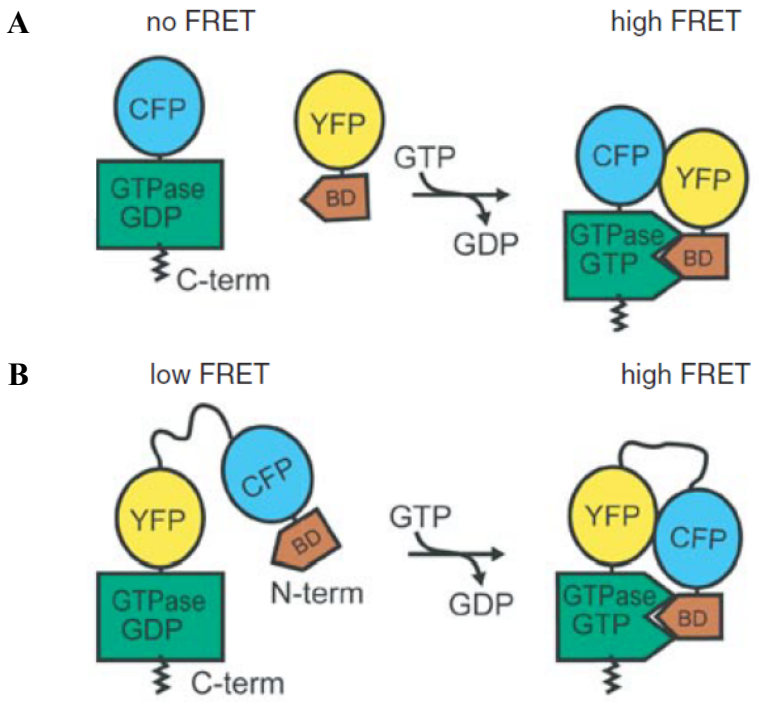

Figure 4.3: FRET-based Biosensors for Measuring Rho GTPase Activity. (**A**) In this approach, a fluorescently labeled Rho GTPase and a fluorescently labeled binding domain from an effector protein (BD) are overexpressed in a cell. If the fluorescently labeled Rho GTPase becomes activated, it can bind to the fluorescently labeled BD. This binding is measured as an increase in FRET between the two fluorphores. (**B**) In this approach, a single fusion protein consisting of the BD, two fluorescent tags, and the Rho GTPase is overexpressed in a cell. If the Rho GTPase becomes activated, it can bind to the BD. This binding is measured as in increase in FRET between the two fluorphores. (This figure was taken from reference 63).

Consistent with the data shown in Fig. 3.8C, the previously published biosensor showed only a weak response to photoactivation of Rac1. However, similar experiments with the new PAK1-based biosensor produced a broad range of values (Fig. 3.10C). One possible explanation for this is that the original PAK1-based construct was overexpressed at such a high level that it functioned more as an

inhibitor of Rac1 rather than a biosensor of Rac1 activity. Indeed, cells expressing the original PAK1-based biosensor produced fewer lamellipodia upon photoactivation of Rac1 than cells expressing the published WASP biosensor or a control biosensor. Alternatively, it is possible that the position of the fluorescent tag in the original PAK1-based biosensor interferes with its ability to bind to active Rac1. Unfortunately, there are currently no structural data for the Rac1/PAK1 complex. However, the structure of Cdc42 in complex with a fragment of the PAK1 GBD has been solved by NMR[64]. And, based on this structure, it would appear that the mCherry fluorescent tag should be tolerated well at either the N-terminus or the C-terminus of the PAK1 GBD fragment (Fig. 4.4).

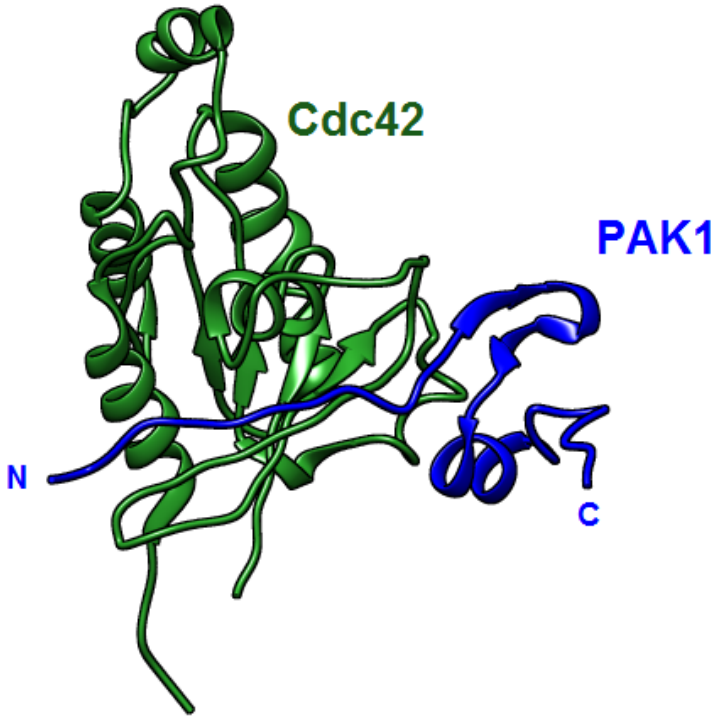

Figure 4.4: NMR Structure of Cdc42 in Complex with a Fragment of the PAK1 GBD.
(PDB Code 1E0A[64]).

Although the new PAK1-based biosensor was more effective than the original PAK1-based biosensor, neither of these sensors are able to distinguish between active Rac1 and Cdc42. Therefore, a new Rac1-specific biosensor based on the GBD of $p67^{phox}$ was also prepared. On average, this new $p67^{phox}$-based biosensor produced a larger relative % change than either the original PAK1-based biosensor or the new PAK1-based biosensor in response to photoactivation of Rac1 (Fig. 3.10A and Fig. 3.10B). Furthermore, two new RhoA biosensors, both based on the GBD of the rhotekin effector protein were also prepared.

Originally all of the biosensors were labeled with mCherry. However, mCitrine versions of the optimized Rac1, Cdc42, and RhoA biosensors have also been prepared. Therefore, two of these biosensors (one labeled with mCherry and the other labeled with mCitrine) could be used to simultaneously measure the activities of two distinct Rho GTPases in a single cell. These biosensors could also be used in combination with blue and cyan fluorescent proteins, such as those described here for reversible recruitment of constitutively active Rho GTPases to the plasma membrane (Fig. 3.20B). Alternatively, these biosensors could be used in combination with optogenetic approaches that use wavelengths of light that fall outside the ranges used to excite mCitrine and mCherry.

4.3 Optogenetic Approaches to Controlling Rho GTPase Activity

Various methods have been proposed to control Rho GTPase activity in living cells. For example, the extracellular growth factor lysophosphatidic acid can be added to cells in order to activate RhoA[3]. Alternatively, the bacterial toxin C3 transferase could be microinjected into a cell in order to inactivate RhoA[65]. Microinjection can also be used to introduce the GEF FGD1 into a cell, which selectively activates Cdc42[3]. However, each of these methods suffers from certain limitations. For example, in addition to activating RhoA, lysophosphatidic acid also activates other signaling pathways[66]. Similarly, bacterial toxins may affect the activities of multiple Rho GTPases[67]. Moreover, microinjection inflicts mechanical stress on cells that can affect their behavior. In fact, a recent study specifically examined rearrangements in the actin cytoskeleton that were induced by puncturing a cell with a microinjection needle[68]. Therefore, recently published optogenetic tools to control Rho GTPase activity using light present attractive alternatives to previous activation methods. One such tool is the photoactivatable Rac1 (PA-Rac1) construct described here.

PA-Rac1 is a fusion protein consisting of the LOV2 domain from Avena sativa (oat) phototropin1 linked to the N-terminus of a constitutively active Rac1 mutant (Fig. 3.7A)[35]. In the dark, the LOV2 domain "cages" the Rac1 mutant and prevents it from interacting with downstream effector proteins (Fig. 3.7A). However, when PA-Rac1 is exposed to light of an appropriate wavelength, the LOV2 domain undergoes structural rearrangements that "uncage" the Rac1 mutant (Fig. 3.7A).

This approach to controlling Rac1 activity has many attractive features. First, because PA-Rac1 is encoded by a single plasmid, this approach is relatively simple to implement. Also, photoactivation of Rac1 is rapid and reversible (Fig. 3.8B). Furthermore, the amount of light required to activate PA-Rac1 is extremely small (Fig. 3.9C). Finally, PA-Rac1 could potentially be locally activated by restricting illumination to a selected region of the cell[35].

In the TIRF setup described here, the positions of the light sources are relatively fixed. However, this setup contains a motorized stage that can be used to control the positions of the cells. Therefore, attempts to locally activate PA-Rac1 by positioning a cell in such a way that part of the cell would be illuminated while the rest of the cell would not were made (Fig. 4.5A). However, in these experiments, Rac1 activity was observed to increase throughout the entire cell upon illumination (data not shown). Although an explanation for these results remains elusive, it is possible that the abnormal localization of PA-Rac1 (Fig. 3.14) may play a role. Therefore, these experiments should be repeated with the optimized PA-Rac1 construct, which localizes primarily to the plasma membrane (Fig. 3.15). Furthermore, it should be noted that these experiments were done before the reversible photoactivation protocol was optimized. Consequently, the amount of light used in these experiments far exceeded that which is necessary to maximally activate PA-Rac1. Therefore, these experiments should be repeated using the optimized photoactivation protocol.

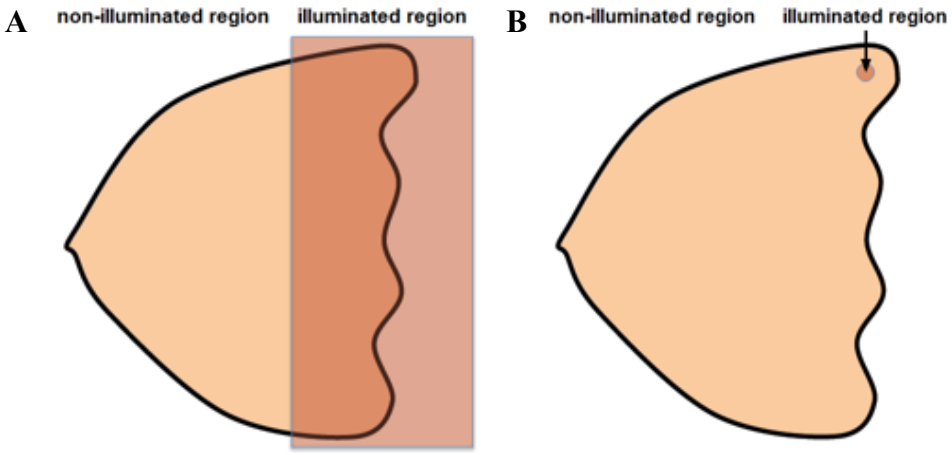

Figure 4.5: Local Activation of PA-Rac1. (**A**) In this approach, the cell is positioned in such a way that part of the cell is illuminated while the rest of the cell is not. (**B**) In this approach, laser light is focused to a small region of the cell.

Recent modifications to the TIRF setup described here included the installation of a new TIRF condensor. With this new condensor, it is possible to focus one laser to a small spot while using the remaining lasers for TIRF microscopy. Although this feature was designed for use in Fluorescence Recovery After Photobleaching (FRAP) experiments, it could also be used to locally photoactivate Rac1 (Fig. 4.5B). Another recent modification to the TIRF setup described here was the installation of a 445 nm laser. Although the primary function of this laser is to excite cyan fluorescent proteins, the evanescent wave produced by this laser could also be used to selectively excite PA-Rac1 within a limited distance of the glass substrate (Fig. 1.15B). And, both of these methods of locally activating PA-Rac1 are currently being explored using the original PA-Rac1 construct and the optimized PA-Rac1 construct.

Despite the many attractive features of PA-Rac1, it is also important to consider other optogenetic approaches to activate Rho GTPases in living cells. For example, Zhou et al. reported a new strategy to cage a protein that is based on the observation that two mutants of the fluorescent protein Dronpa (Dronpa145K and Dronpa 145N) heterodimerize upon illumination with light of one wavelength (~390 nm) and dissociate upon illumination with light of another wavelength (~490 nm) (Fig. 4.6A)[69].

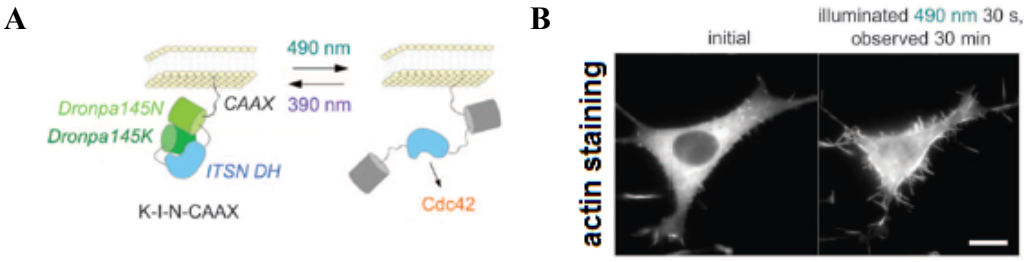

Figure 4.6: Using Light Induced Heterodimerization to Cage a Protein of Interest. (**A**) Cartoon illustrating the concept behind the new caging approach described by Zhou et al.[69]. (**B**) Images of an NIH3T3 cell before (left) and after (right) uncaging of the Dbl homology domain of intersectin. (These images were taken from reference 69).

Zhou et al. expressed a fusion protein (K-I-N-CAAX) containing the Dronpa145K mutant (K), the catalytic Dbl homology domain of a GEF called intersectin (I), the Dronpa145N mutant (N), and the CAAX box of K-Ras (CAAX) in NIH3T3 cells. As expected, this protein localized primarily to the plasma membrane. Furthermore, uncaging of the Dbl homology domain of intersectin led to the formation of filopodia (Fig. 4.6B)[69], a phenotype commonly associated with activation of Cdc42 (Fig. 1.5).

The approach described by Zhou et al. shares many of the attractive features of PA-Rac1. For example, K-I-N-CAAX is entirely encoded by a single plasmid. Furthermore, localized illumination can be used to selectively uncage the Dbl homology domain of intersectin in a particular region of the cell. And, filopodia formation induced by uncaging of this domain appears to be reversible[69]. An additional attractive feature of this approach is that it can be used to activate endogenous Rho GTPases. However, because this method uses a GEF to activate a Rho GTPase, the effects of this activation might be delayed in comparison to direct light-based uncaging of PA-Rac1. For example, although lamellipodia were frequently observed within five minutes of photoactivation of Rac1 (Fig. 3.7C), filopodia formation in response to uncaging of the Dbl homology domain of intersectin may require up to 30 minutes (Fig. 4.6B)[69].

In contrast to the approach described by Zhou et al., where light-induced heterdimerization is used to cage a protein of interest, other optogenetic approaches use light-induced heterdimerization to target a protein of interest to the plasma membrane (Fig. 4.7)[29,70]. In these approaches, one protein module (e.g., PhyB or CIBN) is tethered to the plasma membrane while another protein module (e.g., PIF6 or CRY2) is found predominantly in the cytosol. And, light is used to induce heterodimerization and colocalization of these two protein modules at the plasma membrane.

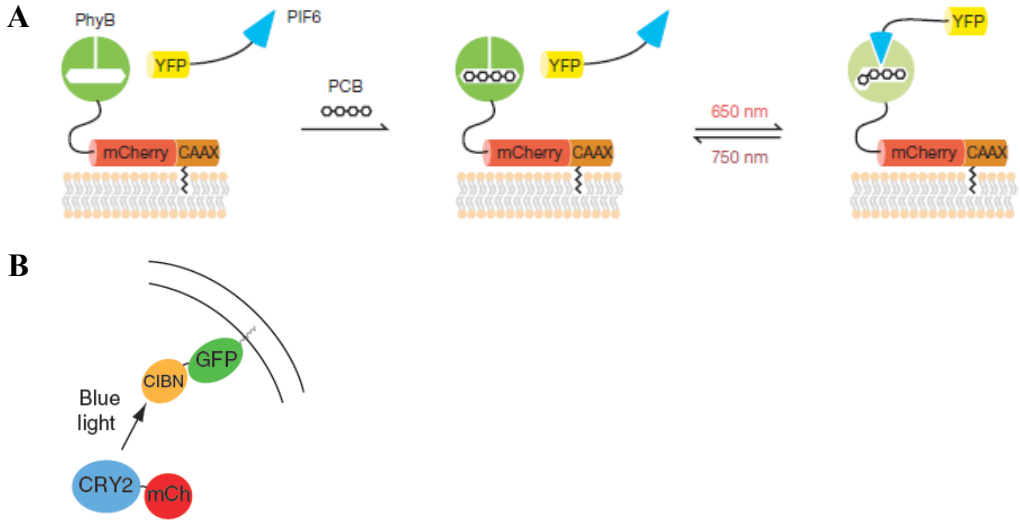

Figure 4.7: Using Light Induced Heterodimerization to Recruit a Protein of Interest to the Plasma Membrane. (**A**) Cartoon illustrating the concept behind the recruitment approach described by Levskaya et al.[29]. (**B**) Cartoon illustrating the concept behind the recruitment approach described by Kennedy et al.[70]. (These images were taken from references 29 and 70).

Unlike the caging strategies described above, where a single protein is used to control Rho GTPase activity, the recruitment approaches shown in Figure 4.7 require two proteins to control the activity of a single Rho GTPase. This makes the recruitment approaches shown in Figure 4.7 more difficult to implement than the caging strategies. Furthermore, because plasma membrane recruitment is monitored using two fluorescent tags, these tags cannot be used to monitor other cellular processes.

Another significant disadvantage to the approach shown in Figure 4.7A is that it requires the addition of a cofactor called phycocyanobilin (PCB). And, isolation of PCB from natural sources can be difficult and time-consuming. Moreover, it should be noted that attempts to reproduce the results described by Levskaya et al. were only partially successful. In particular, the catalytic domains of three different GEFs were rapidly targeted to the plasma membranes of N2a and NIH3T3 cells with this approach. However, activation of Rho GTPases in response to this recruitment was not observed (data not shown). It is also interesting to note that Levskaya et al. claimed that actin-based protrusions were observed within 5-10 minutes of light-induced heterodimerization[29] while Kennedy et al. reported that their approach required up to 30 minutes to produce similar results (Fig. 4.6B)[70]. This is somewhat surprising, given that Levskaya et al. used light-induced heterodimerization to recruit a catalytic GEF domain to the plasma membrane (Fig. 4.7A) while Kennedy et al. used light to uncage a catalytic GEF domain that was already localized to the plasma membrane (Fig. 4.6A).

One major disadvantage shared by all of the optogenetic approaches described here is that the proteins used in these experiments to control Rho GTPase activity absorb light over a broad range of wavelengths, including those commonly used to excite many fluorescent proteins (Fig. 4.8). Therefore, these approaches cannot be easily combined with other approaches that use fluorescent proteins to study cellular processes.

In summary, the subtle advantages and disadvantages associated with each of the optogenetic approaches described here can make it difficult to determine which of these approaches is best suited to study a particular cellular process. Nevertheless, as a whole, these approaches represent an expanding set of tools that use light to control Rho GTPase activity in living cells.

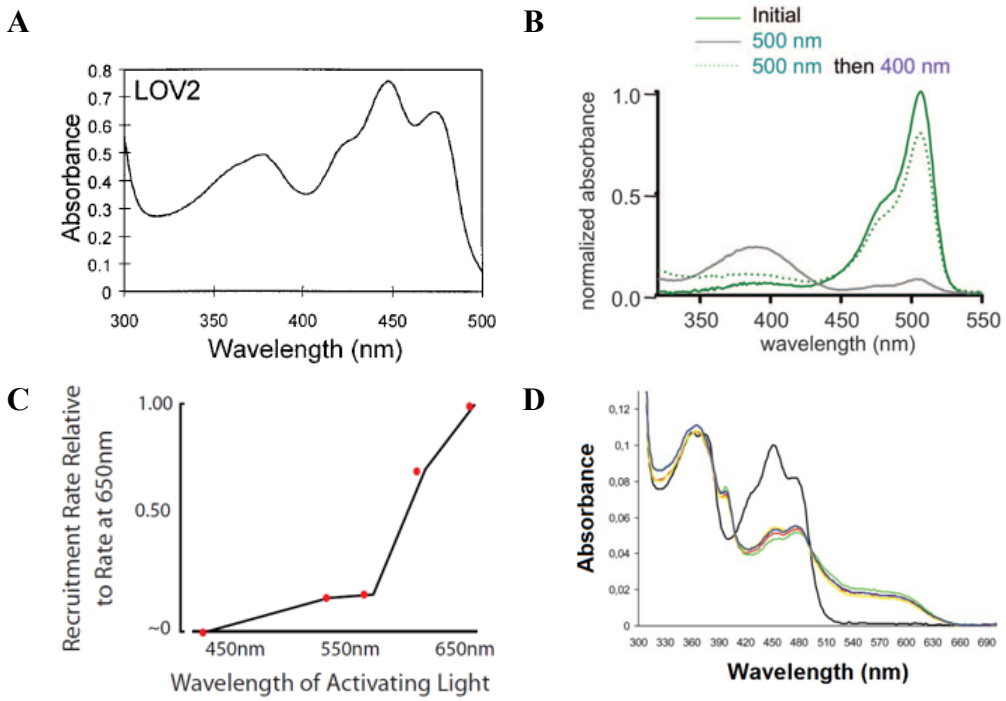

Figure 4.8: Optogenetic Proteins Absorb Light Over Broad Ranges of Wavelengths. (**A**) Absorption spectrum of the LOV2 domain used in PA-Rac1. (This figure was taken from reference 58). (**B**) Absorption spectra showing the range of wavelengths that regulate heterodimerization and dissociation of Dronpa145K and Dronpa145N. (This figure was taken from reference 69). (**C**) Graph showing the range of wavelengths that were observed to induced heterodimerization of PhyB and PIF6. (This figure was taken from reference 29). (**D**) Absorption spectra of CRY2 before (black curve) and after exposure to various durations of blue light (red curve = 5 minutes, yellow curve = 10 minutes, green curve = 25 minutes, and blue curve = 30 minutes). (This figure was taken from reference 71).

4.4 Using CID to Control Rho GTPase Activity

The Chemically Induced Dimerization (CID) system described here can be used to target a protein of interest to the plasma membrane (Fig. 3.16D). This approach is similar to those shown in Figure 4.7. However, instead of using light to induce heterodimerization, a small molecule (referred to as a "dimerizer") is used. This approach also shares some of the same limitations as the light-based recruitment systems described above. In particular, this approach requires two proteins to control the activity of a single Rho GTPase. Furthermore, because plasma membrane recruitment is monitored using two fluorescent tags, these tags cannot be used to monitor other cellular processes.

However, one important advantage to using small molecules to control reversible heterodimerization (Fig. 3.16D) is that this approach can be easily combined with other approaches that use fluorescently labeled proteins. For example, the mCherry and mCitrine biosensors described here can be used to simultaneously monitor how the activities of two Rho GTPases respond to reversible recruitment of a constitutively active Rho GTPase to the plasma membrane (Fig. 3.20B). This makes it possible to directly study the crosstalk between these Rho GTPases within a single cell. However, it is not possible to directly measure this crosstalk with the optogenetic approaches described above because these approaches do not directly measure to what extent the activity of a Rho GTPase changes in response to illumination. For example, when a catalytic GEF domain is uncaged or recruited to the plasma membrane, it is not immediately clear how much of the corresponding endogenous Rho GTPase is activated in response to these perturbations.

Furthermore, unlike some of the optogenetic approaches described above that were only successfully applied to one or two Rho GTPases[69,35], the approach described here was successfully used to control the activities of all three of the most well-studied Rho GTPases (Rac1, Cdc42, and RhoA). Moreover, the CID system developed here was observed to produced rapid and reversible changes in cell morphology and the actin cytoskeleton (Fig. 3.21). However, similar results were not obtained using the approach described by Levskaya et al.[29] (data not shown).

Nevertheless, despite the many advantages associated with the CID system described here, it does suffer from one key limitation. Namely, it would be difficult to use this system to locally activate a Rho GTPase. However, a recent study suggests that, by subjecting cells to a gradient of dimerizer, CID can be used to direct cell migration. In this study, the rapamycin-based CID system was used to control the localization of a Rac1 specific GEF called TIAM1 in HeLa cells (Fig. 4.9A)[72]. In these experiments, cells were observed to migrate towards the direction of the highest dimerizer concentration (Fig. 4.9B)[72]. However, in these experiments, cells did not begin to move until approximately 1-1.5 hours after the gradient was imposed[72]. Furthermore, it is possible that the continuous application of the gradient in these experiments can lead to saturation of all available rapamycin binding sites[72].

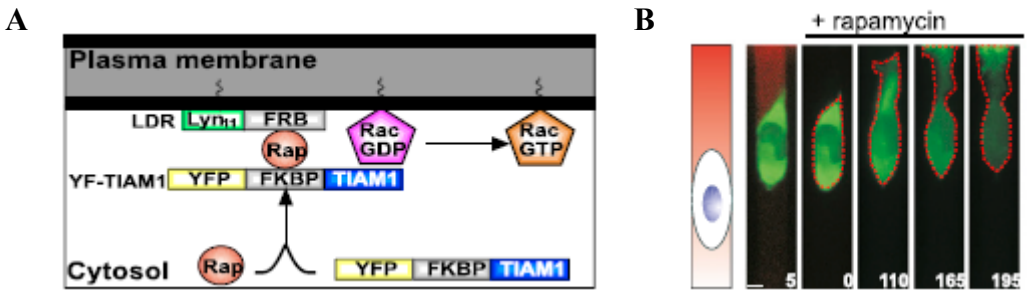

Figure 4.9: Using a Gradient of Dimerizer to Direct Cell Migration. (**A**) Cartoon illustrating the CID system used by Lin et al.[72]. (**B**) A HeLa cell expressing the proteins shown in (A) was subjected to a gradient of the dimerizer rapamycin. Eventually, this cell began to migrate towards the direction of the highest dimerizer concentration. (These images were taken from reference 72).

It should be noted that the CID system described here has two key advantages over the rapamycin-based system. First, because neither of the two protein modules used here are endogenous to mammalian cells, this approach represents a novel bioorthogonal CID system that can be used to control protein function in cells. Second, with this system, heterodimerization can be quickly disrupted by the addition of an inhibitor (Fig. 3.16C).

It should also be noted that current efforts are being made to develop an artificial receptor[73] based on one of the protein modules describe here. Once this artificial receptor has been optimized, the approach described by Gandor et al.[73] can be used to localize this module to specific regions of the plasma membrane. This would make it possible to gain more precise spatial control over the CID-based recruitment system presented here.

4.5 Future Studies

Here, both optogenetic and CID-based approaches were used to perturb Rho GTPase activity in living cells. Furthermore, a series of biosensors was developed to measure Rho GTPase activity. And, these tools were used to examine the crosstalk between Rac1, Cdc42, and RhoA in N2a cells. Currently, these studies suggest that both Cdc42 and RhoA are activated in response to activation of Rac1. This was surprising, as mutual inhibition between RhoA and Rac1 is generally favored in the literature as a mechanism to segregate protrusive (Rac1-based) and contractile (RhoA-based) signals during cell polarization[26].

Future studies will focus on using the tools developed here to identify proteins that play a key role in regulating the crosstalk between Rac1, Cdc42, and RhoA. These studies will also investigate how crosstalk between these Rho GTPases is related to cellular morphogenesis in normal cell function and disease.

5. REFERENCES

1. Revenu C, Athman R, Robine S, Louvard D (**2004**) The co-workers of actin filaments: from cell structures to signals, *Nature Reviews Molecular Cell Biology*, 5:635-46

2. Pak C W, Flynn K C, Bamburg J R (**2008**) Actin-binding proteins take the reins in growth cones, *Nature Reviews Neuroscience*, 9:136-47

3. Alberts B, Johnson A, Lewis J, Raff M, Roberts K, Walter P (**2008**) *Molecular Biology of the Cell*, 5th Edition

4. Svitkina T M, Borisy GG (**1999**) Arp2/3 Complex and Actin Depolymerizing Factor/Cofilin in Dendritic Organization and Treadmilling of Actin Filament Array in Lamellipodia, *Journal of Cell Biology*, 145:1009-1026

5. Tannert R, Milroy L, Ellinger B, Hu T, Arndt H, Waldmann H (**2010**) Synthesis and Structure-Activity Correlation of Natural-Product Inspired Cyclodepsipeptides Stabilizing F-Actin, *Journal of the American Chemical Society*, 132:3063–3077

6. Carter S B (**1967**) Effects of Cytochalasins on Mammalian Cells, *Nature*, 213:261-264

7. Bubb M R, Spector I, Bershadsky A D, Korn E D (**1995**) Swinholide A Is a Microfilament Disrupting Marine Toxin That Stabilizes Actin Dimers and Severs Actin Filaments, *Journal of Biological Chemistry*, 270:3463-3466

8. Milroy L, Rizzo S, Calderon A, Ellinger B, Erdmann S, Mondry J, Verveer P, Bastiaens P, Waldmann H, Dehmelt, Arndt H (**2012**) Selective Chemical Imaging of Static Actin in Live Cells, *Journal of the American Chemical Society*, 134:8480–8486

9. Hall A (**1998**) Rho GTPases and the Actin Cytoskeleton, *Science*, 279:509-514

10. Jaffe A B, Hall A (**2005**) Rho GTPases: biochemistry and biology, *Annual Review of Cell and Developmental Biology*, 21:247–269

11. Nassar N, Hoffman G R, Manor D, Clardy J C, Cerione R A (**1998**) Structures of Cdc42 bound to the active and catalytically compromised forms of Cdc42GAP, *Nature Structural Biology*, 5:1047–1052

12. Rittinger K, Walker P A, Eccleston J F, Smerdon S J, Gamblin S J (**1997**) Structure at 1.65 Å of RhoA and its GTPase-activating protein in complex with a transition-state analogue, *Nature*, 389:758-762

13. Graham D L, Lowe P N, Grime G W, Marsh M, Rittinger K, Smerdon S J, Gamblin S J, and Eccleston J F (**2002**) MgF_3^- as a Transition State Analog of Phosphoryl Transfer, *Chemistry & Biology*, 9:375–381

14. Rossman K L, Der C J, Sondek J (**2005**) GEF means go: turning on RHO GTPases with guanine nucleotide-exchange factors, *Nature Reviews Molecular Cell Biology*, 6:167–180

15. Erickson J W, Cerione R A (**2004**) Structural Elements, Mechanism, and Evolutionary Convergence of Rho Protein-Guanine Nucleotide Exchange Factor Complexes, *Biochemistry*, 43:837-842

16. Wei Y, Zhang Y, Derewenda U, Liu X, Minor W, Nakamoto R K, Somlyo A V, Somlyo A P, Derewenda Z S (**1997**) Crystal structure of RhoA-GDP and its functional implications, *Nature Structure Biology*, 4:699-703

17. Snyder J T, Worthylake D K, Rossman K L, Betts L, Pruitt W M, Siderovski D P, Der C J, Sondek J (**2002**) Structural basis for the selective activation of Rho GTPases by Dbl exchange factors, *Nature Structural Biology*, 9:468-475

18. Cherfils J, Zeghouf M (**2013**) Regulation of Small GTPases by GEFs, GAPs, and GDIs, *Physiologal Reviews*, 93:269–309

19. Canagarajah B, Leskow F C, Ho J Y, Mischak H, Saidi L F, Kazanietz M G, Hurley J H (**2004**) Structural mechanism for lipid activation of the Rac-specific GAP, β2-chimaerin, *Cell*, 119:407–418

20. Roberts P J, Mitin N, Keller P J, Chenette E J, Madigan J P, Currin R O, Cox A D, Wilson O, Kirschmeier P, Der C J (**2008**) Rho Family GTPase Modification and Dependence on CAAX Motif-signaled Posttranslational Modification, *Journal of Biological Chemistry*, 283:25150–25163

21. Garcia-Mata R, Boulter E, Burridge K (**2011**) The “invisible hand”: regulation of RHO GTPases by RHOGDIs, *Nature Reviews Molecular Cell Biology*, 12:493–504

22. Hori Y, Kikuchi A, Isomura M, Katayama M, Miura Y, Fujioka H, Kaibuchi K, Takai Y (**1991**) Post-translational modifications of the C-terminal region of the rho protein are important for its interaction with membranes and the stimulatory and inhibitory GDP/GTP exchange proteins, *Oncogene*, 6:515–522

23. Allal C, Favre G, Couderc B, Salicio S, Sixou S, Hamilton A D, Sebti S M, Lajoie-Mazenc I, Pradines A (**2000**) RhoA prenylation is required for promotion of cell growth and transformation and cytoskeleton organization but not for induction of serum response element transcription, *Journal of Biological Chemistry*, 275:31001–31008

24. Hoffman G R, Nassar N, Cerione R A (**2000**) Structure of the Rho Family GTP-Binding Protein Cdc42 in Complex with the Multifunctional Regulator RhoGDI, *Cell*, 100:345–356

25. Hart M J, Maru Y, Leonard D, Witte O N, Evans T, Cerione R A (**1992**) A GDP-dissociation inhibitor that serves as a GTPase inhibitor for the Ras-like protein Cdc42Hs, *Science*, 258:812–815

26. Guilluy C, Garcia-Mata R, Burridge K (**2011**) Rho protein crosstalk: another social network?, *Trends in Cell Biology*, 21:718-726

27. Mattheyses A L, Simon S M, Rappoport J Z (**2010**) Imaging with total internal reflection fluorescence microscopy for the cell biologist, *Journal of Cell Science*, 123:3621-3628

28. Fish K N (**2009**) Total Internal Reflection Fluorescence (TIRF) Microscopy, *Current Protocols in Cytometry*, 12:18.1-12.18.13

29. Levskaya A, Weiner O D, Lim W A, Voigt C A (**2009**) Spatiotemporal control of cell signalling using a light-switchable protein interaction, *Nature*, 461:997-1001

30. Murakoshi H, Wang H, Yasuda R (**2011**) Local, persistent activation of Rho GTPases during plasticity of single dendritic spines, *Nature*, 472:100-106

31. Bement W M, Benink H A, von Dassow G (**2005**) A microtubule-dependent zone of active RhoA during cleavage plane specification, *Journal of Cell Biology*, 170:91–101

32. Solouk D (**2013**) Design and Characterization of a TIRF-Based Biosensor for the Rho GTPase Rac1, Master's thesis, Ruhr University (Bochum, Germany)

33. Biesemann A (**2009**) Dynamik von kortikalem Dynein in der MAP2c-induzierten Mikrotubuli-Reorganisation, Master's thesis, Ruhr University (Bochum, Germany)

34. Arens J (**2012**) Die Rolle von Mikrotubuli-regulierenden Proteinen während der neuronalen Differenzierung, Doctoral thesis, Technical University of Dortmund (Dortmund, Germany)

35. Wu Y I, Frey D, Lungu O I, Jaehrig A, Schlichting I, Kuhlman B, Hahn K M (**2009**) A genetically encoded photoactivatable Rac controls the motility of living cells, *Nature*, 461:104-110

36. Goedhart J, von Stetten D, Noirclerc-Savoye M, Lelimousin M, Joosen L, Hink M A, van Weeren L, Gadella T W J, Royant A (**2012**) Structure-guided evolution of cyan fluorescent proteins towards a quantum yield of 93%, *Nature Communications*, 3:751

37. Kamentsky L, Jones T R, Fraser A, Bray M A, Logan D J, Madden K L, Ljosa V, Rueden C, Eliceiri K W, Carpenter A E (**2011**) Improved structure, function and compatibility for CellProfiler: modular high-throughput image analysis software, *Bioinformatics*, 27:1179-80

38. Schneider C A, Rasband W S, Eliceiri K W (**2012**) NIH Image to ImageJ: 25 years of image analysis, *Nature Methods*,9:671-5

39. Dehmelt L, Poplawski G, Hwang E, Halpain S (**2011**) NeuriteQuant: An open source toolkit for high content screens of neuronal Morphogenesis, *BMC Neuroscience*, 12:100

40. Anderson M O, Shelat A A, Guy R K (**2005**) A solid-phase approach to the phallotoxins: total synthesis of [Ala7]-phalloidin, *Journal of Organic Chemistry*, 70:4578-84

41. Schuresko L A, Lokey R S (**2007**) A practical solid-phase synthesis of Glu7-phalloidin and entry into fluorescent F-actin-binding reagents, *Angewandte Chemie International Edition*, 46:3547-9

42. Waldmann H, Hu T, Renner S, Menninger S, Tannert R, Oda T, Arndt H (**2008**) Total Synthesis of Chondramide C and Its Binding Mode to F-Actin, *Angewandte Chemie International Edition*, 47:6473 –6477

43. Eggert U, Diestel R, Sasse F, Jansen R, Kunze B, Kalesse M (**2008**) Chondramide C: synthesis, configurational assignment, and structure-activity relationship studies, *Angewandte Chemie International Edition*,47:6478-82

44. Grieco P A, Hon Y S, Perez-Medrano A (**1988**) A convergent, enantiospecific total synthesis of the novel cyclodepsipeptide (+)-jasplakinolide (jaspamide), *Journal of the American Chemical Society*, 110:1630–1631

45. Schmidt U, Siegel W, Mundinger K (**1988**) Total syntheses of jaspamide (jasplakinolide) and geodiamolide A and B - 1. Stereoselective synthesis of (2S,4E,6R,8S)-8-hydroxy-2,4,6-trimethyl-4-nonenoicic acid[1], *Tetrahedron Letters*, 29:1269-1270

46. Chu K S, Negrete G R, Konopelski J P (**1991**) Asymmetric total synthesis of (+)-jasplakinolide, *Journal of Organic Chemistry*, 56:5196–5202

47. Imaeda T, Hamada Y, Shioiri T (**1994**) Efficient syntheses of geodiamolide A and jaspamide, cytotoxic and antifungal cyclic depsipeptides of marine sponge origin, *Tetrahedron Letters*, 35:591-594

48. Ghosh A K, Moon D K (**2007**) Enantioselective Total Synthesis of (+)-Jasplakinolide, *Organic Letters*, 9:2425–2427

49. Letourneau P C, Shattuck T A, Ressler A H (**1987**) "Pull" and "push" in neurite elongation: observations on the effects of different concentrations of cytochalasin B and taxol, *Cell Motility and the Cytoskeleton*, 8:193-209

50. Dehmelt L, Smart F M, Ozer R S, Halpain S (**2003**) The role of microtubule-associated protein 2c in the reorganization of microtubules and lamellipodia during neurite initiation, *Journal of Neuroscience*, 23:9479-90

51. Dehmelt L (**2014**) Cytoskeletal self-organization in neuromorphogenesis, *Bioarchitecture*, 4:75-80

52. Schiff P B, Horwitz S B (**1980**) Taxol stabilizes microtubules in mouse fibroblast cells, *Proceedings of the National Academy of Sciences (U.S.A)*, 77:1561-1565

53. Watanabe N, Mitchison T J (**2002**) Single-Molecule Speckle Analysis of Actin Filament Turnover in Lamellipodia, *Science*, 295:1083-1086

54. Harper S M, Neil L C, Gardner K H (**2003**) Structural Basis of a Phototropin Light Switch, *Science*, 301:1541-1544

55. Harper S M, Neil L C, Day I J, Hore P J, Gardner K H (**2004**) Conformational Changes in a Photosensory LOV Domain Monitored by Time-Resolved NMR Spectroscopy, *Journal of the American Chemical Society*, 126:3390-3391

56. Yao X, Rosen M K, Gardner K H (**2008**) Estimation of Available Free Energy in a LOV2-Jα Photoswitch, *Nature Chemical Biology*, 4:491–497

57. Wu Y I, Wang X, He L, Montell D, Hahn K M (**2011**) Spatiotemporal Control of Small GTPases with Light Using the LOV Domain, *Methods in Enzymology*, 497:393-407

58. Salomon M, Christie J M, Knieb E, Lempert U, Briggs W R (**2000**) Photochemical and Mutational Analysis of the FMN-Binding Domains of the Plant Blue Light Receptor, Phototropin, *Biochemistry*, 39:9401-9410

59. Mackay D J G, Hall A (**1998**) Rho GTPases, *Journal of Biological Chemistry*, 273:20685–20688

60. Timmermann A (**2013**) Analyse und akute Störung des Signalnetzwerks von RhoGTPasen in lebenden Zellen, Master's thesis, Ruhr University (Bochum, Germany)

61. Oda T, Namba K, Maéda Y (**2005**) Position and Orientation of Phalloidin in F-Actin Determined by X-Ray Fiber Diffraction Analysis, *Biophysical Journal*, 88:2727–2736

62. Rizzo S, Milroy L, Calderon A, Bieker V, Schulz I, Tran T, Ellinger B, Sievers S, Waldmann H, Arndt H, Dehmelt L (**2014**) Identification of a Gain-of-function phenotype induced by a Natural Product-Inspired Compound (manuscript in preparation)

63. Hodgson L, Shen F, Hahn K (**2010**) Biosensors for Characterizing the Dynamics of Rho Family GTPases in Living Cells, *Current Protocols in Cell Biology*, 14.11.1-14.11.26

64. Morreale A, Venkatesan M, Mott H R, Owen D, Nietlispach D, Lowe P N, Laue E D (**2000**) Structure of Cdc42 bound to the GTPase binding domain of PAK, *Nature Structural Biology*, 7:384-388

65. C D Nobes, A Hall (**1999**) Rho GTPases Control Polarity, Protrusion, and Adhesion during Cell Movement, *Journal of Cell Biology*, 144:1235-1244

66. Dorsam R T, Gutkind J S (**2007**) G-protein-coupled receptors and cancer, *Nature Reviews Cancer*, 7:79-94

67. Lerm M, Selzer J, Hoffmeyer A, Rapp U R, Aktories K, Schimdt G (**1999**) Deamidation of Cdc42 and Rac by Escherichia coli Cytotoxic Necrotizing Factor 1: Activation of c-Jun N-Terminal Kinase in HeLa Cells, *Infection and Immunity*, 67:496-503

68. Vinzenz M, Nemethova M, Schur F, Mueller J, Narita A, Urban E, Winkler C, Schmeiser C, Koestler S A, Rottner K, Resch G P, Maeda Y, Small J V (**2012**) Actin branching in the initiation and maintenance of lamellipodia, *Journal of Cell Science*, 125:2775-2785

69. Zhou X X, Chung H K, Lam A J, Lin M Z (**2012**) Optical Control of Protein Activity by Fluorescent Protein Domains, *Science*, 338:810-814

70. Kennedy M J, Hughes R M, Peteya L A, Schwartz J W, Ehlers M D, Tucker C L (**2010**) Rapid blue-light–mediated induction of protein interactions in living cells, *Nature Methods*, 7:973-975

71. Banerjee R, Schleicher E, Meier S, Viana R M, Pokorny R, Ahmad M, Bittl R, Batschauer A (**2007**) The Signaling State of Arabidopsis Cryptochrome 2 Contains Flavin Semiquinone, *Journal of Biological Chemistry*, 282:14916-14922

72. Lin B, Holmes W R, Wang C J, Ueno T, Harwell A, Edelstein-Keshet L, Inoue T, Levchenko A (**2012**) Synthetic spatially graded Rac activation drives cell polarization and movement, *Proceedings of the National Academy of Sciences (U.S.A)*, 109:E3668-77

73. Gandor S, Reisewitz S, Venkatachalapathy M, Arrabito G, Reibner M, Schröder H, Ruf K, Niemeyer C M, Bastiaens P I H, Dehmelt L (**2013**) A Protein-Interaction Array Inside a Living Cell, *Angewandte Chemie International Edition*, 52:4790 –4794

ACKNOWLEDGEMENTS

I would like to thank Dr. Leif Dehmelt for giving me the opportunity to come to Germany and to participate in a whole new field of research. It is clear to me that you have a great passion for science and you are always thinking about new ways to answer scientific questions. You also have a great wealth of knowledge. And, you gave me the opportunity to work on multiple projects, which made it possible for me to collaborate with many people and to learn new techniques. And, you even made time for me when I needed to talk about non-scientific matters. Thank you for your guidance.

I would also like to thank Dr. Philippe Bastiaens. Throughout my time in Dortmund, you have given me extremely helpful input regarding my research. And, it continues to amaze me that you are able to oversee so many projects that encompass such a wide range of scientific disciplines. Thank you for your enthusiasm and your guidance.

Thank you as well to Dr. Martin Engelhard for agreeing to review my thesis and for agreeing to participate in my defense.

It has also been my extreme pleasure to work in collaboration with other groups in Dortmund and in Essen. In particular, I would like to thank Dr. Perihan Nalbant, Dr. Yaowen Wu, and Dr. Herbert Waldmann for including me in your research projects. Thank you also to Dr. Reza Ahmadian for helping us to develop the new Rac1 biosensor.

Of course, I must also thank my fellow lab members. In particular, I would like to thank Dr. Tomáš Mazel, Katharina Ruf, and Silke Gandor for welcoming me into the group and for helping me to adjust to life in Germany. Thank you also to Muthu Venkatachalapathy for being such a great friend. And, thank you to our two student helpers, Jana Jungkurth and Ira Schulz, for making sure that the lab runs as it should. Thank you also to Thanh-Thuy Duong for helping me set up a series of confocal experiments.

I was also fortunate enough to have the opportunity to work with two Master's students, Aline Timmermann and Djamschid Solouk. You each have such a positive attitude. And, I wish you both great success during your doctoral studies.

I would also like to thank various students and post-docs from other groups for their help and their friendship. In particular I would like to thank Johannes Koch, Dr. Stefano Rizzo, Dr. Silke Erdmann, Dr. Georgios Konstantinidis, Melanie Gräßl, Jan-Erik Hoffmann, and Sarah Imtiaz. I learned so much from all of you. And, I am truly thankful that I had the opportunity to work with you.

I also have to thank Dr. Sven Müller for keeping our microscopes in working order. You're work is extremely important. And, I want you to know how much I appreciate it.

Thank you also to Dr. Astrid Krämer for taking the time to meet with me and share your advice and wisdom.

Also, because the work described here involved a great deal of cloning, I would like to thank the sequencing staff at the MPI (Walburga Hecker and Nina Ludwigs). And, I would like to thank Jutta Luig for providing our lab with competent cells.

Finally, I would like to thank Tanja Forck for explaining to me the procedures involved in submitting my thesis and scheduling my defense.